THESIS FOR A MASTER'S DEGREE

TITLE:

Research on shear history effect of okra mucilage's viscosity

Supervisor: Obara Hiromichi (Assoc. Prof.)

Date of submission: Month01 Day10 , Year2019

Graduate School of Science and Engineering,
Tokyo Metropolitan University

Department: Mechanical Engineering

Student ID No.: 17883323

Student name: シュ　イシュン(Zhu weijun)

I. Contents

Overview

Background:

Okra known in many English-speaking countries as ladies' fingers or ochro, is a flowering plant in the mallow family and contains soluble fibers from the stems of itself. Because of these soluble fibers, it will make the okra-water mixed liquid become thick and viscous, which is the aqueous phase called mucilage. As we all know, okra is one of the healthy vegetables, it has a variety of uses and functions in pharmacology, food industry or biomedical applications. In the previous rheological research, a low-yield mucilage was described obtained via aqueous extraction of okra fruit, named 'okra mucilage F'. It is a water-soluble, 1.7-million-molecular-weight glycoprotein which produces viscous, shear-thinning, and viscoelastic solutions in water. Some reports showed hot buffer soluble solids solutions are mainly elastic, while chelating agent soluble solids ones are primarily viscous. Because the okra extraction protocols affected the molecular parameters as well as rheological properties of isolates. The mucilage of okra showed very high extensional viscosity, which was two or three orders of magnitude higher than the shear viscosity. And the okra mucilage represented the transition from the shear thinning to the plateau zone approximately at the low shear rate.

Objective:

However, the previous research did not give a clear view on the shear history effect whether having an influence on the okra mucilage rheological properties. In my study, a rheological experiment was set up to discuss these issues. In order to point out the changed rheological properties when okra mucilage was flowing after high shear stress and long sheared time. Trying to find out what would happen when it was dumped into a narrow tube, so as to give predictability if trying to be dumped into the liver.

Method:

Okra pods were brought from the local market. It was cleaned by pipe water in order to get rid of the dirt on their skins. Then the okra pods' seeds were removed and the skins were sliced. After that, the pieces would be store in the pure water at a fixed weight ratio. The mixed solution would be preserved in the refrigerator for a while. The impurity-free okra mucilage was collected by using a combination of weave mesh. The PEO15 solution and jute mucilage were also modulated as a control group. The shear history effect was finished by flowing through a narrow needle with a group of devices.

Results:

At this stage of my experiments, a changed shear viscosity on okra mucilage after high shear stress treatment was observed. All these three solutions showed shear thinning when they were sheared. In the experiment, the okra mucilage viscosity is sensitively changed after the high strain rate comparing with the PEO15 solution and jute mucilage. At low shear rate (from $0.1S^{-1}$ to $100S^{-1}$), the viscosity values almost do not change after the high shear stress impact. However, the okra mucilage which was highly pre-sheared by the narrow needle treatment would be decreased 20%-40% at a high shear rate (from $100S^{-1}$ to $1000S^{-1}$). Moreover, the transaction point around

$50\sim60S^{-1}$ was found in one okra mucilage. And the okra mucilage was influenced by the shear history effect when the shear strain rate must be over the transaction point as a limit.

Conclusion:

Overall, okra mucilage is a very interesting complex fluid. The okra extract structure in the mucilage is changing not only arranged by the rising shear rate but also caused by the shear history effect. In addition, findings suggest that the application of shear history effect irreversibly changes the microstructure of the okra mucilage, and consequently their flow properties. These effects result in that the large soluble okra protein turn into many small crops when the shear stress break the structure as the shear rate researched over transaction point. Moreover, it hints the okra mucilage will flow more and more easily in the microchannel when the flow has been started.

II. Background

1.1 Okra

Okra, (Abelmoschus esculentus), herbaceous hairy annual plant of the mallow family (Malvaceae) which originates from Africa.

When the plant grow up, it can carry a yellow mallow-type blossom and a greenish fruit, which is the okra pod (Fig 1.1). It is an elongated, lantern shape vegetable. In our daily life, the okra pods are usually used for cooking or preserved by freezing or canning (Woolfe et al. 1977). Moreover, okra pod is famously known by its sticky texture when cut open (Fig. 1.2).

Fig. 1.1 The okra pod from the local market

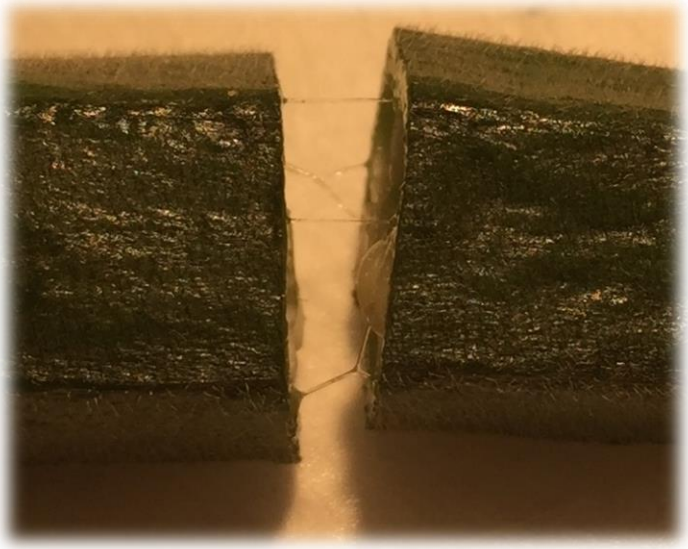

Fig. 1.2 The slimy and sticky texture when okra was cut open

1.1.1 Okra chemical composition/nutrition

From table 1.1, we can find that raw okra contains 90% water, 2% protein, 7% carbohydrates and negligible in fat. That shows the okra pods can be a healthy food to our body.

Table. 1.1 The raw okra's nutrient database from USDA

Source: USDA National Nutrient Database for Standard Reference 1 April 2018 Software v.3.9.5.1_2018-09-23				
Basic Report				
Report Run at: December 02 2018 01:11 EST				
Nutrient data for: Okra, raw				
Nutrient	Unit	1Value per 100 g	1 cup = 100.0g	8.0 pods (3" long) = 95.0g
Proximates				
Water	g	89.58	89.58	85.1
Energy	kcal	33	33	31
Protein	g	1.93	1.93	1.83
Total lipid (fat)	g	0.19	0.19	0.18
Carbohydrate, by difference	g	7.45	7.45	7.08
Fiber, total dietary	g	3.2	3.2	3
Sugars, total	g	1.48	1.48	1.41
Minerals				
Calcium, Ca	mg	82	82	78
Iron, Fe	mg	0.62	0.62	0.59
Magnesium, Mg	mg	57	57	54
Phosphorus, P	mg	61	61	58
Potassium, K	mg	299	299	284
Sodium, Na	mg	7	7	7
Zinc, Zn	mg	0.58	0.58	0.55
Vitamins				
Vitamin C, total ascorbic acid	mg	23	23	21.9
Thiamin	mg	0.2	0.2	0.19
Riboflavin	mg	0.06	0.06	0.057
Niacin	mg	1	1	0.95
Vitamin B-6	mg	0.215	0.215	0.204
Folate, DFE	µg	60	60	57
Vitamin B-12	µg	0	0	0
Vitamin A, RAE	µg	36	36	34
Vitamin A, IU	IU	716	716	680
Vitamin E (alpha-tocopherol)	mg	0.27	0.27	0.26
Vitamin D (D2 + D3)	µg	0	0	0
Vitamin D	IU	0	0	0
Vitamin K (phylloquinone)	µg	31.3	31.3	29.7
Lipids				
Fatty acids, total saturated	g	0.026	0.026	0.025
Fatty acids, total monounsaturated	g	0.017	0.017	0.016
Fatty acids, total polyunsaturated	g	0.027	0.027	0.026
Fatty acids, total trans	g	0	0	0
Cholesterol	mg	0	0	0
Other				
Caffeine	mg	0	0	0

1.1.2 Okra fiber

Bast fiber is a plant fiber collected from the phloem around some plant stems. They will support the conductive cells of the phloem and provide strength to the stems. A more thing of bast fiber is that it contain the fiber node, even it represents a weakness but also provides flexibility to the skin stems.

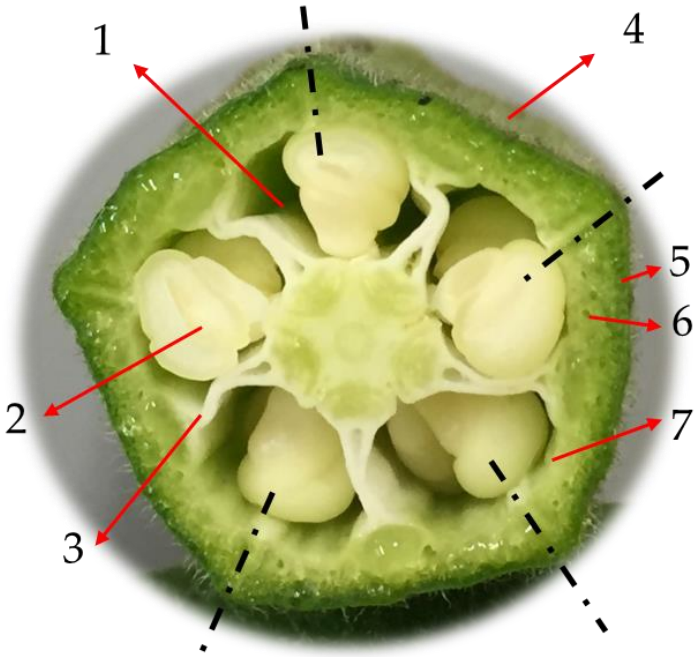

Fig. 1.3 The cross-section of okra pod

(1: Locule; 2: Seed; 3: Septa; 4: Epidermis; 5: Cortex; 6: Bast fibers; 7: Phloem)

Okra bast fiber (Fig. 1.3 6:hollow hole part) was analyzed and the estimated average chemical compositions of okra bast fiber are 67.5 % a-cellulose, 15.4 % hemicelluloses, 7.1 % lignin, 3.4 % pectic matter, 3.9 % fatty and waxy matter and 2.7 % aqueous extract (Fekadu Gemede 2015). It has good characteristics like high molecular weight thus it gives high tensile strength, more dyeability and better color fastness properties (Lousinian et al. 2017).

1.2 Complex fluid

Complex fluids are binary mixtures that have coexistence between two phases: solid-liquid, solid–gas, liquid–gas or liquid-liquid. They exhibit unusual mechanical responses that are applied stress or strain due to the geometrical constraints that the phase coexistence imposes. They are surrounding us in our daily life (Newman J. 2008).

1.2.1 Mucilage

It is well known by everyday experience that the water will be thicken when some plants' roots, leaves, or fruits are left in there. The resulting high-viscosity liquids are collectively known as mucilage. From the table 1.2, there is only 27 kinds of plants can mainly secret the mucilage.

In our daily life, we can find that increasing either in the temperature or in the available surface area of the extraction part typically further increase the intensity of this thickening action.

Table. 1.2 Plants which can extract mucilage

Aloe vera	Liquorice root	Parthenium
Basella alba (Malabar spinach)	Marshmallow	Pinguicula (butterwort)
Cactus	Mallow	Psyllium seed husks
Chondrus crispus (Irish moss)	Drosophyllum lusitanicum	Salvia hispanica (chia) seed
Corchorus (jute plant)	Fenugreek	Mullein
Dioscorea polystachya (nagaimo, Chinese yam)	Flax seeds	Okra
Drosera (sundews)	Kelp	Talinum triangulare (waterleaf)

1.2.2 Mucilage formation (Ritzoulis 2017)

A basic working hypothesis is that the transformation of low-viscosity water into a viscous colloidal dispersion comprises of three distinct stages (Fig 1.4):

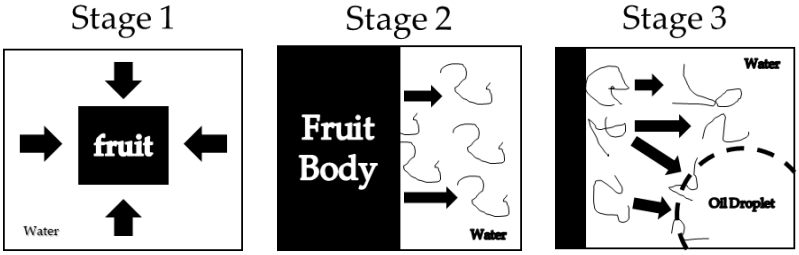

Fig. 1.4 The process of mucilage formation (Ritzoulis 2017)

Stage 1: The macromolecules of the solid matrix are hydrated by the aqueous solvent. The solid object swells, leaving space for the incoming elution of the hydrated macromolecules.

Stage 2: Hydrated macromolecules are transported from the solid matrix to the bulk aqueous phase, increasing the concentration of the macromolecules therein.

Stage 3: Macromolecules arrange themselves and relax in the bulk aqueous phase or are adsorbed onto oil interfaces. This alters the water's rheological properties, turning it into a viscous hydrocolloid.

1.2.3 Okra mucilage components

A low-yield mucilage was described obtained via aqueous extraction of okra fruit, named ‘okra mucilage F’ (Fig. 1.5). Okra mucilage F, a product of the okra, is a water-soluble, 1.7-million-molecular-weight glycoprotein which produces viscous, shear-thinning, and viscoelastic solutions in water. It resulted in a polysaccharide-rich material with a yield of 0.17% containing galactose, rhamnose, and galacturonic acid all occurring at concentrations between 20% and 30% (Meister et al. 1983).

Interestingly, ‘okra mucilage F’ is reported to have similar protein composition with another extract, namely ‘okra mucilage M’, but the branching of the polysaccharide chains is different between the two extracts. That suggested that even small alterations in the extraction protocols can have a substantial impact on the selectivity of larger molecules such as the polysaccharide (Ritzoulis 2017).

Moreover, the intrinsic viscosity of okra extracts is highly dependent on the extraction protocol (Kontogiorgos et al. 2012) (Ndjouenkeu et al. 1996).

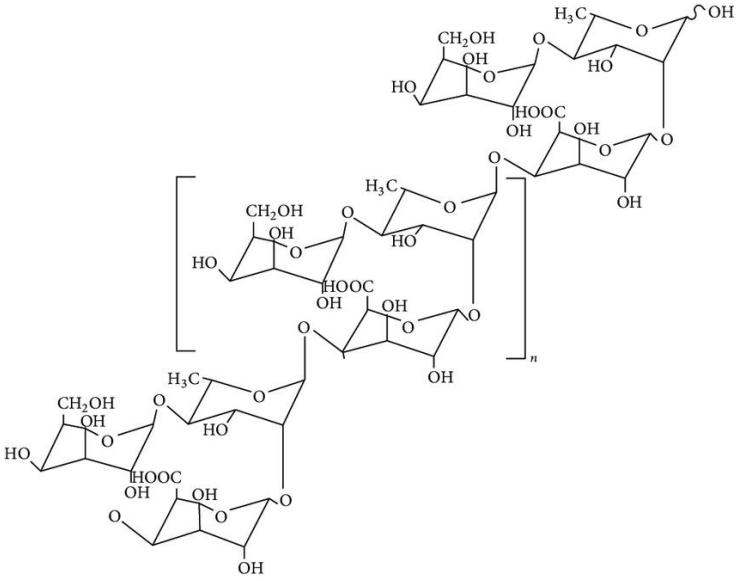

Fig. 1.5 Chemical structure of ‘okra mucilage F’ (Mishra et al. 2008)

1.2.4 Okra polysaccharide components

Okra gum is a NaOH-soluble polysaccharide with a peptide covalently-bound to it (Chen et al. 2014). Isolated okra pectins are rich in rhamnogalacturonan-I segments with varying composition of side chains and molecular weights ranging from 10 ~767x10^3g/mol^{-1} (Sengkhamparn et al. 2009).

As mentioned in previous section, the extraction component would be changed varied with the method that we chose. Because the polyelectrolyte nature and differences in the molecular

structure of extracted pectins significantly affect conformational characteristics of polymer chains within the dilute region (Alba et al. 2015).

The principal polysaccharide populations of okra extract resulting from the hot neutral extraction of okra alcohol-insoluble solids essentially type I acetylated rhamnogalacturonan-I with side branches of 1–2 galactosyl residues, with small amounts of homogalacturonan. The same authors reported that extraction of the remaining materials with EDTA which stand for ethylenediaminetetraacetic acid yielded extracts rich in homogalacturonan and a lesser amount of somehow larger molecules of RG I, reportedly with somehow larger side chains (Sengkhamparn et al. 2009).

Meanwhile, the okra pods from different place of origin have a little different with each other, too. Okra from the southern USA contained an acidic polysaccharide which consisted of galactose, rhamnose, and galacturonic acid as the main sugars (Whistler et al. 1954). An okra polysaccharide from a commercial supplier in Germany also contained glucose and glucuronosyl residues (Lengsfeld et al. 2004). In addition, the galacturonic acid in okra polysaccharides from India was in the L-configuration form (Agarwal et al. 2001). Okra polysaccharides grown in Japan, extracted with cold water and purified using a 10 % chelating agent solution was shown to contain a repeating unit of α-(1,2)-linked rhamnosyl and α-(1,4)-linked galacturonosyl residues and dimeric β-(1,4)-linked galactan side chains which were substituted to O-4 of half of the rhamnosyl residues (Tomada et al. 1980).

Despite these common structural similarities, sugar molar ratios and variability in the HG and rhamnogalacturonan-I domains revealed a range of backbone structures (Kpodo et al. 2017).

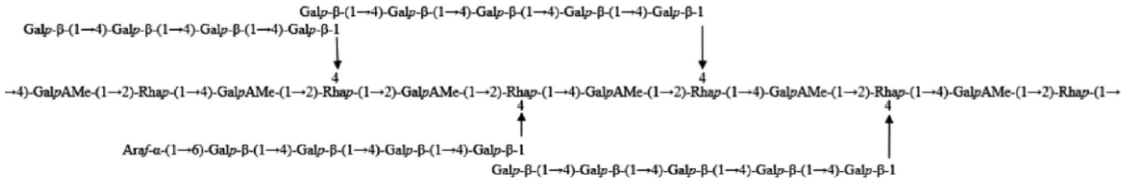

Fig. 1.6 Putative structure of okra polysaccharide rhamnogalacturonan (Liu et al. 2018)

1.2.5 Self-assembly of okra mucilage

Self-assembly is a process in which a disordered system of pre-existing components forms an organized structure or pattern due to specific local interactions between the components themselves, without an external orientation.

Historical reports showed that okra proteins would form a continuous meshwork-like microstructure by self-assembly in aqueous solution, and pure okra proteins in aqueous solution always remained in the liquid state, showing an elasticity performance during the heating-cooling cycle (Chen et al. 2019). The structures are assemblies of a substantial number of individual macromolecules, largely dependent on their thermal history. Hexameric structures were shown as a typical structure of okra mucilage in aqueous systems (Lousinian et al. 2017).

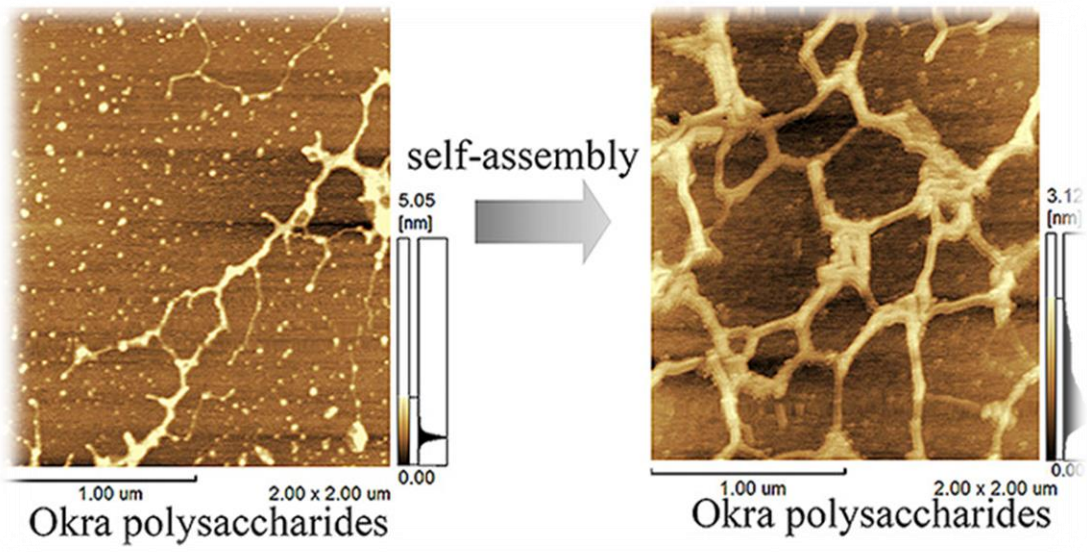

Fig. 1.7 Self-assembly structure of okra mucilage (Chen et al. 2019)

1.3 Application of okra

1.3.1 Food industry

Okra pods were found to be a good source of vital nutrients like crude protein, crude fiber, crude ash, calcium, and iron. Specifically, some okra pod contained significantly higher amounts of crude protein, total ash, crude fat, gross energy, calcium, iron, and zinc than all other accessions and can be recommended as a remedy to alleviate malnutrition in the country (Gemede et al. 2016a) (Gemede et al. 2016b).

In the food industry, the okra water-soluble polysaccharide could be successfully incorporated to control desirable ice cream quality and to retard ice crystal growth during storage. 0.15% okra water-soluble polysaccharide could be used to stabilize ice cream without affecting its sensory perception (Yuennan et al. 2014). Moreover, okra extract has influenced the investigated properties of the starches, either by indirectly controlling water movement or by interacting with amylose as indicated by starch-gel setback outcome (Alamri et al. 2012) (Alamri et al. 2013). Batters prepared by blending alkaline soluble okra gum extract presented higher densities and viscous properties (Qasem et al. 2017). In the presence of okra gum, bread loaf volume was lower, the color was darker, and higher okra increased bread firmness (Alamri 2014).

1.3.2 Industry

On the other hand, for it is inexpensive, easy, eco-friendly and available biodegradable, the okra bast fiber has industrial uses. A bio-flocculant can be successfully extracted from okra using water as a solvent. The bio-flocculant could be used without pH adjustment or addition of a coagulant and exhibited high removal of suspended solids and turbidity and water recovery. And the sludge dewatering performance was verified to be comparable to commercial flocculants (Siah et al. 2015) (Freitas et al. 2015) (Anastasakis et al. 2009).

Okra extract can also be the reinforcement of polymer composites and has a nice prospect to be bio-drag reducer (Coelho et al. 2016).

1.3.3 Pharmacology

Not only because okra extract is non-irritability and biocompatible nature with biological tissues (Kaur et al. 2014), and toxicity against human cells are not expected (Messing et al. 2014). But also, okra extract can be successfully employed to create modified release formulations (Zaharuddin et al. 2014) (Akram et al. 2018) (Ghori et al. 2014). Besides, okra reduced the gastric injuries, lipid peroxidation, ulcerated area, edema, hemorrhage, cell infiltration, epithelial cell loss, and improved antioxidant defense systems (Zafer et al. 2018). Such a property could be exploited in delivering emulsified hydrophobic drugs or nutrients through the acidic environment of the stomach (Ghori et al. 2014). Okra extracts can be strong candidates for emulsification in acidic environments (Alba et al. 2013). Thus, okra polymer can be used as a promising biomaterial for controlled drug delivery.

1.3.4 Biomedical applications

Okra contains rich sources of polysaccharides which could be isolated and further screened for different kinds of biological activities, based on their potential therapeutic applications (Archana et al. 2013).

Okra extract was found to have a hepatoprotective effect (Alqasoumi 2012) (Saravanan et al. 2013). Okra raw and fractionated polysaccharide showed strong bile acid binding capacity (okra > beets > asparagus > eggplant = turnips = beans green = carrots = cauliflower) among the vegetable from our daily life. Thus it may contribute to the hypolipidemic activity, that will prove okra will have potential application in the management of hyperlipidemia and its associated metabolic disorders (H. et al. 2014) (Jenkins et al. 2005).

Okra polysaccharides treatment reduced body weight, lowered serum total cholesterol and low-density lipoprotein cholesterol levels and improved glucose tolerance and insulin sensitivity. Some research shows that okra's peel and seed possess blood glucose normalization and lipid profiles lowering action in diabetic condition (Panneerselvam et al. 2011) (Liu et al. 2018) (Karim et al. 2014) (Huang et al. 2017). Besides its hypoglycemic action, the antioxidant activity of okra may contribute to improved metabolic disorders in high-fat-diet-induced (Zhang et al. 2018) (Mishra et al. 2016) (Majd et al. 2018). Moreover, okra, being non-toxic in nature, this fruit can be easily tried for human trials rather than animal models. Okra based anti-diabetic food, antioxidant-rich food formulation can be thus easily be tried avoiding complicated medical trials (Roy et al. 2014).

A water-soluble polysaccharide mainly composed of galactose and rhamnose from okra promote the phagocytosis, because of production of some kinds of cytokines (Zheng et al. 2014). Okra polysaccharides have a similar stimulatory as carbohydrate polymers activate the innate immune system by interacting with dendritic cells, which are professional antigen-presenting cells that provide an important bridge between innate and adaptive immunity (Sheu & Lai 2012). The polysaccharides of okra especially the high dosage of the polysaccharides showed the most powerful restoration ability of kidney yang deficiency and the ability to relieve physical fatigue (Li et al. 2016) (Xia et al. 2015).

Not only for industrial uses, okra as natural polymeric additives also can be utilized as drag reducing additives in enhancing the blood flow in semi-clogged bloodstreams which can be an alternative treatment for atherosclerosis (Ling & Abdulbari 2017).

1.4 Previous research on okra mucilage's rheological property

Because extraction protocols affected the molecular parameters as well as rheological properties of isolates (Kontogiorgos et al. 2012). Two substances were found. One is the hot buffer soluble solids and the other is chelating agent soluble solids. Oscillation rheological measurements have shown that concentrated hot buffer soluble solids solutions are mainly elastic, while chelating agent soluble solids ones are primarily viscous. The okra chelating agent soluble solids pectin solutions in water have a lower viscosity than hot buffer soluble solids solutions at the same concentration, and also show shear thinning behavior (Sengkhamparn et al. 2010). Upon addition in polyoxyethylene sorbitan monolaurate-stabilized emulsions, hot buffer soluble solids caused flocculation and enhanced creaming at low concentrations (0.125%), while at higher concentrations (1.25%-2.50%) it drastically reduced creaming due to its increase of the continuous phase viscosity. While, chelating agent soluble solids induced flocculation, shear-thinning rheology, and rapid creaming at concentrations above 0.5% (Georgiadis et al. 2011).

From the other different extract method, the crude rude okra polysaccharides (extraction of the powdered okra by deionized water) and refined okra polysaccharides (crude okra polysaccharides were further treated by enzymolysis, precipitation, and dialysis) have different compositions, molecular weight distributions, and rheological properties. Both them showed a shear thinning behavior with increasing shear rates at a concentration of 4%. The refined okra polysaccharides behaved more solid-like as a viscous liquid at higher concentrations (>2%) (Xu et al. 2017).

Okra pectin solutions (>1.0% w/w) showed high viscosity and shear-thinning behavior. A predominantly viscous response(G'< G'') for the okra pectin (in the frequency range of 0.1–10 Hz)was observed. The variation and crossover of G' and G'' values were observed at the highest frequencies for the concentrations tested, demonstrating the weak gel behavior of okra pectin (Chen et al. 2014). Moreover, the okra mucilage represented the transition from the shear thinning to the plateau zone approximately at the low shear rate of 10^{-1}. In the small amplitude oscillatory flow, the okra mucilage obeyed Cox-Merz rule approximately. And the mucilage showed very high extensional viscosity, which was two or three orders of magnitude higher than the shear viscosity (Rheology et al. 2017).

The relationship between okra extract and PH value was also investigated. Okra extracts exhibit high shear viscosity, especially at pH 7 as compared to pH 4, while they show a concentration-dependent self-association pattern. Their character is predominantly elastic throughout the shear frequencies tested. The viscosities are lower at pH 4 due to the aggregation of polymers into fewer, larger, entities. Macromolecular interactions manifest as shear and extensional elasticity. The extensional viscosities are found to be much higher than the respective shear viscosities. The relative contribution of the extensional viscosity is always far greater than the shear one, although the relative importance of the shear interactions increases as the packing of the macromolecular components increases (Yuan et al. 2018a) (Yuan et al. 2018b).

The most charming property of okra mucilage is its structure's self-assembly. This property highly depends on its thermal history and concentration. The power-law exponent for okra in

water decreases as the polymer concentration increases, showing that the solution becomes more shear thinning as polymer concentration increases (Meister et al. 1983). Different rheological approaches agree that specific interactions among polymeric chains influence the rheological behavior of the extracts and are highly dependent on concentration (Kontogiorgos et al. 2012). A possible explanation is that the polysaccharide has a strong tendency to self-association, with the extent of aggregation increasing with increasing concentration. The initial effect of intermolecular association is to form compact 'bundles' with. At higher concentrations, the 'bundles' associate further into larger assemblies with greater overall flexibility (Ndjouenkeu et al. 1996).

1.5 Controlled group

1.5.1 Jute mucilage

Jute (Fig. 1.8) is a long, soft, shiny vegetable fiber that can be spun into coarse, strong threads.

The polysaccharide of its water-leaves mucilage was rich in uronic acid (65%), and consisted of rhamnose, glucose, galacturonic acid, and glucuronic acid in a molar ratio of 1.0: 0.2: 0.2: 0.9: 1.7, in addition to 3.7% of the acetyl group (Ohtani et al. 1995).

Meanwhile, okra contained an acidic polysaccharide which consisted of galactose, rhamnose, and galacturonic acid as the main sugars. Comparing with the components of jute leaves and their common point on fiber carrier, the jute leaves was considered to be a nice contrast with the okra mucilage. Thus, it would be investigated, too.

Fig. 1.8 Jute plant from the local market

1.5.2 PEO solution

Polyethylene glycol (PEG) is a polyether. PEG is also known as polyethylene oxide (PEO) or polyoxyethylene (POE), depending on its molecular weight.

PEO powders are soluble in water. On the rheological properties, the PEO as a polymer was also investigated. Its behavior as both Newtonian and non-Newtonian depend on its concentration. Its behavior could be related to the formation of a three-dimensional network. At the highest polymer concentrations, the local polymer-polymer interactions are the main factor responsible for the rheological behavior of the PEO solutions.

The okra mucilage are formed by the biopolymers. Thus, the PEO15 (Fig. 1.10) powders were selected as an artificial and chemical polymers' control group to be modified a viscous solution, in order to investigate the effect caused by the shear history.

Fig. 1.10 PEO15 powders

1.6 Objective:

In summary, okra is a very promising plant, especially for medical applications. Because it has a significant effect on liver protection and blood sugar lowering. However, these are all from the direction of biochemistry. And it has not been studied from the aspects of fluid's rheological property. Moreover, if the polysaccharides of okra are to be used in biological organisms, the simulation of complex fluids such as the interaction between okra and soft tissue, or okra mucilage flow with blood in micro channels of organisms cannot be ignored. To achieve these experiments, the research and analysis on the rheology view of okra polysaccharide are fundamental at all.

Thus, the rheological study of okra polysaccharide mucilage has also begun gradually from other researchers. Okra mucilage is mainly characterized by its extensional viscosity much higher than its shear viscosity. Meanwhile, its liquid structure is a self-assembled form. It combines with hydrogen bonds from the interaction together with water. The accepted rheological view of okra mucilage is that it is a shear-thinning fluid. And when the shear rate reaches a certain value, it will come to a stable value. On the other hand, the okra mucilage has a certain relationship with the pH value and so on.

But, there is no mention of the effect of shear history on the viscosity of okra mucilage, yet. Besides, the effect of shear history on some mucus does exist. Whether the centrifuge is used during the preparation of liquids, or when the liquid was be cycling in a narrow tube, or the liquid is under a long-term flowing. These will all affect the structures of complex fluids. Irreversible or partial microstructure changes may occur in systems. It would have the influence on fluid's applications.

To get a more thoughtful preparation method of okra mucilage, and to understand the rheological characteristics of the okra polysaccharide mucilage flowing throughout a narrow tube (in order to better investigate the flowing situation if it is pumped into the liver in future), this topic 'Research on shear history effect of okra mucilage's viscosity' was chosen to be studied and investigated.

III. Theory

2.1 Viscosity (Viscosity. 2015. Ideal Fluid. . 1–22)

The viscosity of a fluid is a measure of its resistance to gradual deformation of shear or tensile stress. Viscosity is a property of a fluid that resists relative motion between two surfaces of a fluid moving at different speeds. At the same time, the shear viscosity means that adjacent layers move at different speeds, and as a result, there is frictional resistance which causes energy dissipation due to shearing.

2.1.1 Newton's law of viscosity

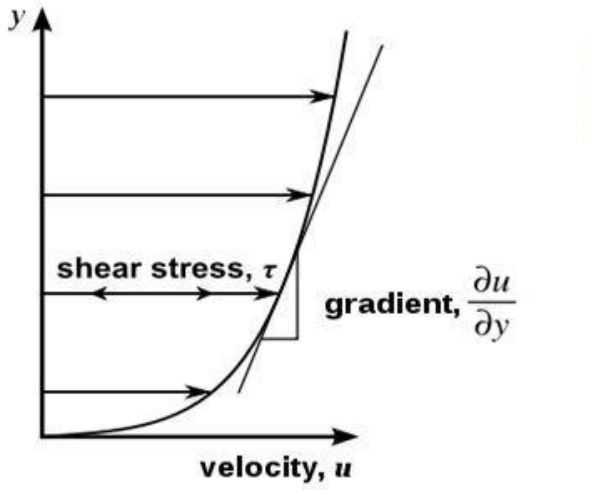

Fig. 2.1 Couette flow (Viscosity. 2015. Ideal Fluid. . 1–22)

The viscosity of a fluid expresses its resistance to shearing flows, in which adjacent fluid layers are in relative motion. A simple example of such a shearing flow is a planar Couette flow (Fig. 2.1), where a fluid is trapped between two infinitely large plates, one fixed and one in parallel motion at constant speed u.

$$\boldsymbol{\tau = \mu \frac{du}{dy}} \qquad \textbf{(1)}$$

Where:

τ is the shear stress, with units of Pa;

μ is the viscosity, with units of Pa · s;

$\frac{du}{dy}$ is the local shear velocity, with units of s^{-1}.

The viscosity μ is sometimes also referred to as the shear viscosity.

2.1.2 Apparent viscosity

Apparent viscosity is the shear stress applied to a fluid divided by the shear rate.

$$\boldsymbol{\eta = \frac{\tau}{\dot{\gamma}}} \quad \textbf{(2)}$$

Where:

τ is the shear stress, with units of Pa;

η is the viscosity, with units of $Pa \cdot s$;

$\dot{\gamma}$ is the shear rate, with units of s^{-1}.

2.2 Non-Newtonian fluid behavior (Chhabra, R.P., 2010)

2.2.1 Normal stress difference

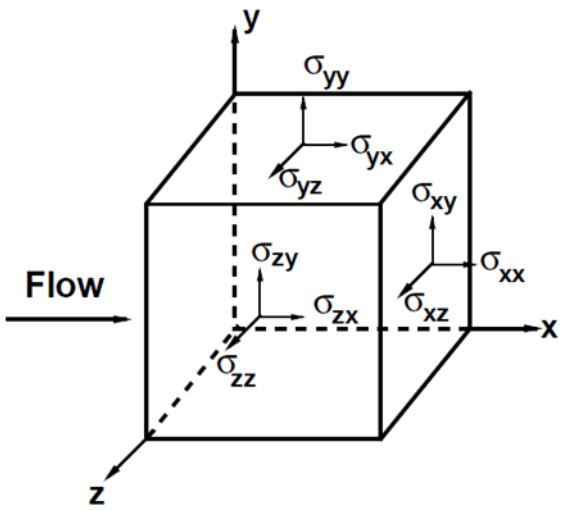

Fig. 2.2 Normal stresses of flowing micro-particle (Chhabra, R.P., 2010)

For an incompressible material, normal stress by itself has no rheological significance, since if the normal stresses are the same in all directions, i.e. the stress is isotropic, there will be no deformation. Only normal stress differences can cause deformation, for example stretching and compression. There are two, independent, normal stress differences, and these are called the first and second normal stress differences. These, along with the viscosity, are functions of shear rate and are called the viscometric functions.

$$\eta(\dot{\gamma}) \equiv \frac{\sigma}{\dot{\gamma}} \quad \textbf{(3)}$$

Primary normal stress difference, $N_1 \equiv \sigma_{xx} - \sigma_{yy}$ **(4)**

Secondary normal stress difference, $N_2 \equiv \sigma_{zz} - \sigma_{yy}$ **(5)**

For any viscometric flow, the three viscometric functions completely describe the rheological behavior of a fluid. In other words, these constitute all the rheological information that can be obtained from measuring the stress components.

2.2.2 Different types of Non-Newtonian fluid

Most commonly, the viscosity of non-Newtonian fluids is dependent on shear rate or shear rate history. Some non-Newtonian fluids with shear-independent viscosity, however, still exhibit normal stress-differences or other non-Newtonian behavior.

In a Newtonian fluid, the relation between the shear stress and the shear rate is linear, passing through the origin, the constant of proportionality being the coefficient of viscosity. In a non-Newtonian fluid, the relation between the shear stress and the shear rate is different. The fluid

can even exhibit time-dependent viscosity. Therefore, a constant coefficient of viscosity cannot be defined.

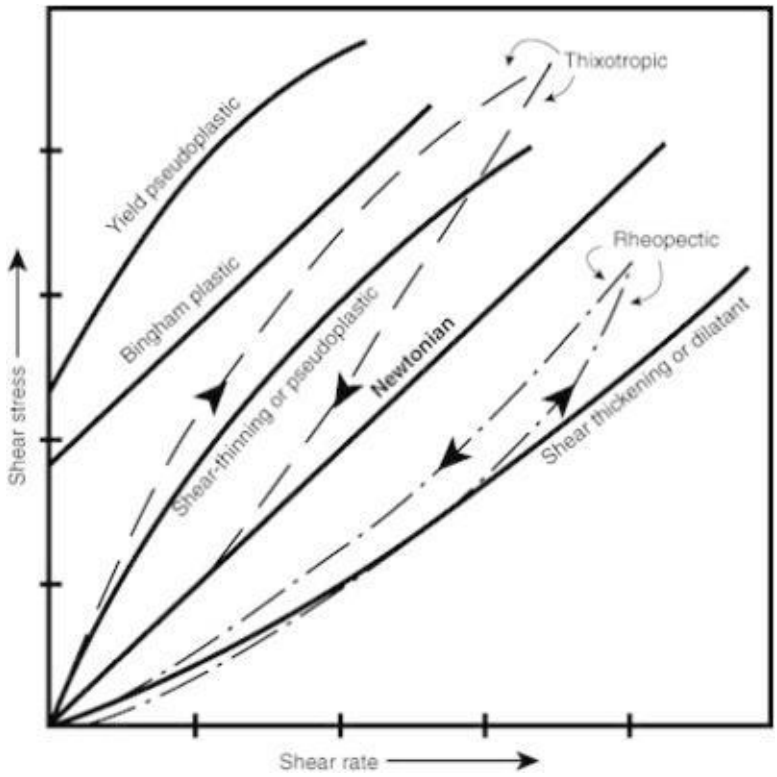

Fig. 2.3 Different types of fluid (Chhabra, R.P., 2010)

Shear thickening fluid: The viscosity of a shear thickening fluid, or dilatant fluid, appears to increase when the shear rate increases.

Shear thinning fluid: On the opposite, there is a shear thinning fluid, or pseudo plastic fluid. The viscosity of a shear thinning fluid appears to decrease when the shear rate increases.

Bingham plastic: Fluids that have a linear shear stress/shear strain relationship require finite yield stress before they begin to flow.

Rheopectic or Thixotropic: There are also fluids whose strain rate is a function of time. Fluids that require a gradually increasing shear stress to maintain a constant strain rate are referred to as rheopectic. An opposite case of this is a fluid that thins out with time and requires decreasing stress to maintain a constant strain rate (thixotropic).

2.2.3 Microstructure and non-Newtonian

There is a direct link between the type and extent of non-Newtonian fluid behavior and the influence of the externally applied stress on the state of the structure (Fig. 2.4).

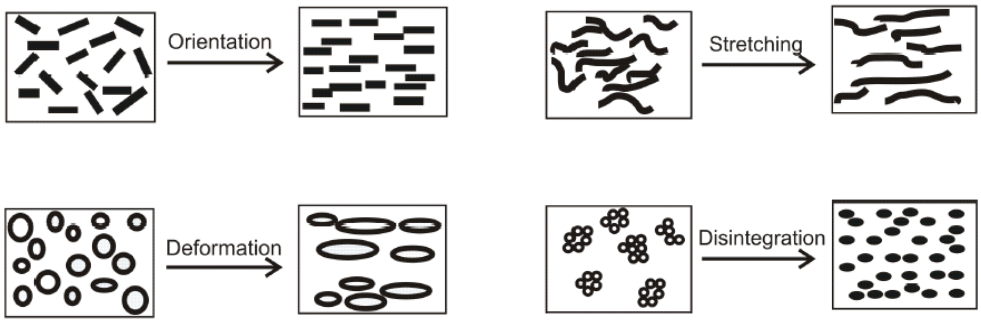

Fig. 2.4 Different ways of structure changing for complex fluid (Chhabra, R.P., 2010)

2.2.4 Master Curve (Yuan et al. 2018a)

The rheological behavior of viscoelastic materials varies with both solvent and shear rate. Normalization of flow curves by the viscosity of the solvent at an arbitrary experimental shear rate nullifies the effect of these two variables (shear rate and solvent viscosity) on the data.

Thus, allowing the underlying effect of polysaccharides on viscosity to be studied:

$$\frac{(\eta-\eta s)}{\eta 0-\eta s} = f(\frac{\dot{\gamma}}{\dot{\gamma}_{\frac{1}{2}}}) \quad (6)$$

Where:

η is the viscosity of the omplex fluid,

η_s is the viscosity of the solvent,

η_0 is the initial viscosity of the complex fluid,

$\dot{\gamma}_{\frac{1}{2}}$ is the shear rate where viscosity equal to half of the max viscosity.

2.2.5 Changed viscosity index

To describe the large difference after shear history effect, a factor, changed viscosity index was induced.

$$\eta_c = \frac{\overline{\eta(\dot{\gamma})}-\overline{\eta_{Ps}(\dot{\gamma})}}{\overline{\eta(\dot{\gamma})}} \quad (7)$$

Where:

η_c is the changed viscosity index,

$\overline{\eta(\dot{\gamma})}$ is the no shear history effect average viscosity at plateau zone,

$\overline{\eta_{Ps}(\dot{\gamma})}$ is the average viscosity at plateau zone of a pre-sheared mucilage.

The higher the value of the changed viscosity index, the system would be affected by shear history much more deeply.

2.3 Shear-Thinning fluid (Chhabra, R.P., 2010)

2.3.1 Shear-Thinning Fluids behavior

This is perhaps the most widely encountered type of time-independent non-Newtonian fluid behavior in engineering practice.

It is characterized by an apparent viscosity η which gradually decreases with increasing shear rate.

$$\lim_{\dot{\gamma}\to 0} \frac{\tau}{\dot{\gamma}} = \eta_0 \, , \lim_{\dot{\gamma}\to \infty} \frac{\tau}{\dot{\gamma}} = \eta_\infty \quad (8)$$

$$\eta_0 > \eta_\infty \quad (9)$$

Where:

η_0 is the zero shear viscosity,

η_∞ is the infinite shear viscosity.

2.3.2 Power Law or Ostwald de Waele Equation

Often the relationship between shear stress − shear rate plotted on log-log coordinates for a shear-thinning fluid can be approximated by a straight line over an interval of shear rate.

$$\tau = K(\dot{\gamma})^n \quad (10)$$

Where:

K is the flow consistency index (SI units Pas^n),

n is the flow behavior index (dimensionless)

2.3.3 The Cross viscosity equation

A cross fluid is a type of fluid whose viscosity depends upon shear rate according to the following equation:

$$\eta = \eta_\infty + \frac{\eta_0 - \eta_\infty}{1+(C\dot{\gamma})^m} \quad (11)$$

Where:

η_0 is the zero shear viscosity,

η_∞ is the infinite shear viscosity.

m is known as the rate constant.

c is known as the cross time constant and has dimensions of time.

2.4 Time Dependent Behavior (Chhabra, R.P., 2010)

Many substances, notably in food, pharmaceutical and personal care product manufacturing sectors display flow characteristics which cannot be described by a simple mathematical expression. This is so because their apparent viscosities are not only functions of the applied shear stress or the shear rate, but also of the duration for which the fluid has been subjected to shearing as well as their previous kinematic history. For instance, the way the sample is loaded into a viscometer, by pouring or by injecting using a syringe, etc. influences the resulting values of shear stress or shear rate.

Depending upon the response of a material to shear over a period of time, it is customary to sub-divide time-dependent fluid behavior into two types, namely, thixotropy and rheopexy (or negative thixotropy).

2.4.1 Thixotropic Behavior

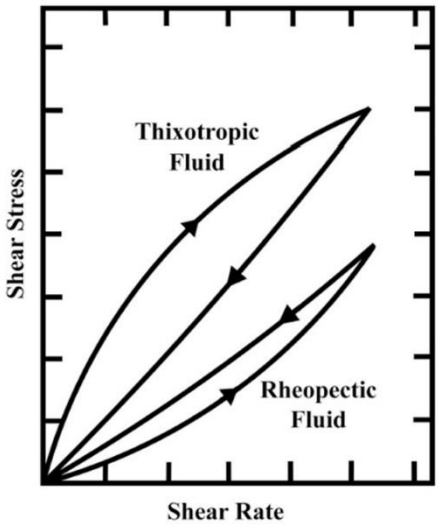

Fig. 2.5 Thixotropic and rheopectic fluid (Chhabra, R.P., 2010)

Thixotropy is a time-dependent shear thinning property. Certain gels or fluids that are thick, or viscous, under static conditions will flow (become thin, less viscous) over time when shaken, agitated, sheared or otherwise stressed (time dependent viscosity). They then take a fixed time to return to a more viscous state.

Some non-Newtonian pseudo plastic fluids show a time-dependent change in viscosity; the longer the fluid undergoes shear stress, the lower its viscosity. A thixotropic fluid is a fluid which takes a finite time to attain equilibrium viscosity when introduced to a steep change in shear rate.

Some thixotropic fluids return to a gel state almost instantly, such as ketchup, and are called pseudo plastic fluids. Others such as yogurt take much longer and can become nearly solid. Many gels and colloids are thixotropic materials, exhibiting a stable form at rest but becoming fluid when agitated. Thixotropy arises because particles or structured solutes require time to organize.

The quantification of thixotropy was accomplished through specific descriptors as thixotropic area, thixotropic index (Ghica et al. 2016).

2.4.2 Thixotropic area (Ghica et al. 2016)

Thixotropy area (hysteresis loop area, S_{thix}) is the surface between the forward curve (S_{fwd}) and the backward curve (S_{bw})

$$\boldsymbol{S_{thix} = S_{fwd} - S_{bw}} \quad \textbf{(12)}$$

Where:

S_{thix} is the thixotropic area;

S_{fwd} is the area of forward curve;

S_{bw} is the area of backward curve.

The hysteresis area value is an indicator for the degree of system destructuration, higher values for thixotropic area indicating a higher thixotropy.

2.4.3 Thixotropic index (Ghica et al. 2016)

$S_{thix\%}$ is the thixotropy index, is the relative thixotropy area, expressed as a percentage of the area rheodestroyed by stirring at maximum rotational speed, compared to the backward area:

$$\boldsymbol{T_{hyst}\%} = \left[\frac{(\boldsymbol{S_{fwd} - S_{bw}(t)})}{\boldsymbol{S_{fwd}}}\right] * \mathbf{100}\% \quad \textbf{(13)}$$

Where:

$S_{thix\%}$ is the thixotropy index;

T is the stirring time.

The higher the value of the thixotropy index, the system becomes more thixotropic.

2.4.4 Indirect microstructural theories (Armstrong et al.)

Most workers in this area have developed mathematical theories of thixotropy based on the numerical scalar measure of structure, often designated by λ. The thixotropy is usually introduced via the time derivative of the structure parameter, dλ/dt, which is given by the sum of the buildup and breakdown terms, which, in the simplest theories, are only controlled by the shear rate and the current level of structure λ.

$$\frac{\mathbf{d\lambda}}{\mathbf{dt}} = \mathbf{g}(\dot{\boldsymbol{\gamma}}, \boldsymbol{\lambda}) = \mathbf{a}(\mathbf{1} - \boldsymbol{\lambda})^{\mathbf{b}} - \mathbf{c}\boldsymbol{\lambda}\dot{\boldsymbol{\gamma}}^{\mathbf{d}} \quad \textbf{(14)}$$

Where:

a,b,c,d are constants for any one system.

If the value of dλ/dt is negative, the system is breaking down towards equilibrium; if it is positive, it is building up towards equilibrium. At equilibrium, for every value of $\dot{\gamma}$ there is a particular value of λ which in this equation is found by setting dλ/dt to zero.

The relationship between viscosity and structure is given by

$$\boldsymbol{K = 1 - \left(\frac{\mu_\infty}{\mu_0}\right)^{0.5}} \quad \textbf{(15)}$$

$$\boldsymbol{\lambda = (1 - \left(\frac{\mu_\infty}{\mu}\right)^{0.5})/K} \quad \textbf{(16)}$$

Where:

η is the current value of viscosity,

λ is the structure parameter,

K is a kinetic constant with units of inverse time.

2.5 Visco-elastic behavior (Schets & De Man 2017)

2.5.1 Viscoelasticity

Viscoelasticity is the property of materials that exhibit both viscous and elastic characteristics when undergoing deformation.

Viscous materials resist shear flow and strain linearly with time when a stress is applied.

Elastic materials strain when stretched and immediately return to their original state once the stress is removed.

Viscoelastic materials have elements of both of these properties and, as such, exhibit time-dependent strain. Whereas elasticity is usually the result of bond stretching along crystallographic planes in an ordered solid, viscosity is the result of the diffusion of atoms or molecules inside an amorphous material.

2.5.2 Elastic characteristics

Elasticity is a material property that generates recovering force at an application of an external force to deform the material. When an external force is applied to a material and the material is in an equilibrium deformation, the external force is balanced by an inner force. The inner force is the recovering force. For deformation:

$$\boldsymbol{\varepsilon = \frac{L - L_0}{L_0}} \quad \textbf{(17)}$$

Where

ε is the strain of the subject;

L is the final length a subject;

L_0 is the initial length of a subject.

For small strains, a Hookean relation,

$$\boldsymbol{\sigma \propto \varepsilon} \quad \textbf{(18)}$$

The proportionality factor is defined as a modulus and the modulus is a material's constant. If the material was deformed by a tensile force, the modulus is defined as Young's modulus. If the Deformed was caused by a shear force, the modulus is the shear modulus.

$$\boldsymbol{\sigma = E\varepsilon} \quad \textbf{(19)}$$

$$\boldsymbol{\sigma = G\varepsilon} \quad \textbf{(20)}$$

Where:

σ is the stress;

E is the Yong's modulus,

G is shear modulus.

After eliminating the external force, the recovering force and the deformation are completely diminished. Elasticity is a property of a material to resist the deformation by the external force.

Fig. 2.6 The beam under elastic deformation

2.5.3 Viscous characteristics

Viscosity is a characteristic nature of a fluid. The shear is generated by an applied force causing the flow and an internal force against the former. The internal force is also transformed into a stress generated in the flow.

$$\sigma \propto \frac{d\gamma}{dt} \quad (21)$$

Where:

γ is the shear strain;

t is the time.

Newton postulated the quantitative relationship between the stress and the shear rate as:

$$\sigma = \eta \frac{d\gamma}{dt} \quad (22)$$

Viscous character is a property of a fluid to resist the force for flow. The fluid described by the equation is classified as Newtonian. After stopping the flow, the fluid maintains its deformation strain at the time of stopping.

2.5.4 Stress relaxation and creep

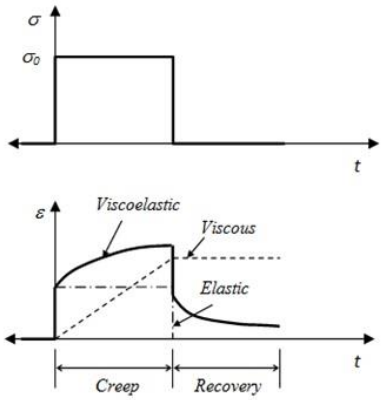

Fig. 2.7 Creep and recovery of complex fluid (Lakes, R.S., 1999)

In materials science, creep is the tendency of a solid material to move slowly or deform permanently under the influence of mechanical stresses. On the other hand, stress relaxation is the observed decrease in stress in response to strain generated in the structure.

The material responds to the stress with a strain that increases until the material ultimately fails, if it is a viscoelastic liquid.

To the linear elastic part,

$$\boldsymbol{\varepsilon = \frac{1}{E}\sigma} \quad \textbf{(23)}$$

To the linear viscous part,

$$\boldsymbol{\varepsilon(t) = \sigma_0 J(t),\ J(t) = \frac{t}{\eta}} \quad \textbf{(24)}$$

Where:

σ_0 is the applied load,

J is the compliance function.

2.6 Oscillatory shear rheology (Chhabra, R.P., 2010)

2.6.1 Oscillatory shear motion

Another common form of motion used to characterize visco-elastic fluids is the so called oscillatory shearing motion. It is useful to consider here the response of a Newtonian fluid and of a Hookean solid to a shear strain which varies sinusoidally with time as:

$$\boldsymbol{\gamma = \gamma_m \sin \omega t} \quad \textbf{(25)}$$

Where:

γ_m *is the amplitude;*

ω *is the angle speed of applied strain;*

t is the time.

For elastic part:

$$\boldsymbol{\sigma = G\gamma = G\gamma_m \sin \omega t} \quad \textbf{(26)}$$

For viscous part:

$$\boldsymbol{\sigma = \eta\dot{\gamma} = \eta\gamma_m \omega \sin\left(\frac{\pi}{2} + \omega t\right)} \quad \textbf{(27)}$$

Thus, there is no phase shift between the shear stress and shear strain in the elastic behavior. On the other hand, the resulting of viscous part, shear stress is out of phase by 90 degree from the applied strain. Thus, the measurement of the phase angle δ which can vary between zero (purely elastic response) and 90 degree (purely viscous response) provides a convenient means of quantifying the level of viscoelasticity of a substance.

2.6.2 Complex viscosity

For the linear visco-elastic region, one can define the complex viscosity η* as follows:

$$\boldsymbol{\eta^* = \eta' + i\eta''} \quad \textbf{(28)}$$

Where:

η^* is the complex viscosity;

η' is the real part;

η'' is the imaginary part.

2.6.3 The storage and loss moduli

The storage and loss modulus in viscoelastic materials measure the stored energy, representing the elastic portion, and the energy dissipated as heat, representing the viscous portion.

The storage: $\boldsymbol{G' = \frac{\sigma_m}{\gamma_m} \cos \delta}$ **(29)**

$$\text{The loss: } \boldsymbol{G'' = \frac{\sigma_m}{\gamma_m} \sin \delta} \quad \textbf{(30)}$$

Where:

σ_m is the amplitude;

G' is the storage moduli;

G'' is the loss moduli.

$$\textbf{In shear: } \boldsymbol{\tan \delta = \frac{G''}{G'}} \quad \textbf{(31)}$$

The ratio between the loss and storage modulus in a viscoelastic material is defined as the tanδ, which provides a measure of damping in the material. tanδ can also be visualized in vector space as the tangent of the phase angle δ between the storage and loss modulus.

2.6.4 The Cox-Merz rule (Principles et al.)

For many materials, linear data G' and G" is relatively easy to measure for various angular frequencies ω(rad/s). When applicable, the shear viscosity can be estimated by applying the Cox-Merz empirical rule. This empirical rule states that the modulus of the complex viscosity matches the nonlinear shear viscosity, as shown in the following equation.

$$\boldsymbol{\eta(\gamma)=\eta^*(\omega) \quad \& \quad N1=2G'} \quad \textbf{(32)}$$

Where:

η(γ) is the steady viscosity,

η*(ω) is complex viscosity,

N1 is the first normal stress difference,

G' is the storage moduli.

It is important in the application of the rule to ensure that the appropriate values for η(γ) and η*(ω) are used. For example, in both cases it is the steady state values which are required, i.e. any transient effects due to flow or oscillation start-up, inertia, or thixotropy must have fully decayed.

2.7 Shear history effect

2.7.1 Hagen–Poiseuille equation (PFITZNER 1976)

In nonideal fluid dynamics, the Hagen–Poiseuille equation is a physical law that gives the pressure drop in an incompressible and Newtonian fluid in laminar flow flowing through a long cylindrical pipe of constant cross section. It can be successfully applied to the flow through a drinking straw or through a hypodermic needle.

$$\Delta \boldsymbol{P} = \frac{\boldsymbol{8\mu LQ}}{\boldsymbol{\pi R^4}} \quad \textbf{(33)}$$

Where:

ΔP is the pressure difference between the two ends,

L is the length of pipe,

μ is the dynamic viscosity,

Q is the volumetric flow rate,

R is the pipe radius.

2.7.2 Momentum analysis of flow systems (Systems)

Next to mass and energy, momentum is an important quantity in fluid mechanics. Momentum is mass times velocity. Since velocity is a vector quantity, momentum also is a vector quantity. A momentum balance therefore is a vector equation. However, in many cases in this course we will only consider momentum is one specific direction, and one component of the momentum balance.

For steady flow with one inlet and one outlet:

$$\sum \vec{\boldsymbol{F}} = \dot{\boldsymbol{m}}(\boldsymbol{\beta_2}\vec{\boldsymbol{V}}_{\boldsymbol{2}} - \boldsymbol{\beta_1}\vec{\boldsymbol{V}}_{\boldsymbol{1}}) \quad \textbf{(34)}$$

Where:

$\dot{m}$ is the mass flow rate,

β is the momentum-flux correction factor,

V is the velocity.

2.7.3 Hagen-Poiseuille (laminar Flow) for Power Law Fluid

For momentum balance:

$$\boldsymbol{p_1 S_1 - p_2 S_2 - F_w - F_g = \dot{m}(\beta_2 \vec{V}_2 - \beta_1 \vec{V}_1)}$$
$$\boldsymbol{2\pi r L \tau_{rz} = \pi r^2 (\Delta p)}$$

Thus:

$$\boldsymbol{2\frac{L}{r}\tau_{rz} = \Delta p}$$

For the power law fluid:

$$\boldsymbol{\tau_{rz} = K\left(\frac{du_z}{dr}\right)^n}$$

Combine these two equation:

$$\boldsymbol{\frac{du_z}{dr} = \left(\frac{1}{2}\frac{\Delta p}{KL}\right)^{\frac{1}{n}} r^{\frac{1}{n}}}$$

According to the boundary condition:

$$\boldsymbol{r = R, u_z = 0}$$

Thus, velocity profile of power law fluid circular conduit is:

$$\boldsymbol{u_z = \left(-\frac{1}{2}\frac{\Delta p}{KL}\right)^{\frac{1}{n}}\left(\frac{n}{n+1}\right)\left(R^{\frac{n+1}{n}} - r^{\frac{n+1}{n}}\right)}$$

For the bulk average velocity:

$$\boldsymbol{\bar{V} = \frac{1}{S}\int u dS = \frac{1}{\pi R^2}\int (2\pi r u_z) dr}$$

$$\boldsymbol{\bar{V} = \left(-\frac{1}{2}\frac{\Delta p}{KL}\right)^{\frac{1}{n}}\left(\frac{n}{3n+1}\right)R^{\frac{n+1}{n}}}$$

Thus, Hagen-Poiseuille equation for Power Law Fluid:

$$\boldsymbol{\Delta p = -\frac{2^{n+2}\left(\frac{3n+1}{n}\right)^n LK\bar{V}^n}{D^{n+1}}} \quad \textbf{(35)}$$

Where:

$\bar{V}$ is the mean velocity,

D is the diameter of the pipe,

L is the length of the pipe.

K is the power law flow consistency index,

n is the power law flow behavior index.

IV. Method

3.1 Mucilage/solution preparations

3.1.1 Okra mucilage

Fresh okra pods were brought from the local market (Fig. 3.1). The origin will vary from seasons.

Fig. 3.1 Okras from the local market

Fig. 3.2 The qualified okra pods

Okra pods are cleaned by pipe water in order to get rid of the dirt on their skins. Then dry the okra pods at ventilated and dry environment. In addition, in the clean stage, the okra fruits were checked and selected for uniformity of size and color. To ensure that they had no visible wounds and rottenness as well (Fig. 3.2).

After that, the middle part of okra pods were chosen, because the shape of the middle body is regular pentagon and has much more uniform components rather than top and bottom body (Fig. 3.3).

Fig. 3.3 The middle body of okra pods

Fig. 3.4 Okra skins

The okra skins were cut into rectangle through the lines of the pentagon. In order to, remove the seeds and the septa (Fig. 3.4). Because the seeds and septa of okra pods do not contain any mucilage.

In order to let the okra skins have much more active surface area to interact with the solvent, the okra skins would be sliced into 3~5mm in width and 5~6mm in length (Fig. 3.5).

Fig. 3.5 Sliced okra skins

Fig. 3.6 A cup of okra pieces for extracting mucilage

Fig. 3.7 Okra water mixture

Then, the okra pieces would be store in the pure water as weight ratio which was adjusted to 1 okra skin pieces part to 2 pure water parts (Japanese Pharmacopoeia, 500ml) at least. So that the okra skin pieces can be perfectly covered by the pure water (Fig. 3.7). The mixed liquid would be preserved in the refrigerator at 6°C for 12 hours, in order to form enough mucilage and protect the okra skins from the biological oxidative decay.

Then, the insoluble materials would be filtered out from okra mucilage by using a combination of weave mesh (0.56mm, 300μm) from Tokyo Screen CO,. LTD (Fig. 3.8).

Finally, the fresh okra mucilage for experiment would be collected (Fig. 3.9).

Fig. 3.8 Okra mucilage under filtering

Fig. 3.9 Okra mucilage for test

3.1.2 Jute mucilage

As a control group from another plant recourse, jute mucilage was also modulated. Fresh jute plants were brought from the local market (Fig. 3.10). The jute mucilage was modulated almost following the okra mucilage extract steps.

Fig. 3.10 Jute plant from the local market

Different from the okra pods, the mucilage of jute would secret from their leaves. So that, the jute leaves were checked and selected for uniformity of size and color. Ensure that they had no visible wounds and rottenness as well (Fig. 3.11).

Fig. 3.11 Selected jute leaves

Fig. 3.12 Middle part of a jute leave

In order to get enough mucilage, the jute leaves would be sliced into 6~8mm in width and 6~8mm in length (Fig. 3.13).

Fig. 3.13 Sliced jute leaves

Fig. 3.14 A cup of jute leaves for mucilage extract

After, the okra pieces would be store in the pure water as weight ratio which was adjusted to 1 okra skin pieces part to 4 pure water parts. Because the jute leaves pieces to have much more volume comparing with the okra skins pieces. At weight ratio 1 to 2, these leaves would be well immerse in pure water (Fig. 3.15). Then the mixed liquid would be preserved in the refrigerator at 6°C for 12 hours, in order to form enough mucilage and protect the leaves from the oxidative decay, as well.

Then, using a combination of weave mesh to filter the mucilage, in order to get rid of the residues of leaves and other some insoluble maters (Fig. 3.16).

Finally, the fresh jute mucilage for experiment would be collected (Fig. 3.17).

Fig. 3.15 Jute leaves-pure water mixture

Fig. 3.16 Jute mucilage under filtering

Fig. 3.17 Jute mucilage

3.1.3 PEO15-water solution

The polyethylene oxide 15 (PEO15) whose average molecular weight is 3.3*10^6 ~ 3.8*10^6 g/mol was selected and set concentration at 0.15wt% as a chemical control group. Because, at high shear rate, its solution's viscosity is close to the okra (Philippines) mucilage's.

The aqueous solutions of PEO15 were prepared by dissolving the appropriate amount of PEO in the pure water. And stirring it to achieve complete homogenization.

Finally, the PEO15 soultion for experiment would be made (Fig. 3.19).

Fig. 3.18 Polyethylene oxide 15

Fig.3.19 PEO15 0.15wt% solution

3.2 Shear history effect

Shear history effect is designed to be the effect of pre-shearing (rotation/needle) on mucilage before the rheological experiments.

3.2.1 Non-sheared treatment

Samples would be collected from the syringe pump (Fusion 200 Classic from Chemyx Inc.) and syringe (ss-10ESzp, 10ml, from Terumo Corporation) combination (Fig. 3.20).

To normal mucilage (non-sheared treatment):

The syringe pump would push the syringe at a fixed flow rate (1ml/min).

Fig. 3.20 Syringe pump and syringe

3.2.2 Needle pre-sheared treatment

The shear history effect was finished by mucilage flowing through a narrow needle. The needles (27G*3/4", ϕ0.40*L19mm, from Terumo Corporation) were used (Fig. 3.21).

To needle pre-sheared mucilage:

The syringe pump would push the syringe at a fixed flow rate (10ml/min) to achieve the shear history effect on okra mucilage.

Fig. 3.21 Syringe 10ml and needle G27

3.2.3 Rotation pre-sheared treatment

To rotation pre-sheared mucilage:

The mucilage would be rotated on the cone and plate of rheometer (HAAKE Rheostress 600) at shear rate $10s^{-1}$ and $500s^{-1}$ for 8min (Fig. 3.22), then it would be collected as a rotation pre-sheared mucilage.

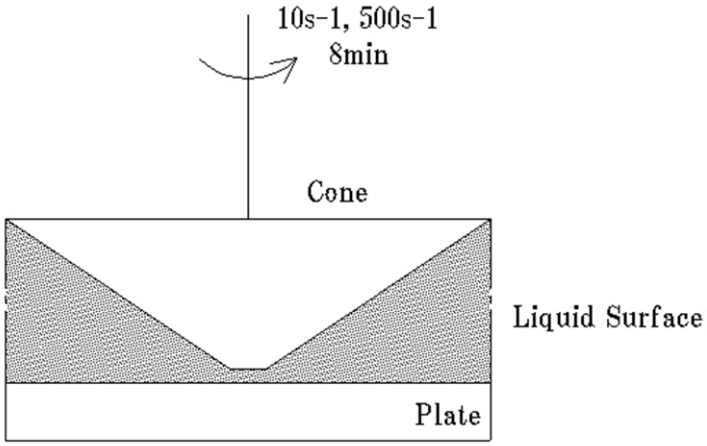

Fig. 3.22 Rotation pre-sheared treatment

3.3 Rheological test equipment

3.3.1 HAAKE Rheostress 600

To do the testes on mucilage and solution's rheological properties, the HAAKE Rheostress 600 (Fig. 3.23) from Thermo Electron Corp was used.

The Thermo Scientific HAAKE RheoStress 600 instrument is compatible with a whole range of sensor systems made from titanium for the rotating part and stainless steel for the stationary part. Aluminum is used for the disposable systems.

Fig. 3.23 HAAKE Rheostress 600

3.3.2 Cone and plate's type

Table. 3.1 Cone and plate sensor system descriptions from the handbook of RS600

Cone and plate sensor system			
Sensor	C60/1	C35/1	C20/1
Application	Low viscosity, less volume, easy wash	Medium viscosity	High viscosity paste, molten material
Example	Ink, polymer solution	Honey, gel	Paste
Sample volume	$1cm^3$	$0.2cm^3$	$0.05cm^3$
Maximum particle size	0.02mm	0.03mm	<0.02mm
Viscosity range	2-10^5mPas	100-10^6mPas	10^3-10^8mPas
Shear rate range	$0.006-9000S^{-1}$	$0.006-9000S^{-1}$	$0.006-9000S^{-1}$

In most of all cases, rheological investigations on polymers were performed using a rheometer with plate/plate or cone/plate measuring geometry.

According to the table from the handbook of HAAKE Rheostress 600, the cone C60/1 Ti (Fig. 3.24), whose diameter is 60mm, the geometry angle is 1°and cone and plate's gap is 0.052mm, was selected. Wet tissues were put surround the plate to maintain the humidity and protect from the mucilage's rapid loss of moisture while all rheological testing, in order to get precise results (Fig. 3.25).

Fig. 3.24 Cone 60/1 Ti

Fig. 3.25 Wet tissues surrounding the plate

3.4 Rheological experiment

3.4.1 Steady shear viscosity (Fig. 3.26)

The best way to measure the measure of a non-Newtonian sample at a constant temperature and known shear rate is to pregame a time test. Since both the measuring instrument and the sample need a finite time to reach constant conditions, in other words until the whole system is in equilibrium, it is necessary to wait a certain time before measured values are obtained that can be evaluated.

Table. 3.2 Shear rate ranges of different samples for experiments

Situation	Shear Rate Range	Examples
Sedimentation of fine powders in liquids	10^-6 to 10^-3	Medicines, Paints, Salad dressing
Leveling due to surface tension	10^-2 to 10^-1	Paints, Printing inks
Draining off surfaces under gravity	10^-1 to 10^1	Toilet bleaches, paints, coatings
Extruders	10^0 to 10^2	Polymers, foods
Chewing and Swallowing	10^1 to 10^2	Foods
Dip coating	10^1 to 10^2	Confectionery, paints
Mixing and stirring	10^1 to 10^3	Liquids manufacturing
Pipe Flow	10^0 to 10^3	Pumping liquids, blood flow
Brushing	10^3 to 10^4	Painting
Rubbing	10^4 to 10^5	Skin creams, lotions
High-speed coating	10^4 to 10^6	Paper manufacture
Spraying	10^5 to 10^6	Atomization, spray drying
Lubrication	10^3 to 10^7	Bearings, engines

Okra mucilage was trying to pump into the liver for future plan. Thus, from the table 3.2, a much more detail at a low shear rate, the shear rate range $0.1S^{-1}$~$1000S^{-1}$ was chosen. The test steps would be 23 during this shear rate. The instrument's waiting time was set at least 5s. And maximum waiting time was 30s. In another word, those whose viscosity's error under 1% in minimal 5s would be recorded. For the values which were always out of 1% error in 5s, the system would let it develop for maximal 30s and pick up the last spot's viscosity as the step's viscosity. Meanwhile the room temperature, 20℃, was selected as the constant temperature, in order to get rid of the influence of temperature on viscosity.

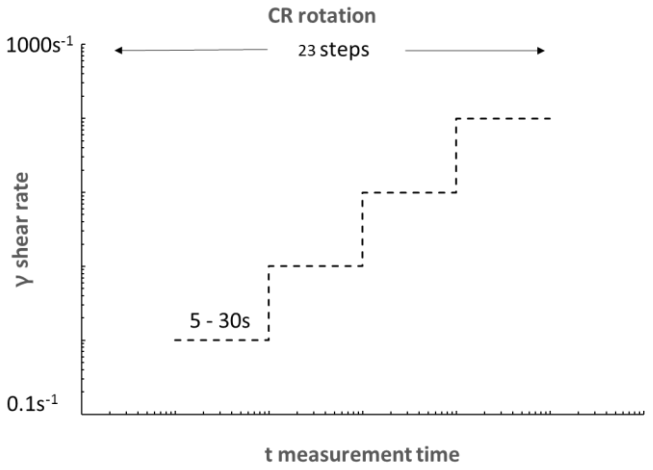

Fig. 3.26 Steady shear viscosity experiment's parameters

3.4.2 Oscillation stress sweep

The oscillation stress sweep is first of all used to determine a material's linear viscoelastic range, which is to say that the measurement parameters are set in this manner that stress and strain amplitude have a linear relationship which can be describe by the following equation:

$$\boldsymbol{\tau_0 = G * \gamma_0} \quad \textbf{(36)}$$

A more practical way to identify the linear viscoelastic range is to look for the region where the material functions. That is to say, I need to find a stress value which is good for all frequencies. Then I will pick this stress value to run a frequency sweep.

3.4.3 Oscillation frequency sweep

The frequency sweep is used to characterize test materials. The sample is not supposed to change its properties throughout the test time.

The stress value I pick needs to be in the linear viscoelastic range. It also needs to create a reasonable deformation. In this stage, 0.1mPa was chosen form the previous linear viscoelastic range test.

Moreover, the start frequency was set at 0.1592Hz, which equals the angle speed 0.1rad/s. On the other hand, the 15.92Hz was set as the end frequency standing for the angle speed 1000rad/s.

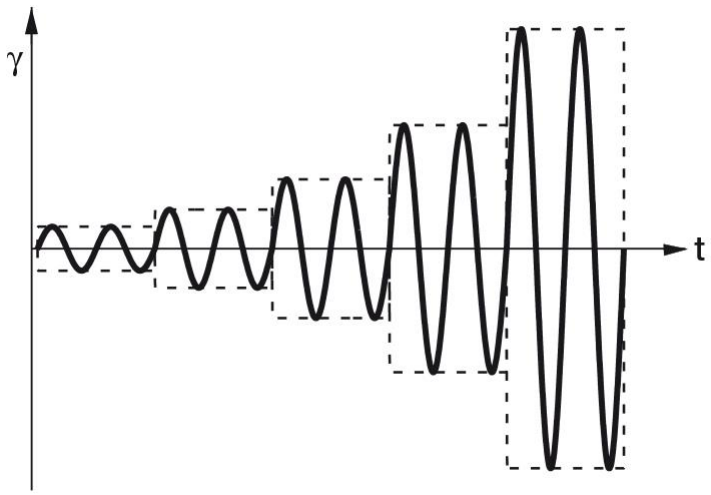

Fig. 3.27 Shear stress amplitude sweep, with controlled shear stress

3.4.4 Creep test (Fig 3.28)

This measurement procedure provides important information regarding the viscoelastic properties of a substance.

Constant shear stress, which 0.001mPa was selected, is applied instantaneously. The resulting deformation is measured as a function of time. The creep time was set at 10s in order to get a fully developed test curve.

An analysis of creep-curve enables the deformation, for example, the zero shear viscosity h_0, the elastic deformation g_{eo} and the steady state compliance $J_{(to)}$.

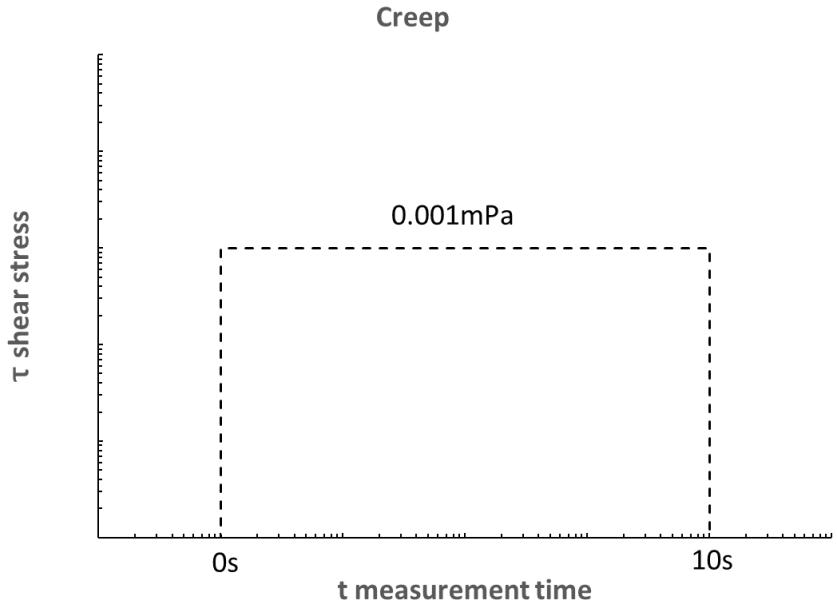

Fig. 3.28 Creep experiment's parameters

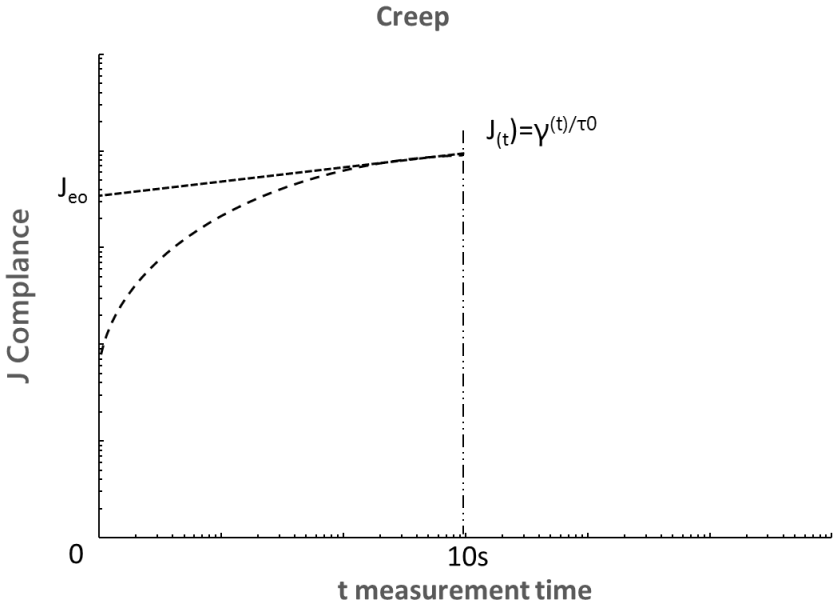

Fig. 3.29 Analysis of creep experiment

3.4.5 Recovery test (Fig 3.30)

Usually, a recovery segment is linked to a creeping segment. The shear stress was set to 0Pas. With this measurement, the recoverable elastic portion of the deformation can be determined. The recovery time was set at the 60s to let okra mucilage have enough time to recover.

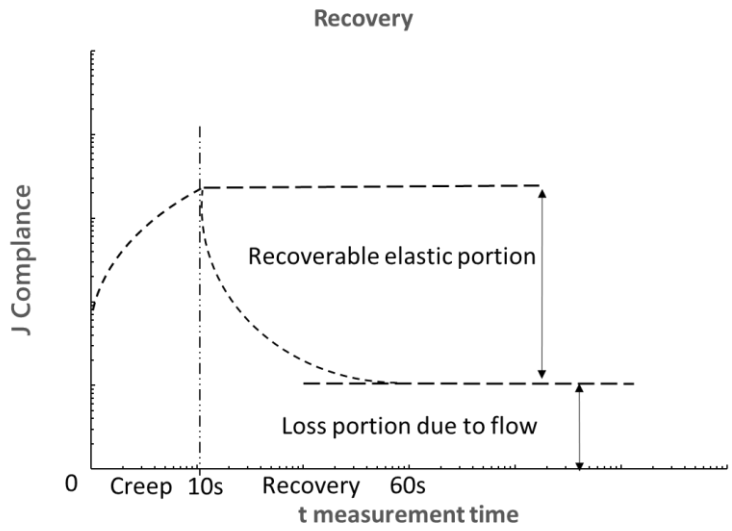

Fig. 3.30 Creep and recovery experiment's parameters

3.4.6. Rotation ramp test (Fig. 3.31)

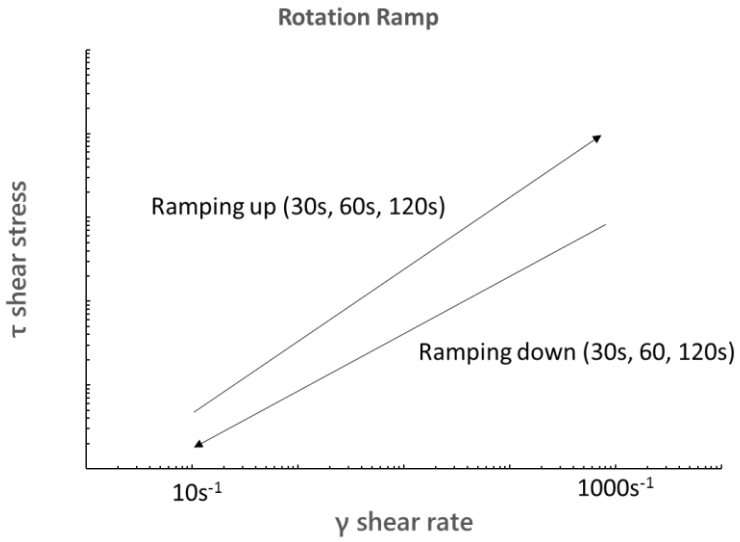

Fig. 3.31 Rotation ramp experiment's parameters

In this measurement's procedure, the shear rate is continuously altered either continuously increased or continuously decreased. The resulting shear stress is measured and displayed without waiting for equilibrium conditions.

To understand the thixotropic behavior of okra mucilage, a loop was investigated. For the forward route, the shear rate from $10s^{-1}$ which was believed to be a transition point of okra mucilage was selected as a beginning shear rate of this test and end at $1000s^{-1}$. On the other hand, the backward route's shear rate was from $1000s^{-1}$ to $10s^{-1}$. Three different loops' time, 60s, 120s, 240s, were set.

3.4.7 Rotation time curve test (Fig. 3.33)

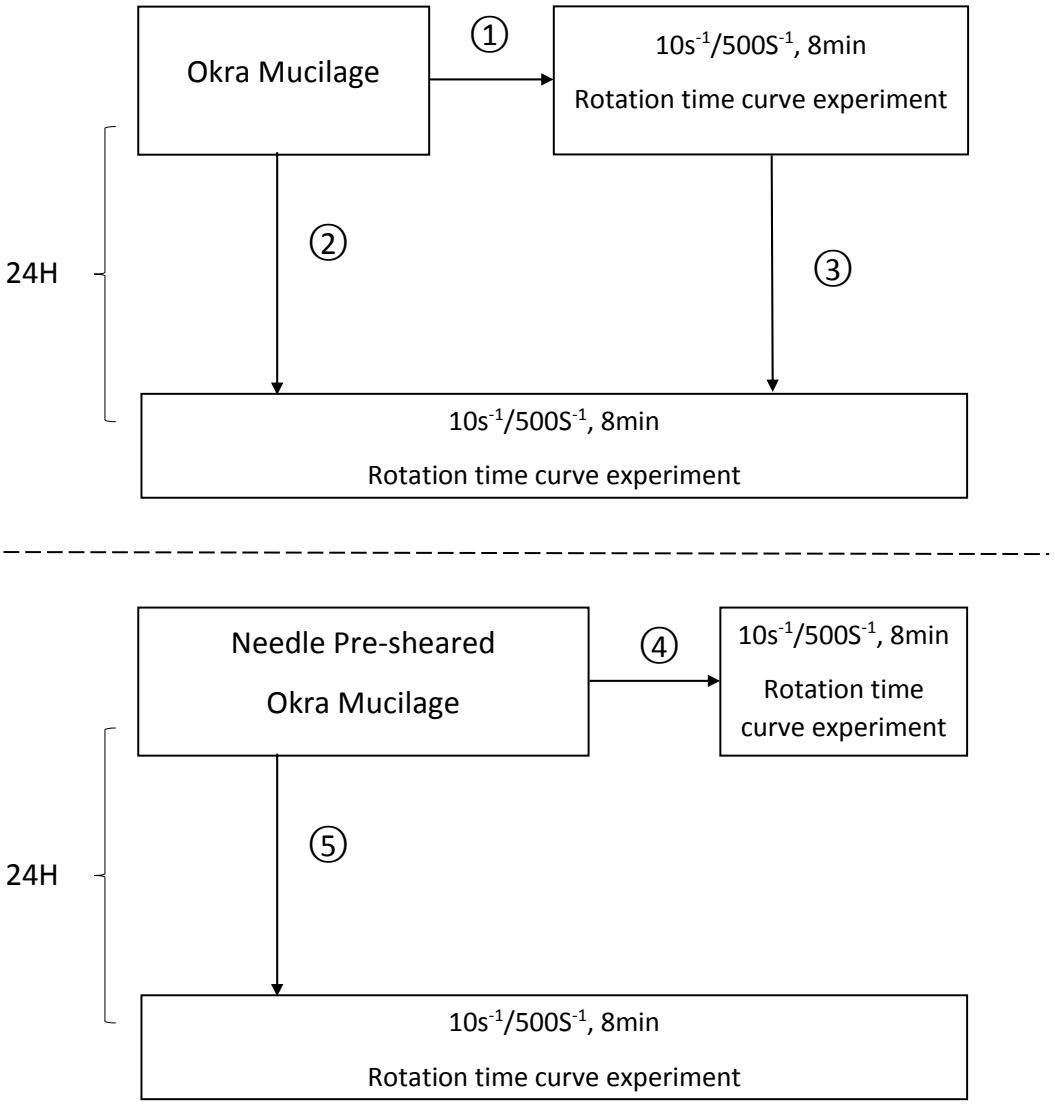

Fig. 3.32 The procedure of rotation time curve experiment

In this measurement's procedure, a constant shear rate and a constant temperature are defined for a fixed time. The resulting shear viscosity is measured and display.

The test time was set at 8min to give the mucilage enough time to develop and reach a stable value. Meanwhile, the fixed shear rates were chosen at $10s^{-1}$ which was believed to be the beginning of okra mucilage's transition point, and $500s^{-1}$ which was over the transition point.

1. Fresh okra mucilage would be tested after filtering and stirring well.

2. Okra mucilage would keep in the fridge at 6°C for one day to observe the one day preservation time wether would have the biological degradation on okra mucilage.

3. Okra mucilage would be collected again from the rheometer's plate to get the rotation pre-sheared okra mucilage. Then, put them in the fridge at 6°C for one day. After that, the cone and plate pre-sheared okra mucilage would be tested to observe whether there was the recovery of structures or not.

4. Fresh needle pre-sheared okra mucilage would be tested.

5. The needle pre-sheared okra mucilage would be tested after a day preservation. Trying to observe the recovery phenomenon and find the difference comparing with the shear history effect from rotation (③).

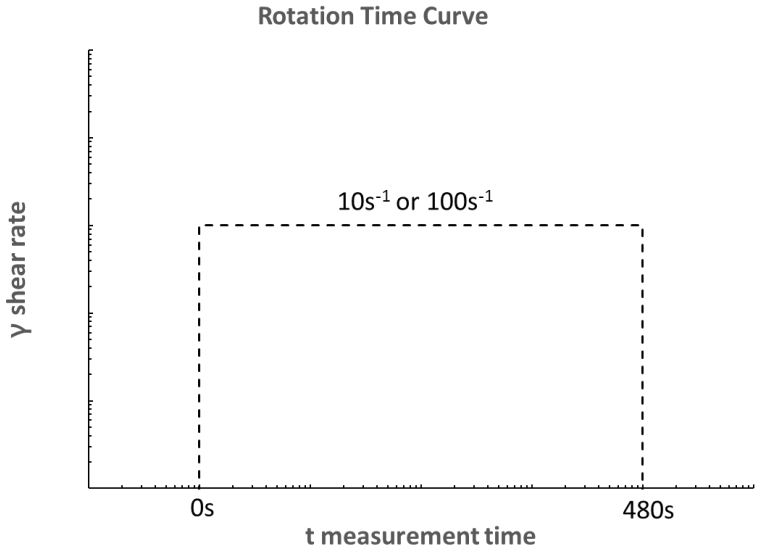

Fig. 3.33 Rotation time curve experiment's parameter

3.5 Basic information of materials

Table. 3.3 The basic information of the tested samples

Jute	**Origin**	**Density (g/cm^3)**	**Concentration (wt%)**	**Material:Water**
	Gunma	**1.02**	**0.21**	**1 -- 4**
	k (mPas^n)	**n**	**ΔP (Pa)**	**R^2**
Test 1	**16.26**	**0.46**	**376.94**	**0.82**
Test 2				**0.70**
Test 3				**0.68**
PEO	**Origin**	**Density (g/cm^3)**	**Concentration (wt%)**	**Material:Water**
	-	**1.05**	**0.15**	**0.15 -- 100**
	k (mPas^n)	**n**	**ΔP (Pa)**	**R^2**
Test 1	**9.84**	**0.82**	**8537.45**	**0.99**
Test 2				**0.99**
Test 3				**0.98**
Okra 1	**Origin**	**Density (g/cm^3)**	**Concentration (wt%)**	**Material:Water**
	Kagawa (JP)	**1.04**	**0.12**	**1 -- 4**
	k (mPas^n)	**n**	**ΔP (Pa)**	**R^2**
Test 1	**19.37**	**0.70**	**5138.77**	**0.95**
Test 2				**0.96**
Test 3				**0.97**
Okra 2.1	**Origin**	**Density (g/cm^3)**	**Concentration (wt%)**	**Material:Water**
	Kagoshima (JP)	**1.05**	**0.29**	**1 -- 2**
	k (mPas^n)	**n**	**ΔP (Pa)**	**R^2**
Test 1	**158.44**	**0.54**	**8180.81**	**0.87**
Test 2				**0.85**
Test 3				**0.84**
Okra 2.2	**Origin**	**Density (g/cm^3)**	**Concentration (wt%)**	**Material:Water**
	Kagoshima (JP)	**1.02**	**0.2**	**1 -- 3**
	k (mPas^n)	**n**	**ΔP (Pa)**	**R^2**
Test 1	**85.81**	**0.58**	**6607.84**	**0.90**
Test 2				**0.91**
Test 3				**0.91**
Okra 2.3	**Origin**	**Density (g/cm^3)**	**Concentration (wt%)**	**Material:Water**
	Kagoshima (JP)	**0.99**	**0.12**	**1 -- 4**
	k (mPas^n)	**n**	**ΔP (Pa)**	**R^2**
Test 1	**63.43**	**0.58**	**4884.46**	**0.92**
Test 2				**0.92**
Test 3				**0.92**
Okra 2.4	**Origin**	**Density (g/cm^3)**	**Concentration (wt%)**	**Material:Water**
	Kagoshima (JP)	**0.99**	**0.1**	**1 -- 5**
	k (mPas^n)	**n**	**ΔP (Pa)**	**R^2**
Test 1	**49.90**	**0.61**	**5184.52**	**0.93**
Test 2				**0.95**
Test 3				**0.94**

(Continued) Table. 3.3 The basic information of the tested samples

Okra 3	**Origin**	**Density (g/cm^3)**	**Concentration (wt%)**	**Material:Water**
	Kouchiken (JP)	**0.98**	**0.12**	**1 -- 4**
	k ($mPas^n$)	**n**	**ΔP (Pa)**	**R^2**
Test 1	**54.78**	**0.62**	**6288.89**	**0.93**
Test 2				**0.92**
Test 3				**0.92**
Okra 4	**Origin**	**Density (g/cm^3)**	**Concentration (wt%)**	**Material:Water**
	Phillppines	**1.01**	**0.1**	**1 -- 4**
	k ($mPas^n$)	**n**	**ΔP (Pa)**	**R^2**
Test 1	**17.28**	**0.69**	**3987.30**	**0.96**
Test 2				**0.97**
Test 3				**0.97**
Okra 5	**Origin**	**Density (g/cm3)**	**Concentration (wt%)**	**Material:Water**
	Thai	**1.01**	**0.11**	**1 -- 4**
	k ($mPas^n$)	**n**	**ΔP (Pa)**	**R^2**
Test 1	**22.72**	**0.65**	**3518.37**	**0.92**
Test 2				**0.98**
Test 3				**0.98**

From the table 3.3, the basic details of the tested samples were shown.

Looking at the whole table 3.3, all the okra mucilages' densities were close to the pure water which was $1g/cm^3$. It is the same result from (Rheology et al. 2017). Meanwhile, jute mucilage and PEO15 (0.15wt%) were also had the densities around $1g/cm^3$.

Comparing the result in report (Rheology et al. 2017), even both experiments were used the cold pure water to extract the okra mucilage, due to the different parts immersed within the water, the okra mucilage's weight content concentration which was made following the weight ratio of 1 to 4, was around 0.12wt% rather than 0.22wt% reported by (Rheology et al. 2017). As common sense, the concentration would be increased as the okra plant-pure water weight ratio is increasing, observed from the data of okra 2.1~2.4.

In order to estimate the value of the press drop of the process that syringe pump pushing the fluid though the needle by using the Hagen–Poiseuille equation for non-Newtonian fluid, the power law parameters of non-sheared fluid were calculated after the steady shear viscosity experiment. The Ostwald-de Wale flow behavior index displayed in table 3.3 showed that all the sample liquid were pseudo plastic fluid. The jute mucilage had been given the minimal shear history effect. On the other hand, the PEO solution and the okra mucilage sample 2.1 were suffered the highest needle shear history effect, due to the largest flow consistency (okra 2.1) index and largest flow behavior index (PEO).

3.6 Brief flow chart

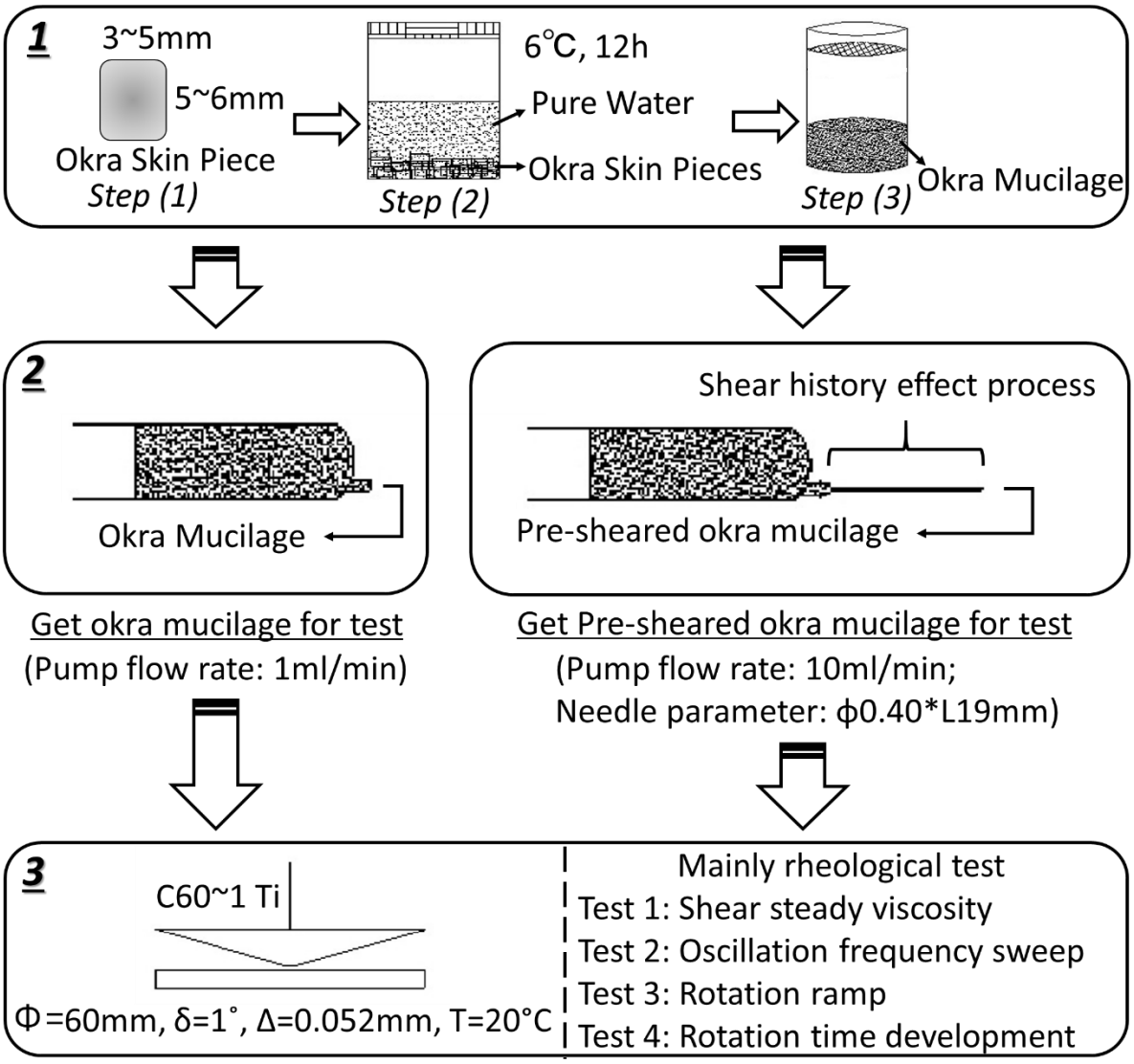

Fig. 3.34 Brief flow chart of a series of experiments on okra mucilage

3.7 Observation

3.7.1 Okra protein observation

20ml stirring-well non-sheared okra mucilage, needle pre-shear okra mucilage would be put under the green laser light to observe the proteins.

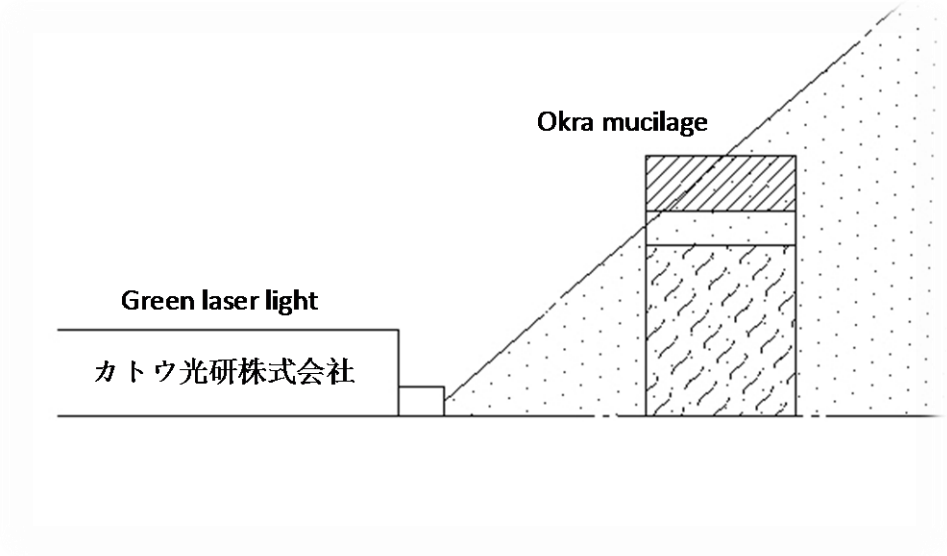

Fig. 3.35 Okra protein observation

3.7.2 Fluorescent-adding mucilage's state observation

12ml stirring-well non-sheared okra mucilage and needle pre-shear okra mucilage were added by 1g fluorescent microspheres (70μm, from Thermo Fisher). Then, both two mucilage-microsphere mixture would be mixed well by shaking 50 times and put under the UV light to observe the liquid-solid state.

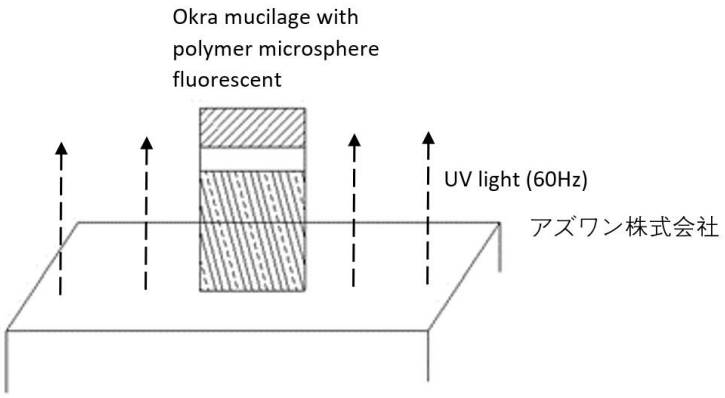

Fig. 3.36 Fluorescent-adding mucilage's state observation

3.7.3 Dry result observation

Either the non-sheared and needle pre-sheared mucilage would be poured on the glass at the volume of 1cm^3. Then both samples would be stored at a cool and ventilated environment to let them dry for one day. The result would be observed through the microscope IX83 from Olympus.

Fig. 3.37 Olympus IX83 microscope

V.Result and discussion

4.1 Steady shear experiment

The apparent viscosities of PEO and jute samples as a function of shear rate were shown in the following Fig. 4.1 to Fig. 4.2. For okra samples, Fig. 4.3 to Fig. 4.10 were displayed.

It was not hard to find that all the okra mucilage were shear thinning because the apparent viscosity was decreasing as the shear strain speed increasing. This same property was already reported in (Yuan et al. 2018a)(Rheology et al. 2017)(Meister et al. 1983)(Kontogiorgos et al. 2012)(Ndjouenkeu et al. 1996) as a previous researches' result. Moreover, the system were still shown shear thinning after the needle shear history effect.

As the same time, a plateau zone started around the shear rate $10s^{-1}$ was found in both okra mucilage and needle pre-sheared okra mucilage. The plateau zone behavior was caused by that the increasing the shear rate would force the fluid elements to follow the direction of the fluid current. When the fluid structure would well deform, including breaking aggregates at a certain shear rate, which would result in viscosity limitations (Björn et al. 2012). And this value was the same as the value which reported in (Rheology et al. 2017) by extracting the okra mucilage from okra pods' skins and seeds. Because the seeds' part of okra mucilage did not contain any mucilage (Woolfe et al. 1977). Hence, the okra mucilage's mesh networks were still dominant.

The PEO 15 solution and jute mucilage's flow behavior were also pseudo plastic.

The PEO15 solution was following the power law when it was posted on the shear stress as a function of shear rate. It is a type of generalized Newtonian fluid. Thus the Cross model was used to fit the PEO15 solution for its behavior. The parameters determination of PEO solution's Cross model were calculated following the steps reported by (Xie & Jin 2016). And their parameters were shown in table 4.2.

$$\text{Cross model: } \boldsymbol{\eta = \eta_{\infty} + \frac{\eta_0 - \eta_{\infty}}{1 + (C\dot{\gamma})^m}} \quad \textbf{(11)}$$

On the other hand, the jute and okra mucilage were not a generalized Newtonian fluid, because they were dependent upon the history of deformation. Meanwhile, the relationship between shear stress and shear rate of jute mucilage hinted that it was a Bingham plastic fluid. Thus, this model was selected and built. The results were shown in the table 4.1.

$$\text{Bingham plastic fluid: } \boldsymbol{\tau = \tau_y + \mu_p \dot{\gamma}} \quad \textbf{(37)}$$

For okra mucilage, it shown that it had shear thinning behavior and a low yield stress. However, unlike the jute mucilage, the Bingham plastic model could not fit them well. Thus, a piecewise function of two Ostwald–de Waele equation was introduced. The transition point, shear rate $10s^{-1}$, was selected as the boundary. These parameters were shown in the table 4.3 to table 4.10.

$$\begin{cases} \boldsymbol{\tau_1 = K_1(\dot{\gamma})^{n_1}} & \boldsymbol{(\dot{\gamma} \leq 10 s^{-1})} \\ \boldsymbol{\tau_2 = K_2(\dot{\gamma})^{n_2}} & \boldsymbol{(\dot{\gamma} \geq 10 s^{-1})} \end{cases} \quad \textbf{(10)}$$

Table. 4.1 Model fitting for jute mucilage

Jute	μ_y (mPas)	τ_p (mPa)	R^2
Test 1	1.13	13.61	0.98
Test 2			0.95
Test 3			0.95
Jute PS	μ_y (mPas)	τ_p (mPa)	R^2
Test 1	1.05	1.18	0.95
Test 2			0.97
Test 3			0.99

PS: Needle pre-sheared

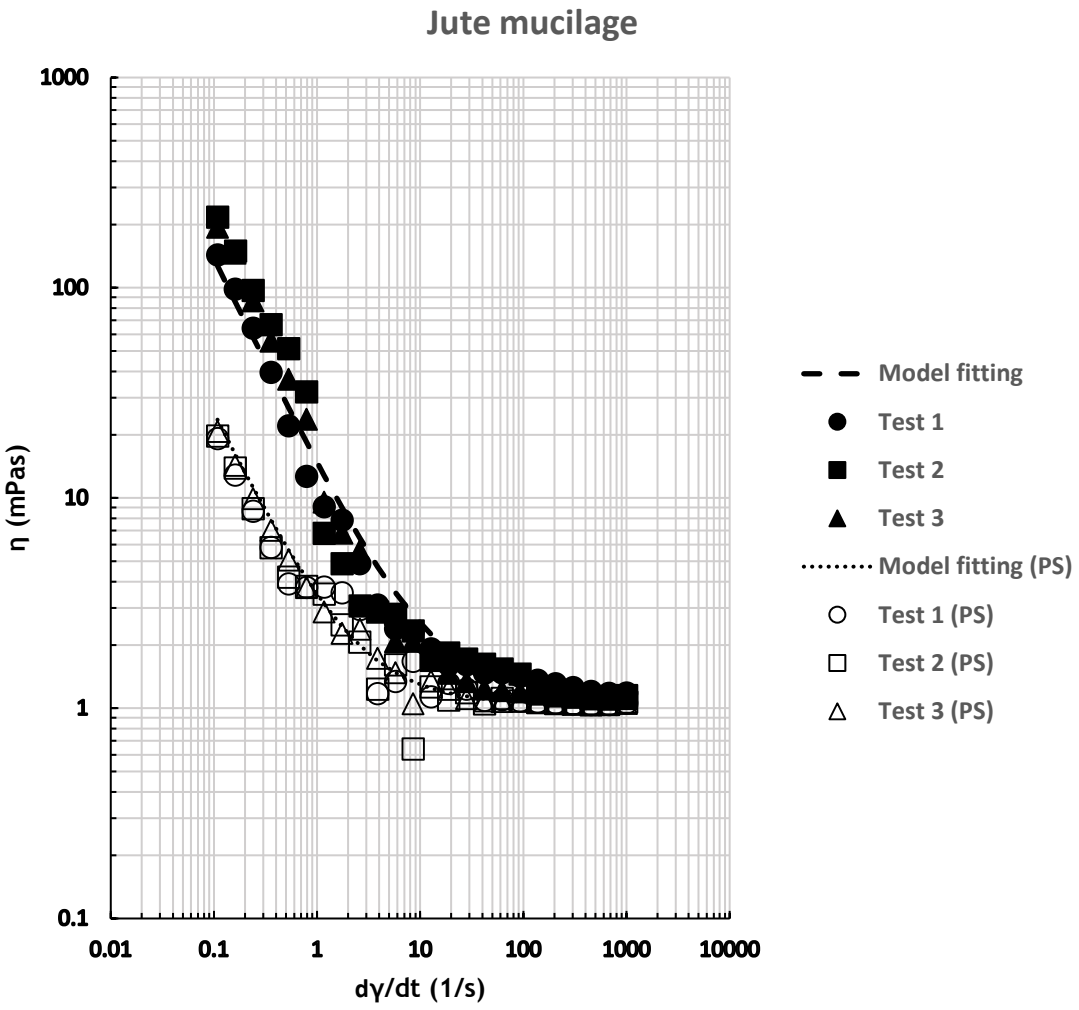

Fig. 4.1 Steady shear viscosity as a function of jute mucilage

Table. 4.2 Ostwald–de Wale model fitting for PEO15 (0.15wt%) solution

PEO	η_0 (mPas)	η_{inf} (mPas)	C (s)	m	R^2
Test 1	30.76	4.10	7.00	0.82	0.92
Test 2					0.93
Test 3					0.83
PEO PS	η_0 (mPas)	η_{inf} (mPas)	C (s)	m	R^2
Test 1	31.52	3.80	7.00	0.82	0.90
Test 2					0.94
Test 3					0.92

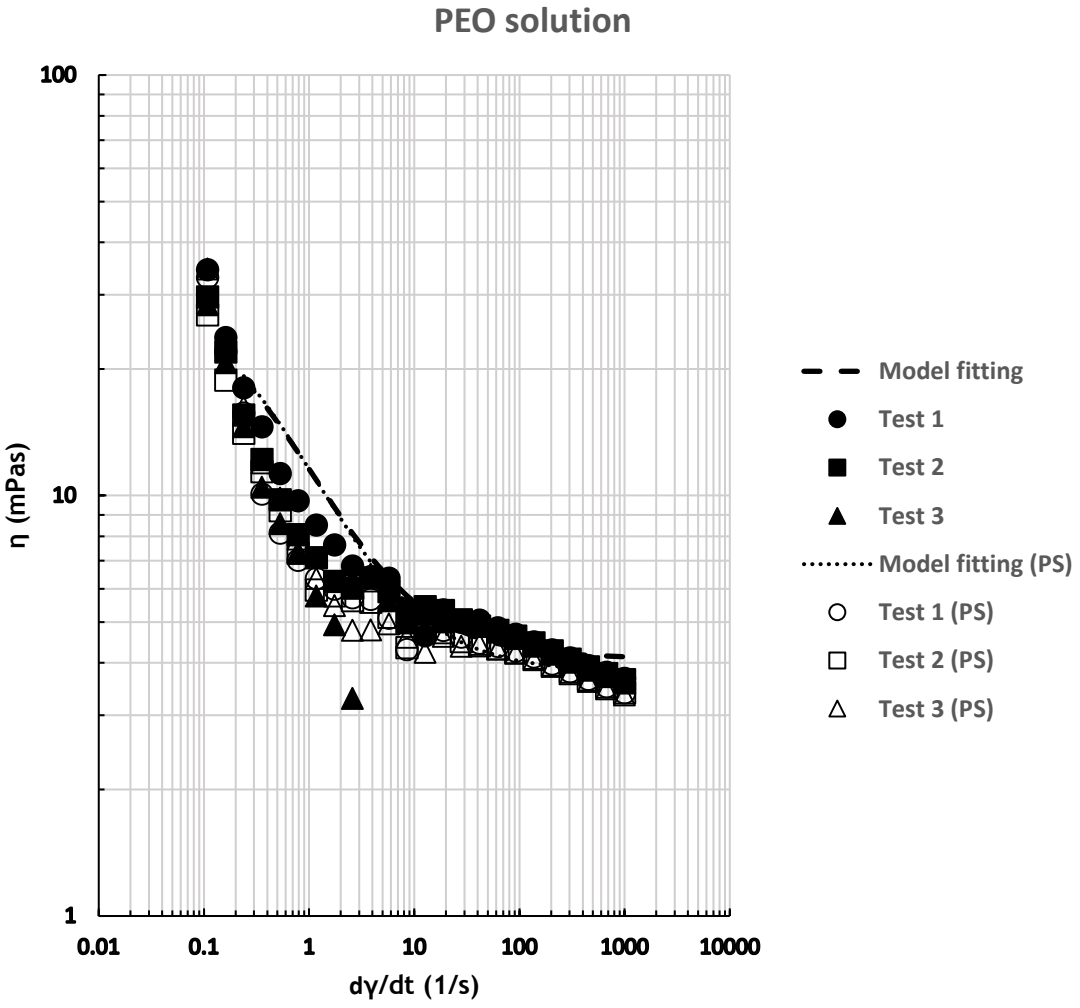

Fig. 4.2 Steady shear viscosity as a function of PEO15 (0.15wt%) solution

Table. 4.3 Model fitting for okra mucilage from Kagawa

Okra 1	k_1 (mPas^n)	n_1	k_2(mPas^n)	n_2	R^2
Test 1	19.59	0.47	6.89	0.93	0.97
Test 2					0.97
Test 3					0.96
Okra 1 PS	k_1(mPas^n)	n_1	k_2(mPas^n)	n_2	R^2
Test 1	16.08	0.61	8.35	0.84	0.98
Test 2					0.92
Test 3					0.98

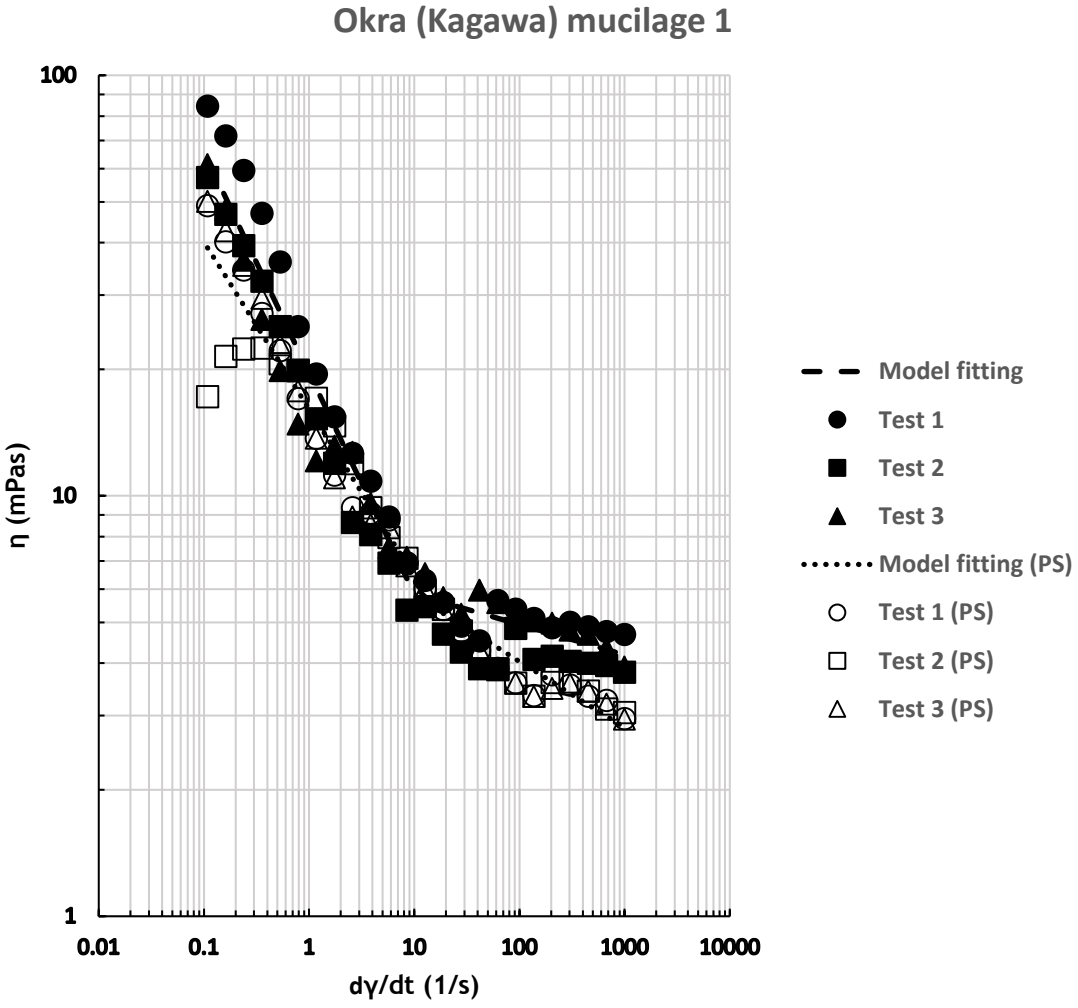

Fig. 4.3 Steady shear viscosity as a function of okra mucilage from Kagawa

Table. 4.4 Model fitting for okra mucilage (0.29wt%) from Kagoshima

Okra 2.1	k_1 (mPas^n)	n_1	k_2(mPas^n)	n_2	R^2
Test 1	164.07	0.24	27.82	0.91	0.99
Test 2					0.99
Test 3					0.99
Okra 2.1 PS	k_1(mPas^n)	n_1	k_2(mPas^n)	n_2	R^2
Test 1	162.35	0.21	30.58	0.85	0.99
Test 2					0.99
Test 3					0.99

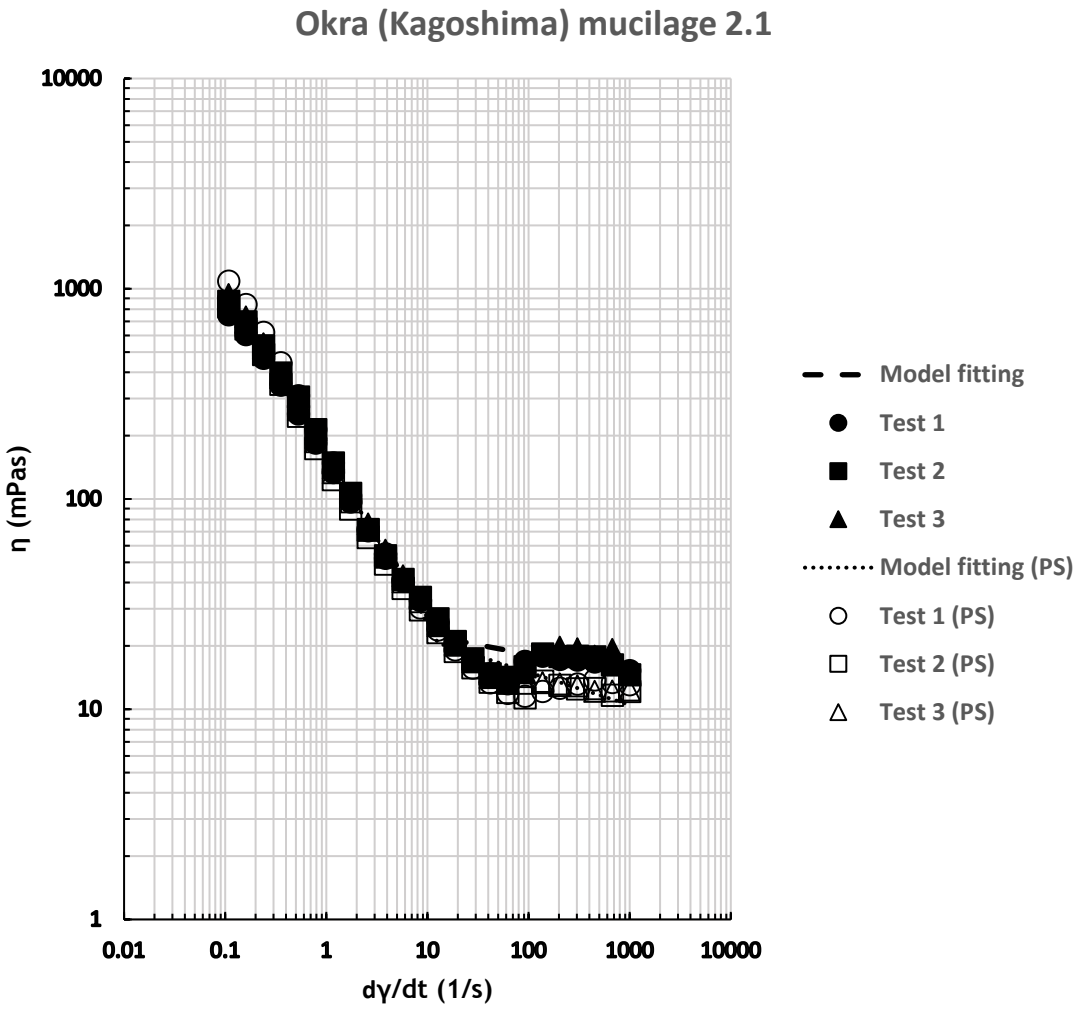

Fig. 4.4 Steady shear viscosity as a function of okra mucilage (0.29wt%) from Kagoshima

Table. 4.5 Model fitting for okra mucilage (0.2wt%) from Kagoshima

Okra 2.2	k_1 (mPas^n)	n_1	k_2(mPas^n)	n_2	R^2
Test 1	88.63	0.31	18.28	0.91	0.99
Test 2					0.99
Test 3					0.99
Okra 2.2 PS	k_1(mPas^n)	n_1	k_2(mPas^n)	n_2	R^2
Test 1	91.73	0.31	26.89	0.79	0.99
Test 2					0.99
Test 3					0.99

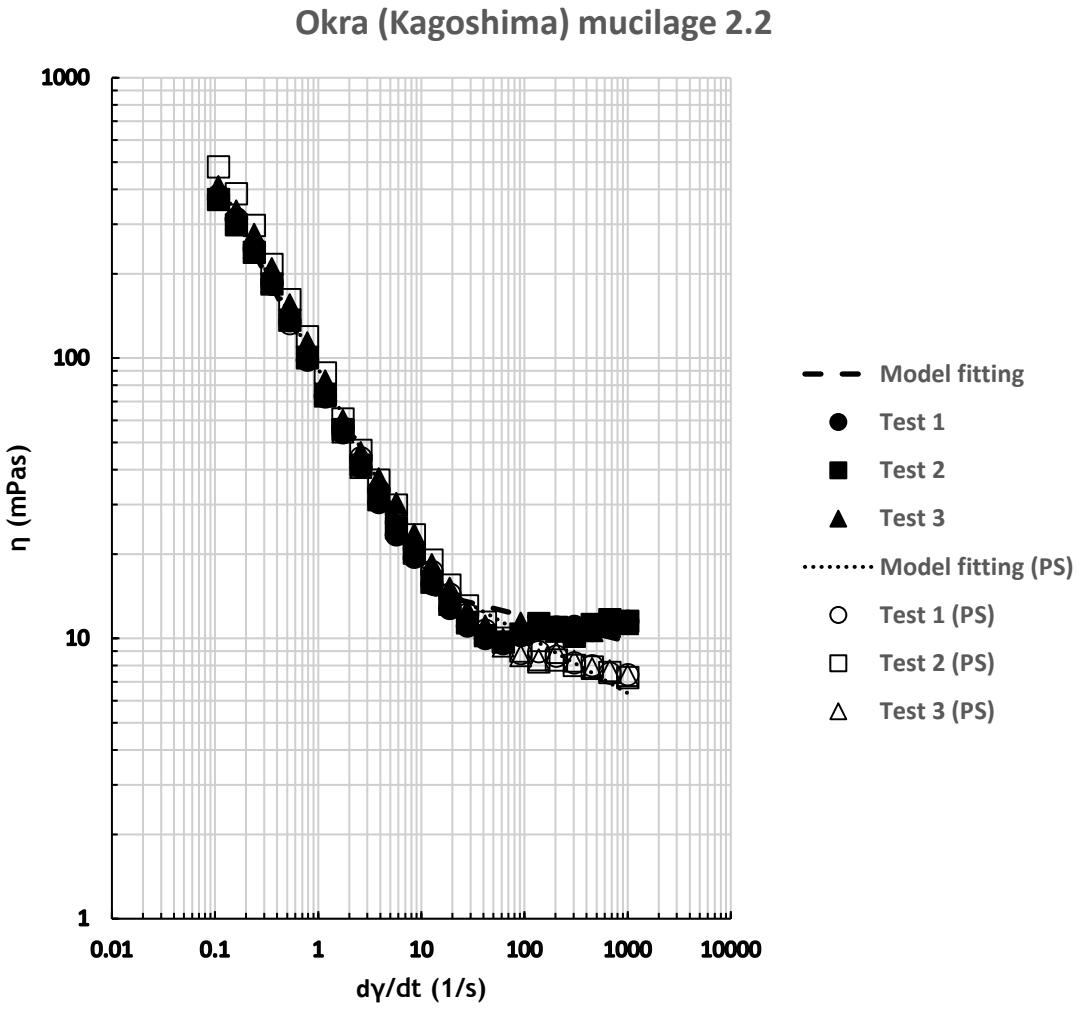

Fig. 4.5 Steady shear viscosity as a function of okra mucilage (0.2wt%) from Kagoshima

Table. 4.6 Model fitting for okra mucilage (0.12%) from Kagoshima

Okra 2.3	k_1 (mPas^n)	n_1	k_2(mPas^n)	n_2	R^2
Test 1	65.34	0.35	16.99	0.86	0.99
Test 2					0.99
Test 3					0.99
Okra 2.3 PS	k_1(mPas^n)	n_1	k_2(mPas^n)	n_2	R^2
Test 1	52.92	0.44	20.98	0.77	0.99
Test 2					0.99
Test 3					0.99

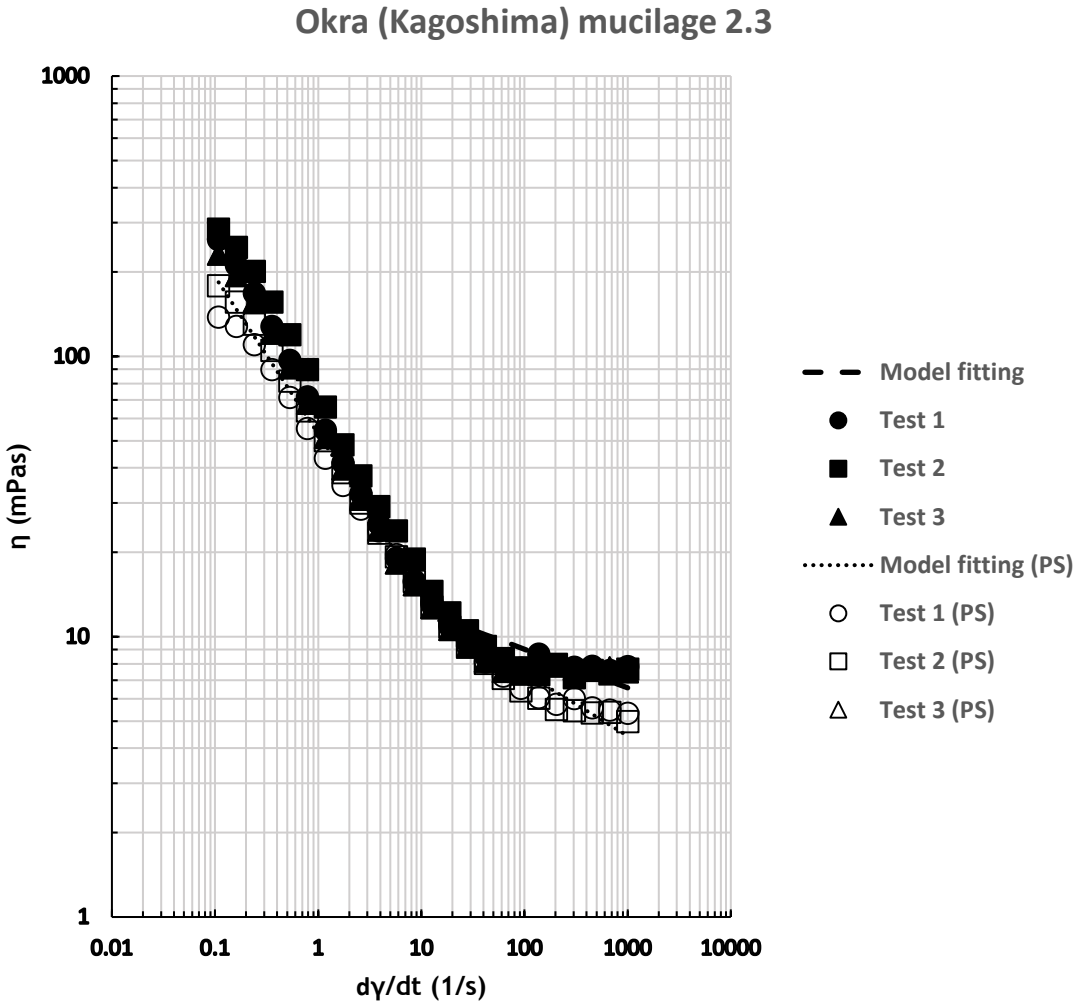

Fig. 4.6 Steady shear viscosity as a function of okra mucilage (0.12wt) from Kagoshima

Table. 4.7 Model fitting for okra mucilage (0.1wt%) from Kagoshima

Okra 2.4	k_1 (mPas^n)	n_1	k_2(mPas^n)	n_2	R^2
Test 1	51.26	0.39	14.51	0.87	0.99
Test 2					0.99
Test 3					0.99
Okra 2.4 PS	k_1(mPas^n)	n_1	k_2(mPas^n)	n_2	R^2
Test 1	50.49	0.41	17.69	0.81	0.99
Test 2					0.99
Test 3					0.99

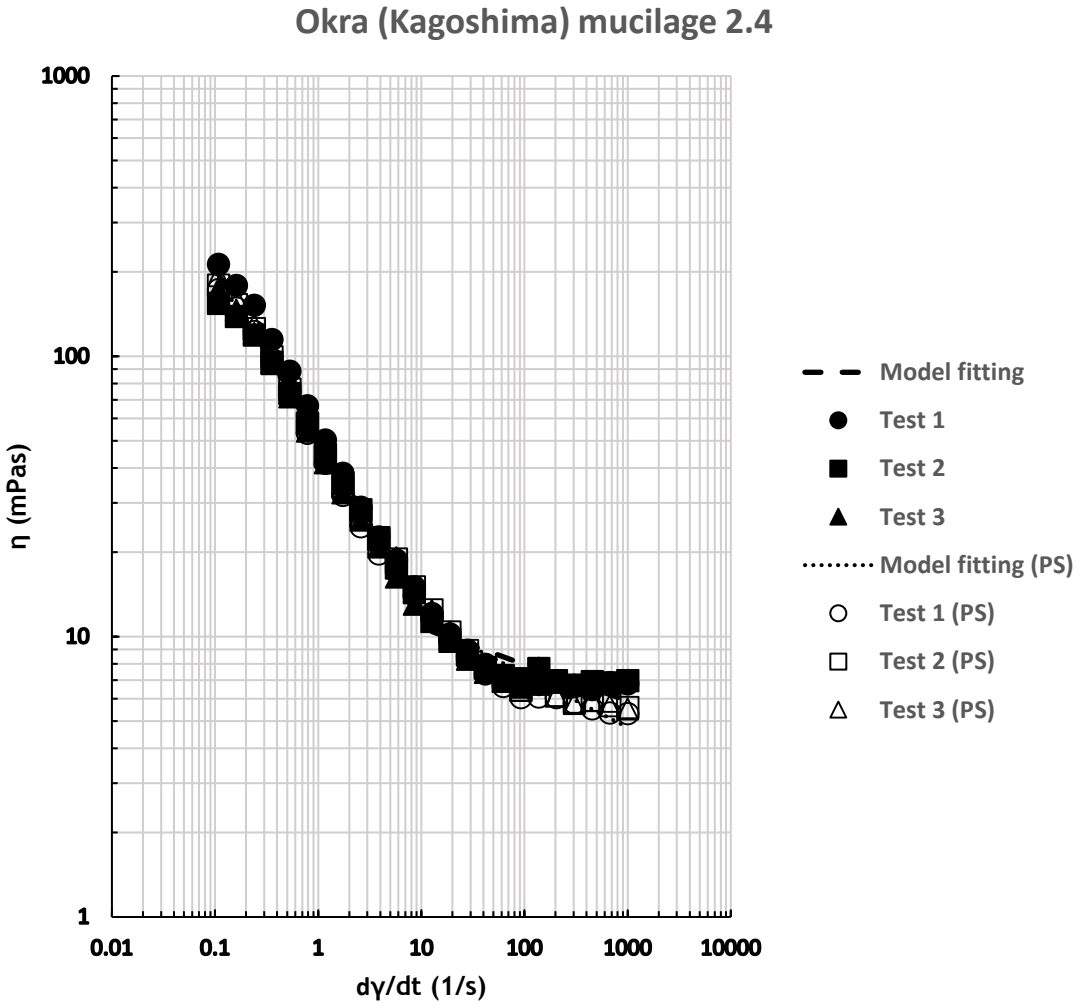

Fig. 4.7 Steady shear viscosity as a function of okra mucilage (0.1wt%) from Kagoshima

Table. 4.8 Model fitting for okra mucilage from Kouchiken

Okra 3	k_1 (mPas^n)	n_1	k_2(mPas^n)	n_2	R^2
Test 1	56.66	0.35	10.91	0.96	0.99
Test 2					0.99
Test 3					0.99
Okra 3 PS	k_1(mPas^n)	n_1	k_2(mPas^n)	n_2	R^2
Test 1	56.92	0.37	16.88	0.83	0.99
Test 2					0.99
Test 3					0.99

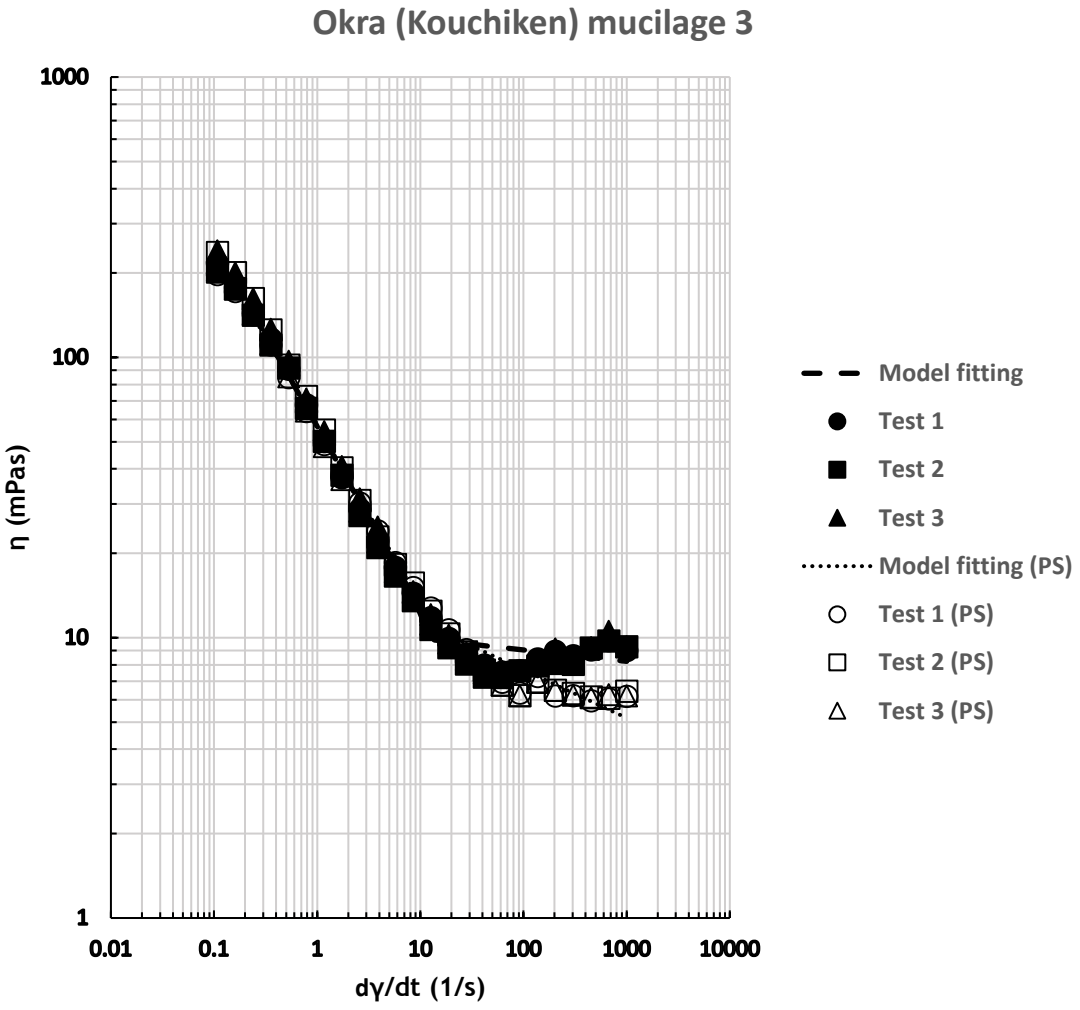

Fig. 4.8 Steady shear viscosity as a function of okra mucilage from Kouchiken

Table. 4.9 Model fitting for okra mucilage from the Philippines

Okra 4	k_1 (mPas^n)	n_1	k_2(mPas^n)	n_2	R^2
Test 1	17.45	0.48	6.22	0.91	0.99
Test 2					0.96
Test 3					0.97
Okra 4 PS	k_1(mPas^n)	n_1	k_2(mPas^n)	n_2	R^2
Test 1	9.96	0.63	5.71	0.84	0.93
Test 2					0.97
Test 3					0.99

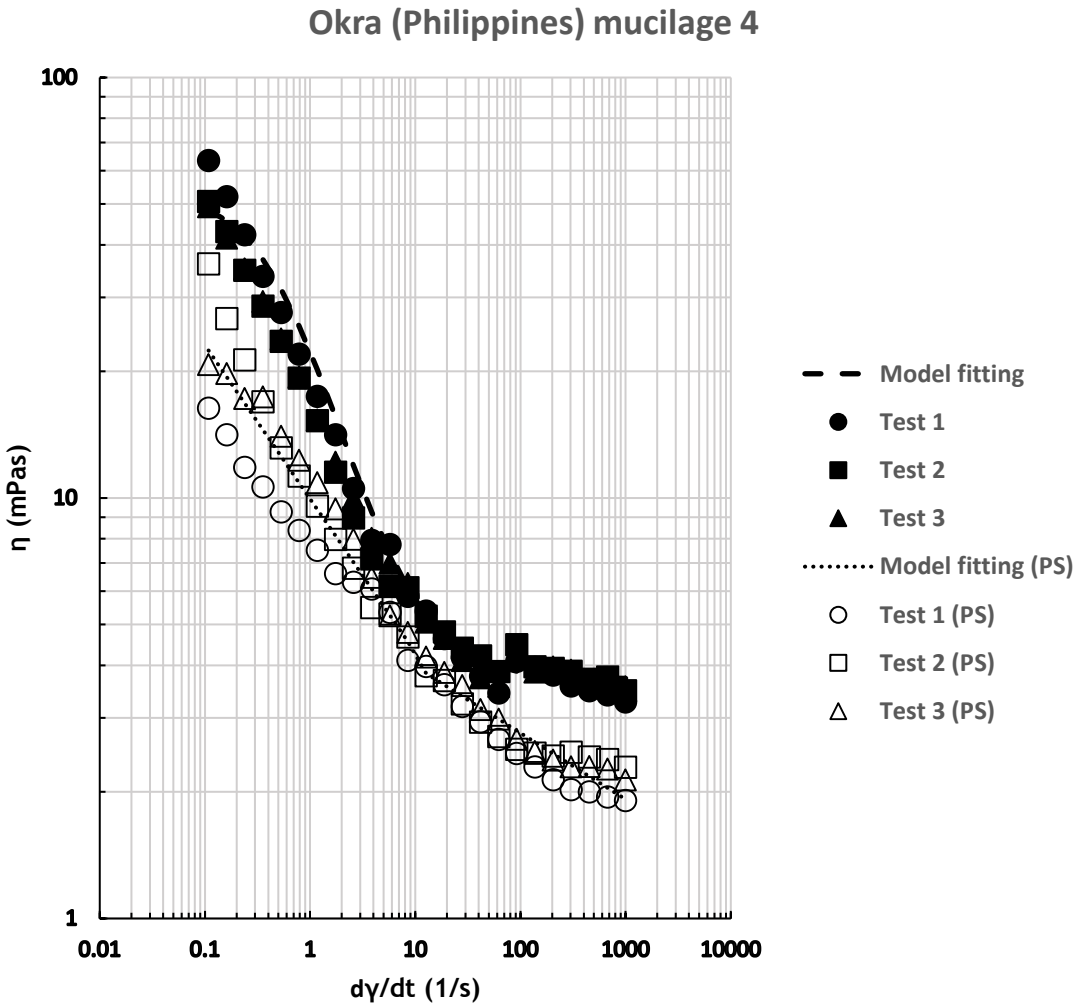

Fig. 4.9 Steady shear viscosity as a function of okra mucilage from the Philippines

Table. 4.10 Model fitting for okra mucilage from Thailand

Okra 5	k_1 (mPas^n)	n_1	k_2(mPas^n)	n_2	R^2
Test 1	23.66	0.49	9.65	0.83	0.94
Test 2					0.99
Test 3					0.88
Okra 5 PS	k_1(mPas^n)	n_1	k_2(mPas^n)	n_2	R^2
Test 1	13.68	0.65	9.67	0.77	0.91
Test 2					0.91
Test 3					0.86

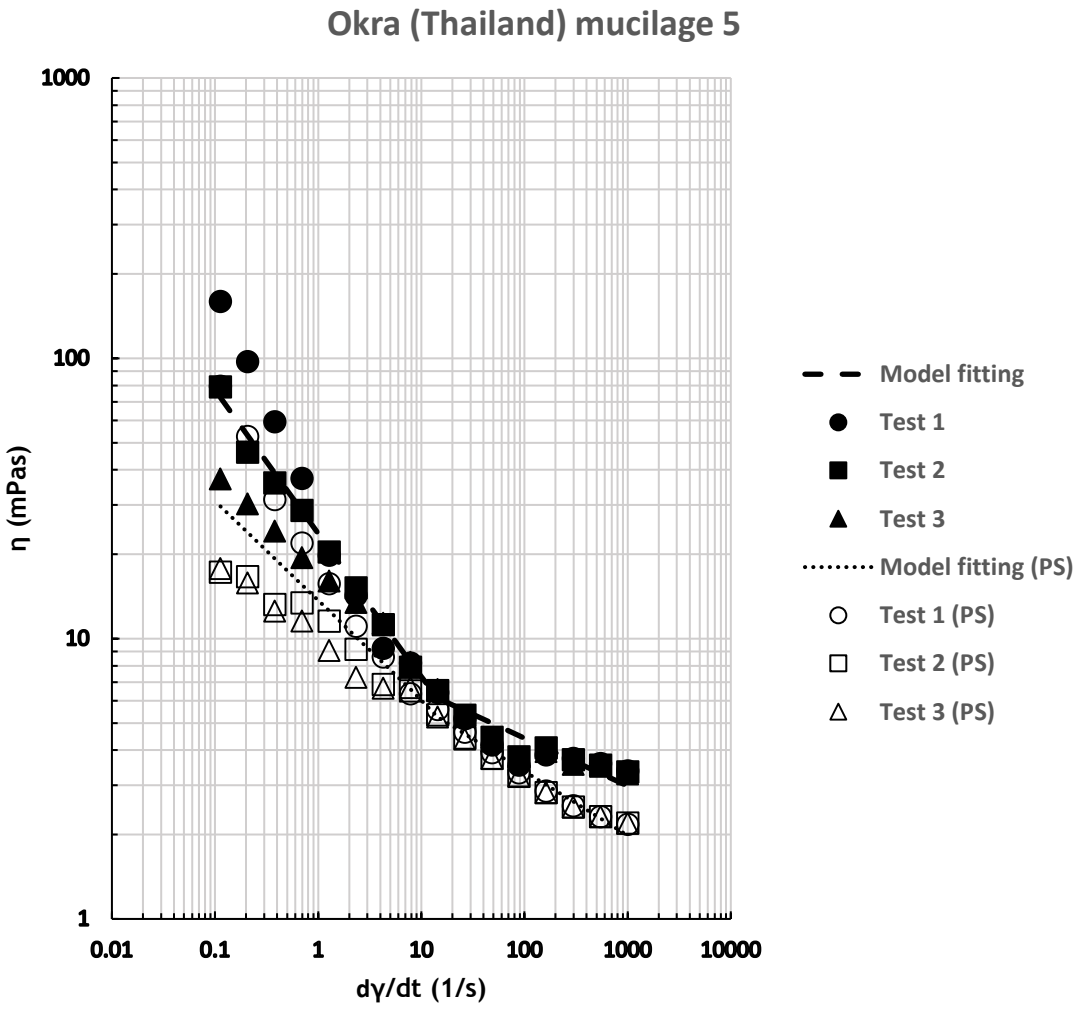

Fig. 4.10 Steady shear viscosity as a function of okra mucilage from Thailand

Observed from the Fig. 4.2, the nearly coincident curves between PEO solution and needle pre-sheared one were found. That showed the PEO solution would be stable after been suffered from a large magnanimity of shear history effect. On the other hand, the jute and okra mucilage comparing with their pre-sheared viscosity curves shown difference. A large distance at the low shear rate range ($0.1s^{-1}$~$100s^{-1}$). That might because the jute mucilage's biopolymer would be distributed in another way after shear history effect. However, when the shear rate was increasing, the viscosity still would tend to be the same. This was because the pre-shearing would damage the material structure (Sun & Gunasekaran 2009). Thus, the yield stress decreased.

Comparing with the control groups (Jute mucilage and PEO solution), that the pre-sheared okra mucilage's infinity viscosity at high shear rate range ($100s^{-1}$ ~ $1000s^{-1}$) were lower than the okra mucilage's as a common point was found. These changed viscosity's magnanimity would be described in η_c, an introduced parameter, to show the amplitude.

$$\eta_c = \frac{\overline{\eta(\dot{\gamma})} - \overline{\eta_s(\dot{\gamma})}}{\overline{\eta(\dot{\gamma})}} \quad (7)$$

Table. 4.11 The rate of changed viscosity from $100s^{-1}$ ~$1000s^{-1}$

Samples	Jute	PEO	Okra 1	Okra 2.1	Okra 2.2
η_c	7.82	7.00	26.70	26.30	25.61
Samples	Okra 2.3	Okra 2.4	Okra 3	Okra 4	Okra 5
η_c	27.17	13.60	29.71	39.10	31.96

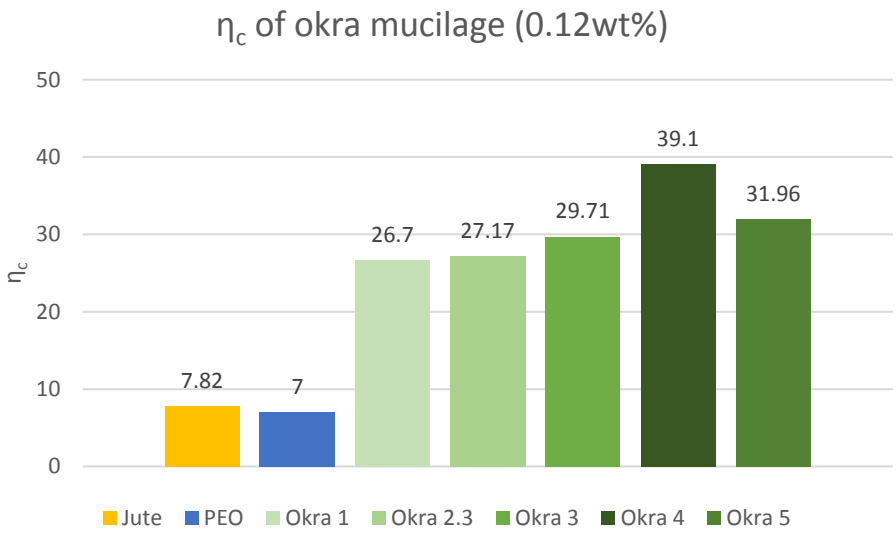

Fig. 4.11 η_c of samples (≈0.12wt%) from $100s^{-1}$ ~$1000s^{-1}$

The rates of changed viscosity of all samples from $100s^{-1}$ ~$1000s^{-1}$ were shown in the table 4.11. Regardless of the concentration's influence, the rate of changed viscosity of those samples whose concentrations were around 0.12wt% were charted in Fig. 4.11. Different from the jute mucilage's result, the shear history effect would have an influence on okra mucilage at high shear

rate range was found. This was because that the okra mucilage's shear viscosity was dominated by extensional viscosity (Yuan et al. 2018a). This might because the small shear strain speed did not have significant effects as deformation. It might be too small to stretch and expose association sites nor maintain any existing network structures (Wee et al. 2015). The broken structure of the okra mucilage would be buried under the entanglements of their networks which was shown in the Fig. 4.12.

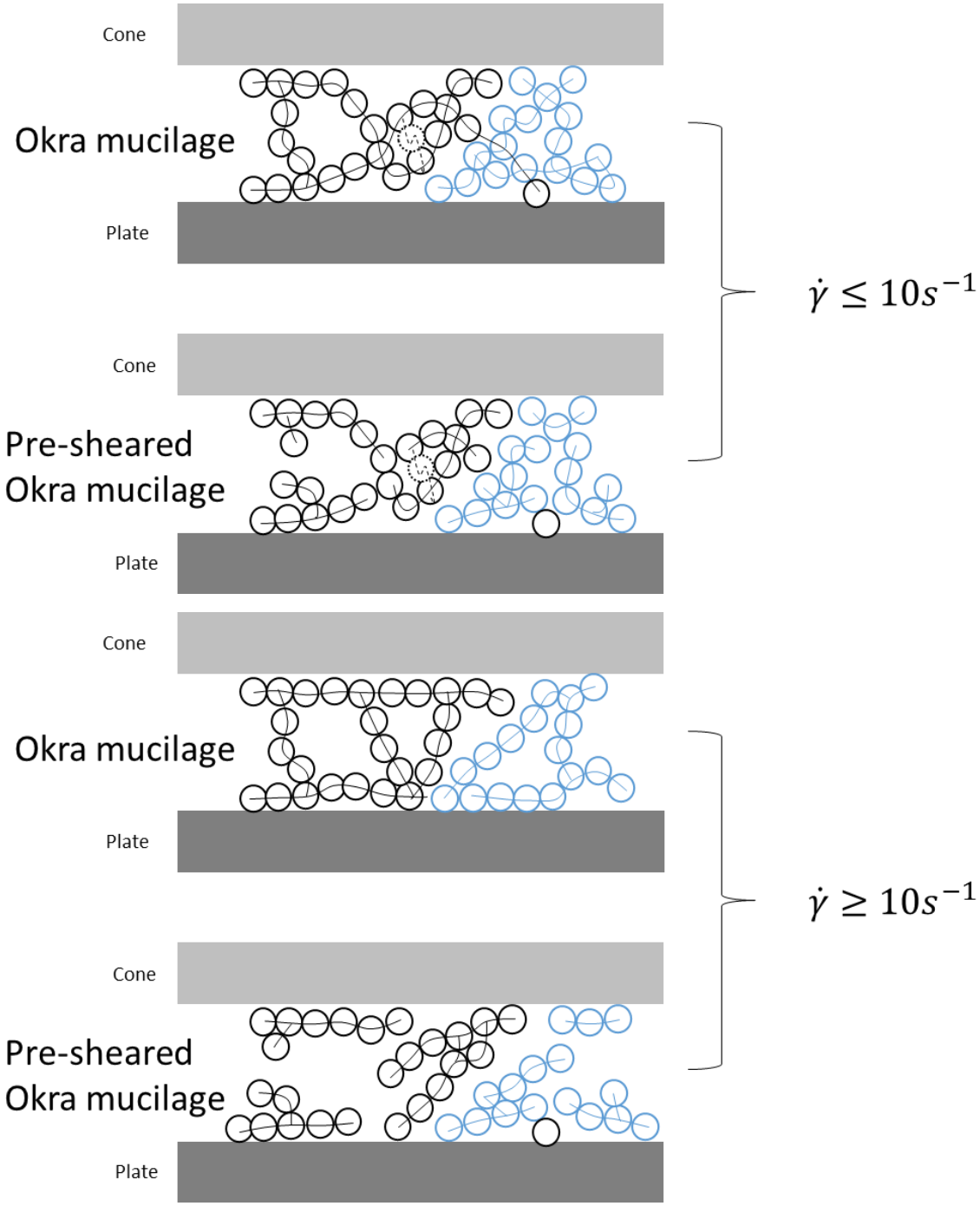

Fig. 4.12 Schematic illustration of viscosity changed rate depend on shear rate

Comparing all the pre-sheared okra mucilage's curves among these five samples, it was found that the pre-sheared okra mucilage from Japan (Okra 1~3 PS) were more stable than Thai's and Philippine's at low shear rate range ($0.1s^{-1}$~$10s^{-1}$) comparing with the non-sheared one. It can be explained that differentiation in rheological behavior is also attributed to the fine structure of the chains and not only to differences in molecular weight of the samples (Kontogiorgos et al. 2012). Thus, the Japanese okra seemed to have a more stable interaction with water.

In Fig. 4.13, all the samples whose concentration were close to 0.12wt% were plotted. The okra viscosity curves from different places were also different. It was because the different origin's okra polysaccharides components were different (Whistler et al. 1954) (Lengsfeld et al. 2004) (Agarwal et al. 2001) (Tomada et al. 1980). The different structure would cause different rheological properties. But even that, they would still show shear thinning. Because their backbone structures were revealed by rhamnogalacturonan-I mainly.

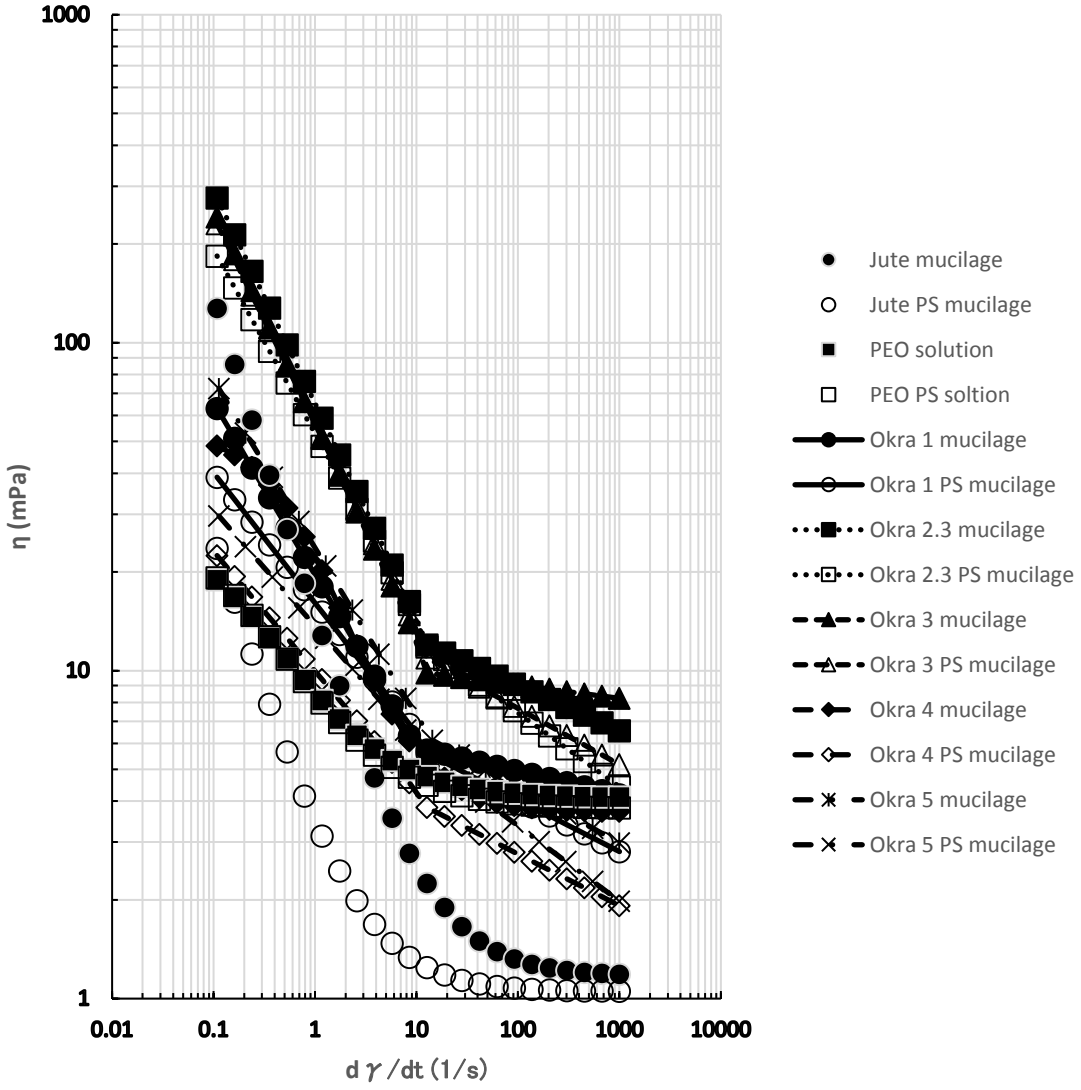

Fig. 4.13 All samples' (≈0.12wt%) viscosity as a function of shear rate

To investigate changed fluid's rheological properties, the most reasonable consideration is that the structure of the complex fluid has been changed.

Meanwhile, the structure of the okra mucilage has a close relationship of the concentration. Thus, the different concentration of the okra mucilage had been made. The concentration of okra mucilage 2.1; 2.2; 2.4 was made by setting the material water ratio 1-2,1-3 and 1-5, which was almost fitted 0.1wt%, 0.2wt%, and 0.3wt%. But the rate of changed amplitude in table 4.11 did not show the relationship. That may because the viscosity also has the connection with the solvent, when the concentration increased, the base number of interaction with water is increasing as well.

Considering that shear-thinning curves for disordered polysaccharide solutions have the same shape, irrespective of structural details and conditions of measurement such as biopolymer concentration or temperature (Morris et al., 1981). Thus, their concentration dependent properties and interactions with water were displayed. Normalization of flow curves by the viscosity of the solvent at an arbitrary experimental shear rate nullifies the effect of these two variables (shear rate and solvent viscosity) on the data (Yuan et al. 2018a) (Kontogiorgos et al. 2012). Allowing the underlying effect of polysaccharides on viscosity to be studied. In the master curve, the concentration and the shear history effect were mentioned.

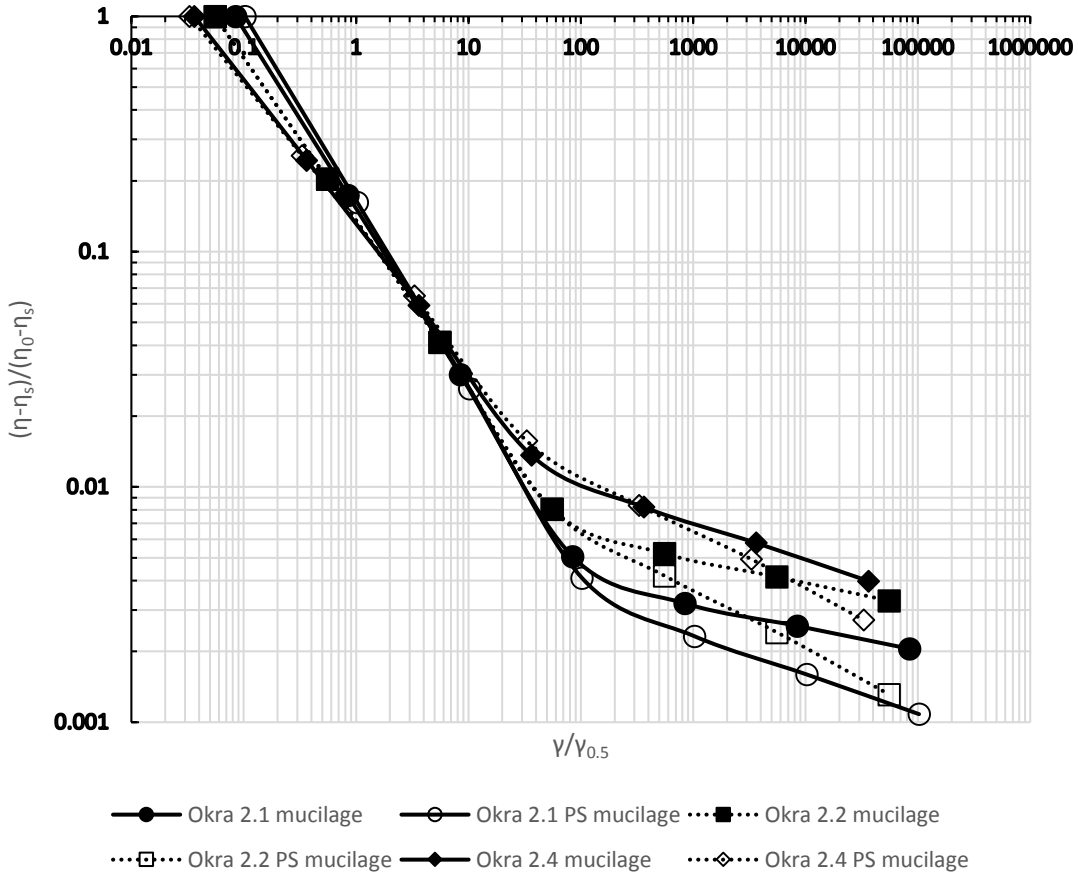

Fig. 4.14 Master curves of different concentration on non/pre sheared okra mucilage

From the Fig. 4.14, the relationship of the concentration of polysaccharides was shown. The larger mass fraction okra mucilage had, the lower master curve it would be. In general, solutions containing stiff polysaccharide chains are more pseudo plastic; the degree of pseudo plasticity increases with the polysaccharide concentration and molecular weight (Cui & Wang 2005). In other words, each concentration results in a further increase of the steepness of the curve, the polymers alter their self-assembled structure with each increase in concentration. A far greater number of smaller particles is counted, and is of much smaller size in the higher concentration mucilage. (Yuan et al. 2018a).

Moreover, when the shear history effect applied, the curves would get lower at high relate shear rate. This suggested that the individual bio-polymeric entities that can be broken up when shear history effect exist in the form. That might hint that the shear history may let the large groups of polysaccharides dissolve well into the small crops. This interaction would increase the number concentration of okra bio-polymers.

4.3 Creep and recovery

The creep and recovery experiments had been held, and the curves had been posted in figure 4.15. The parameters were calculated and shown in table 4.12. The creep and recovery curves of the okra mucilage showed that the okra mucilage was a typical viscoelastic liquid (Mitchell. 1980). From the table 4.12, the low yield stress and zero viscosity of okra (Kagawa) mucilage was found. The yield stress was close 8.8Pa, and the zero viscosity was close 71mPas. It met the previous description of okra mucilage that it was mucilage with a low yield stress in the report (Meister et al. 1983). Meanwhile, according to the table, the system needs almost 4.8s to return into the equilibrium. And after removing the stress, around 82% part of whole strain would have an elastic recovery. On the opposite, the 18% part would be the permanent flow (viscous part). According to the instantaneous strain part in the creep testes, equilibrium shear compliance was nearly 67Pa^{-1}.

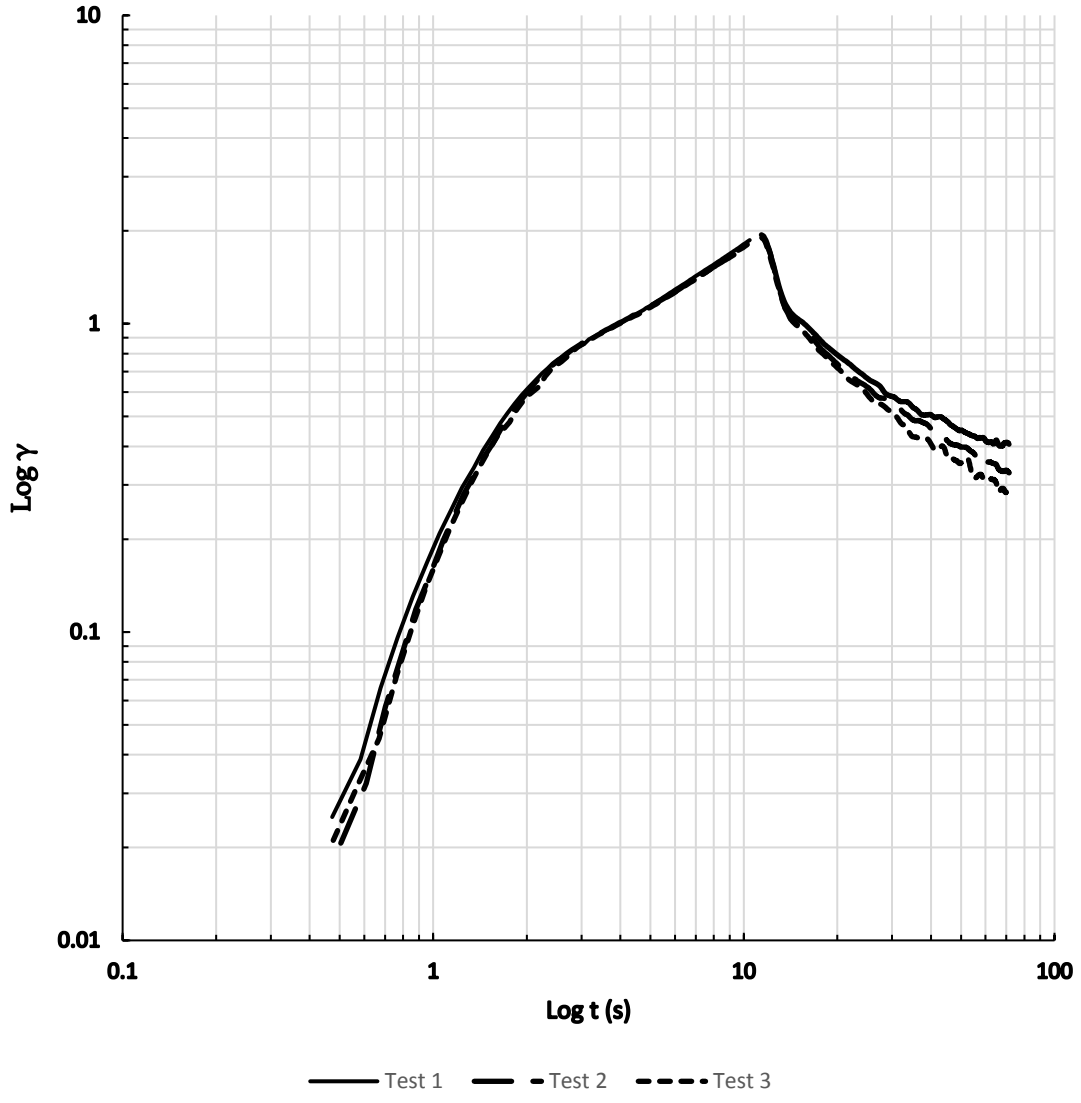

Fig. 4.15 Creep and recovery curves of non/pre-sheared okra (Kagawa) mucilage

Table. 4.12 The list of okra (Kagawa) mucilage basic viscoelasticity information

Okra (Kagawa)	Test 1	Test 2	Test 3
τ_0 (Pa)	0.00884	0.00884	0.00884
η_0 (Pas)	0.06967	0.07272	0.07225
$d\gamma/dt$ (s^{-1})	0.1269	0.1216	0.1224
γ_{e0}	0.5907	0.5981	0.5992
J_e (Pa^{-1})	66.83	67.66	67.79
γ_{rec}	1.535	1.577	1.604
$\gamma_{rec}/\gamma_{max}$ (%)	79.05	82.76	84.59
J_{rec}	173.7	178.3	181.5
J_{rec}/γ_{max} (%)	79.05	82.76	84.59
ψ (Pas^2)	0.6487	0.7156	0.7077
λ (s)	4.656	4.9	4.897
G (Pa)	0.01496	0.01478	0.01475

4.4 Oscillation

4.4.1 Oscillation stress sweep

Oscillation stress sweep was shown in figure 4.16. When doing the oscillation frequency sweep the stress must under the linear viscoelastic range, to okra mucilage, the stress range must below 80mPa.

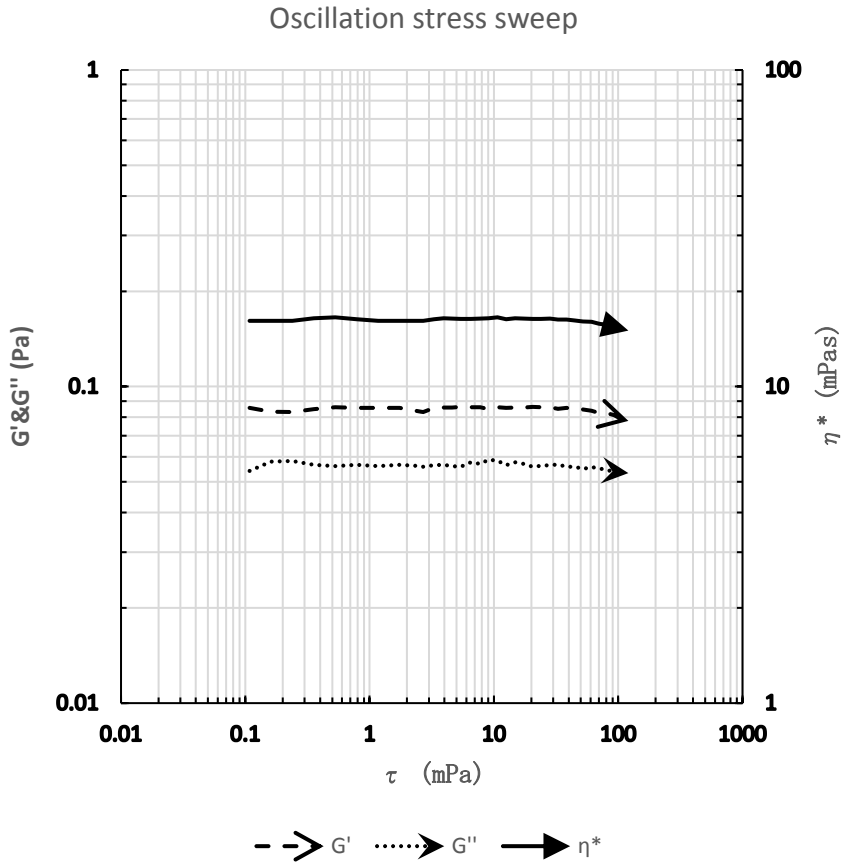

Fig 4.16 Linear viscoelastic range of okra (Kouchiken) mucilage

4.4.2 Oscillation frequency sweep

Small-stress deformation experiments were held after a frequency sweep, as to make sure that all measurements were well within the linear viscoelastic region for the stress used. The result of oscillation frequency sweep was shown in Fig. 4.17.

The storage moduli were higher than the loss moduli in both non-sheared okra mucilage and pre-sheared okra mucilage. Thus, to both okra mucilage and pre-sheared one, in this range, the stored energy of okra mucilage was higher than the energy dissipated as heat.

However, in the figure 4.17, a lower elastic modulus curve was found in pre-sheared okra mucilage curve compared with the non-sheared one. On the opposite, the viscous modulus curve

became a bit higher. That hints the shear history effect would weaken the elastic behavior of the okra mucilage and strengthen the viscous behavior.

To both non/pre-sheared okra mucilage, at shear rate a little bit after $10S^{-1}$, the storage moduli and loss moduli were trying to crossover. It indicated commencement of chain entanglement and becoming unstable. In another word, the time scales involved in the experiments were shorter than the relaxation times of the macromolecular entities, thus after 10rad/s, the motion would irreversibly alter their networks. This result double checked that shear rate $10S^{-1}$ was the transition point of okra mucilage.

For many materials, linear data G' and G" is relatively easy to measure for various angular frequencies $\omega(rad/s)$. When applicable, the shear viscosity can be estimated by applying the Cox-Merz empirical rule. This empirical rule states that the modulus of the complex viscosity matches the nonlinear shear viscosity, as shown in the following equation.

$$\eta(\gamma)=\eta^*(\omega) \quad \& \quad N1=2G' \quad (32)$$

For all the okra mucilage values at a shear rate from $0.1S^{-1}$ to $10S^{-1}$ have no transient effects due to flow or oscillation start-up, inertia, or thixotropy which are under steady state, thus the empirical Cox-Merz rule was suggested to be valid.

Thus, the complex viscosity and steady viscosity were plotted on the Fig. 4.17. The complex viscosity was almost fit with the steady viscosity for both non/pre-sheared okra mucilage. Meanwhile, the complex viscosity curve of both non/pre-sheared okra mucilage were basically coincided. That hinted that the altered rheological property by the shear history effect would not display until the shear rare reach a limit where the networks could fully stretch out.

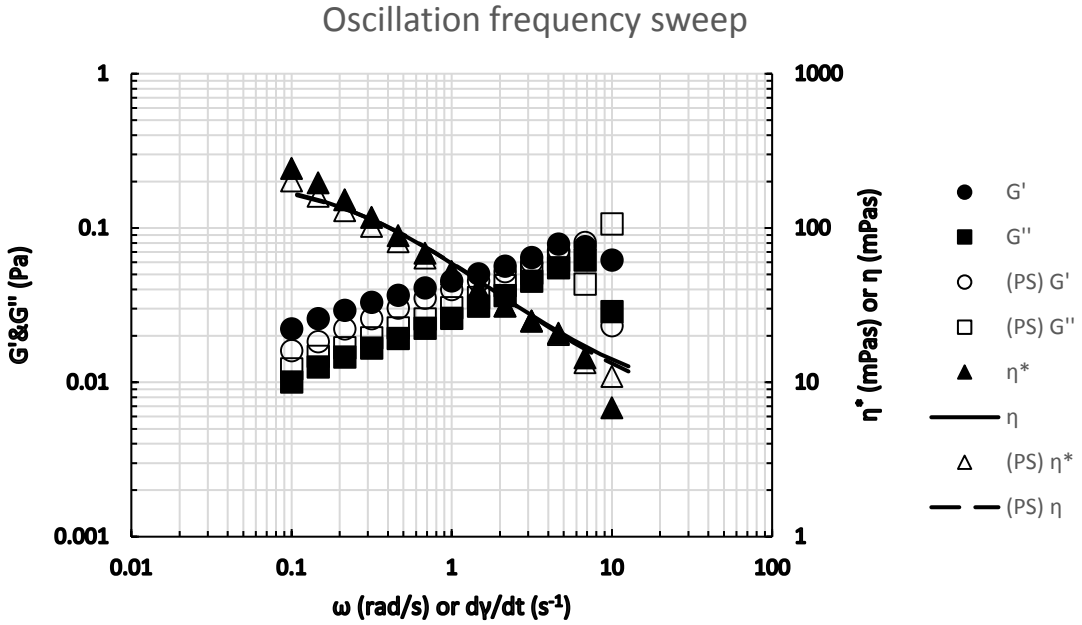

Fig 4.17 Frequency sweep of non/pre-sheared okra (Kouchiken) mucilage

4.5 Stress ramp experiment

For pseudoplastic fluids the viscosity is not affected by the amount of time the shear stress is applied as these fluids are non-memory materials i.e. once the force is applied and the structure is affected, the material will not recover its previous structure (Schramm, 2000). Thus, the hysteresis loop under a shear rate from 10s-1 ~ 1000s-1 of okra mucilage was tested. From the Fig. 4.18 to Fig. 4.20, the thixotropic behavior of okra mucilage was found. The power law was used to fit the stress and shear rate relationship, so that the thixotropic parameter could be calculated easily. From the table 4.13 to Fig.4.15, the thixotropic property was studied. The thixotropic indexes of each loop were posted on the Fig. 4.21.

$$S_{thix}\% = \left[\frac{(S_{fwd} - S_{bw}(t))}{S_{fwd}}\right] * 100\% \quad \textbf{(13)}$$

Table. 4.13 Parameters of okra (Thai) mucilage hysteresis loop (60s/loop)

Okra 5	Test	loop time (s)	k (mPas^n)	n	R^2	S_{thix} (mPa/s)	S_{thix}
1st loop	1st Forward	120	11.17	0.88	0.97	1812000	53%
	1st Backward		14.15	0.79	0.99		
2nd loop	2nd Forward	120	15.18	0.86	0.86	1.93E+06	57%
	2nd Backward		15.31	0.78	0.78		
3rd loop	3rd Forward	120	16.4	0.84	0.84	2.01E+06	59%
	2nd Backward		9.48	0.84	0.84		

Table. 4.14 Parameters of okra (Thai) mucilage hysteresis loop (120s/loop)

Okra 5	Test	loop time (s)	k (mPas^n)	n	R^2	S_{thix} (mPa/s)	S_{thix}
1st loop	1st Forward	120	11.17	0.88	0.97	941000	32%
	1st Backward		14.15	0.79	0.99		
2nd loop	2nd Forward	120	15.18	0.86	0.86	1.00E+06	34%
	2nd Backward		15.31	0.78	0.78		
3rd loop	3rd Forward	120	16.4	0.84	0.84	1.21E+06	41%
	2nd Backward		9.48	0.84	0.84		

Table. 4.15 Parameters of okra (Thai) mucilage hysteresis loop (240s/loop)

Okra 5	Test	loop time (s)	k (mPas^n)	n	R^2	S_{thix} (mPa/s)	S_{thix}
1st loop	1st Forward	120	11.17	0.88	0.97	531000	20%
	1st Backward		14.15	0.79	0.99		
2nd loop	2nd Forward	120	15.18	0.86	0.86	8.60E+05	32%
	2nd Backward		15.31	0.78	0.78		
3rd loop	3rd Forward	120	16.4	0.84	0.84	1.49E+06	56%
	2nd Backward		9.48	0.84	0.84		

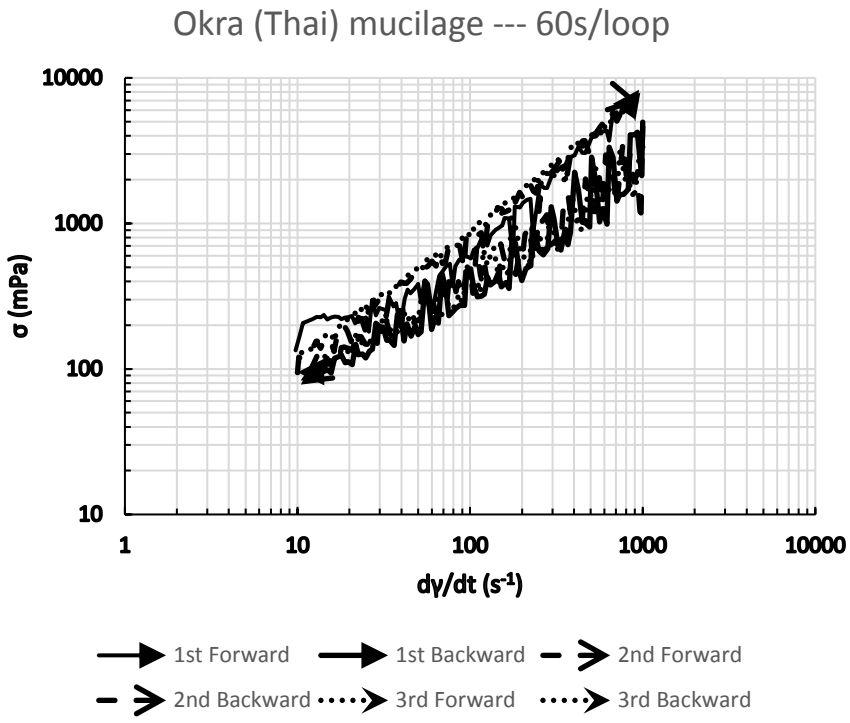

Fig. 4.18 Stress ramp (60s/loop) test of okra (Thai) mucilage

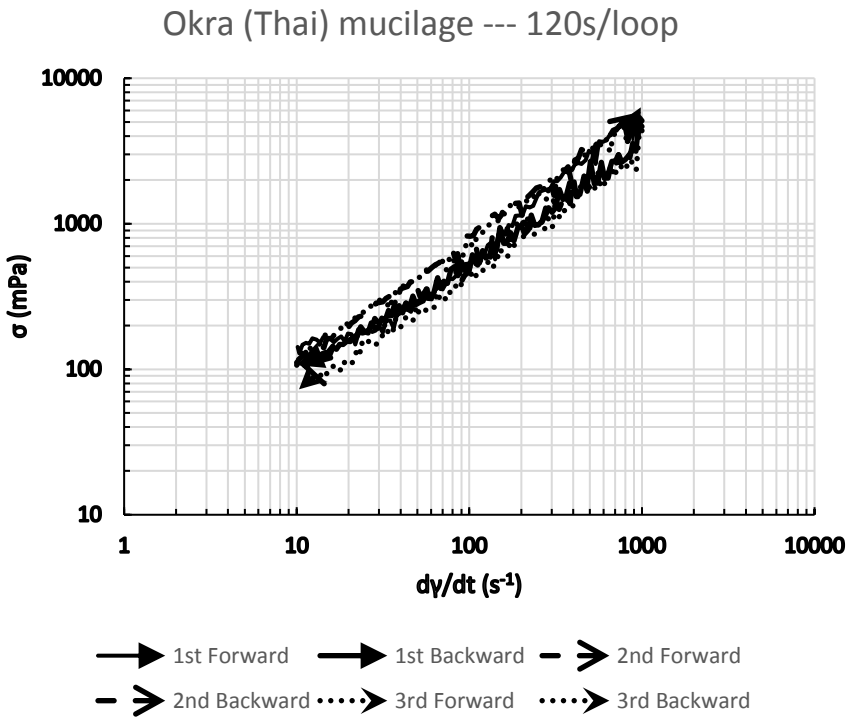

Fig. 4.19 Stress ramp (120s/loop) test of okra (Thai) mucilage

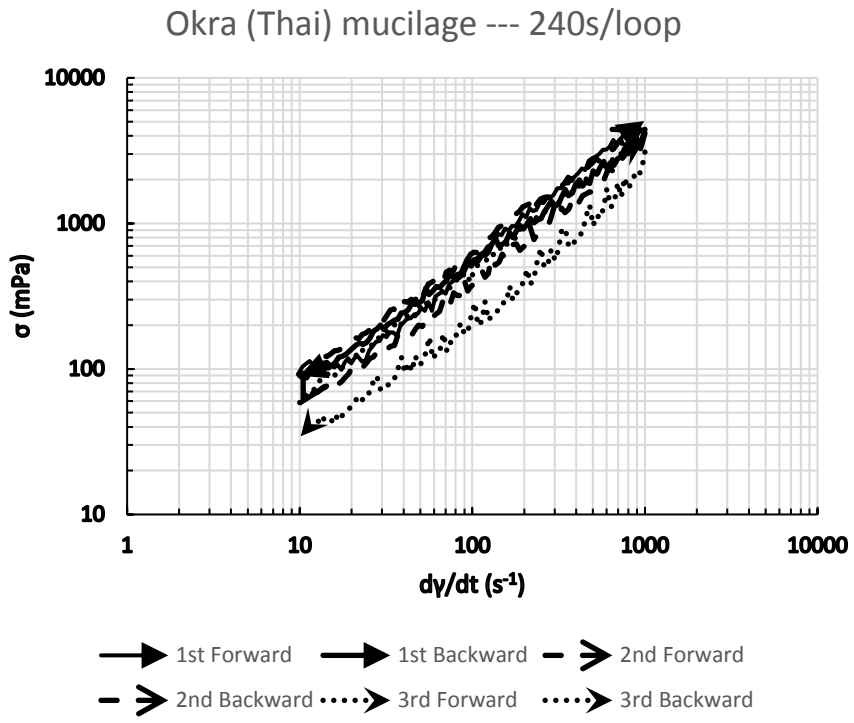

Fig. 4.20 Stress ramp (240s/loop) test of okra (Thai) mucilage

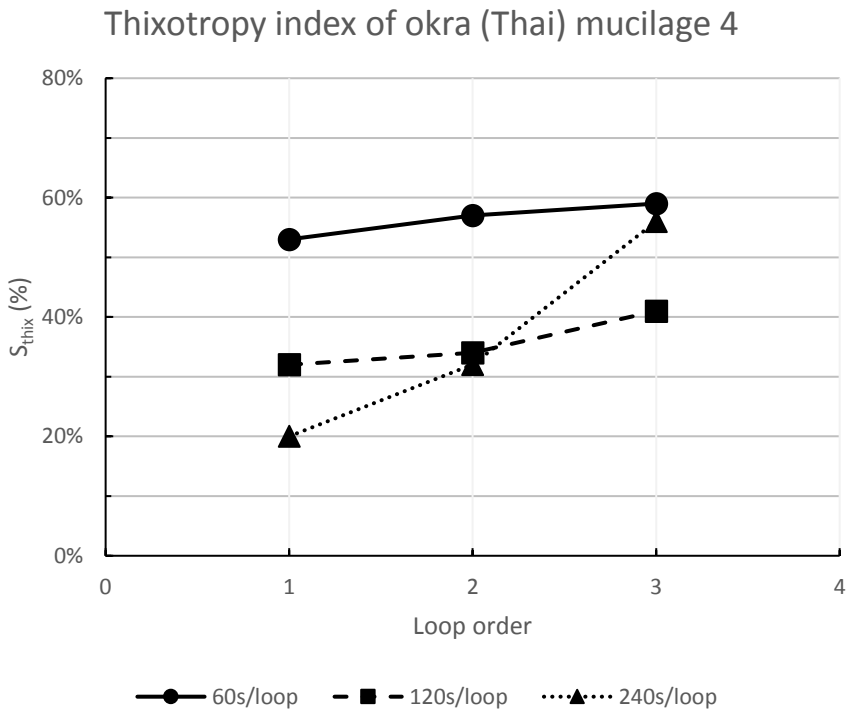

Fig. 4.21 Thixotropy index of each okra (Thai) mucilage ramp tests

According to Fig. 4.21, it showed that the thixotripic index was increasing as the loop's order increasing. In another word, the increasing of shearing time was favorited by the stronger time dependence behavior. It proved that the okra mucilage had a close relationship with the shear history effect.

But, most interesting points in the Fig. 4.21 were the last two spots of the last curve. These two spots' growth rate were far higher than the former two curve's.

To discuss this strange behavior, the structure parameters were introduced.

$$\boldsymbol{K = 1 - \left(\frac{\mu_\infty}{\mu_0}\right)^{0.5}} \quad \textbf{(15)}$$

$$\boldsymbol{\lambda = (1 - \left(\frac{\mu_\infty}{\mu}\right)^{0.5})/K} \quad \textbf{(16)}$$

The viscosity and structure parameter as a function of shearing time were calculated and posted on the Fig. 4.22 to Fig. 4.24.

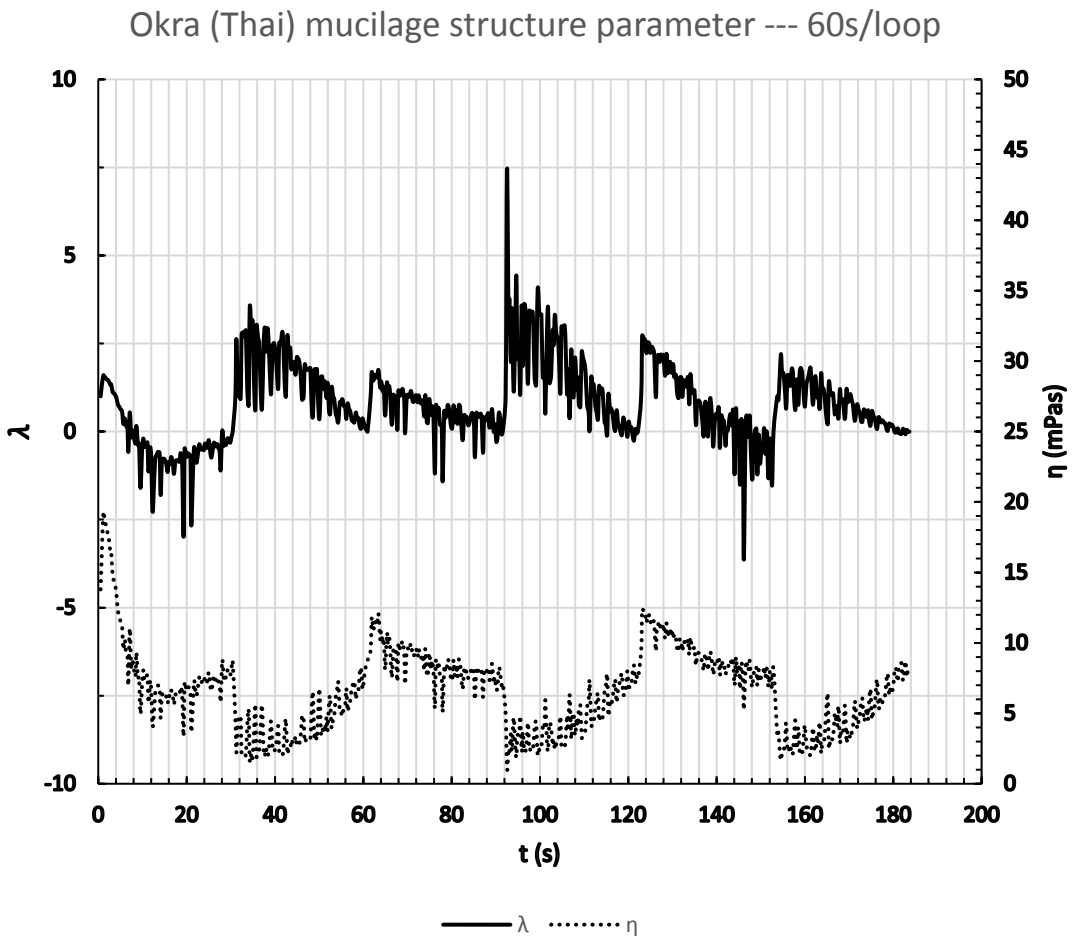

Fig. 4.22 Structure parameter of okra (Thai) mucilage (60s/loop)

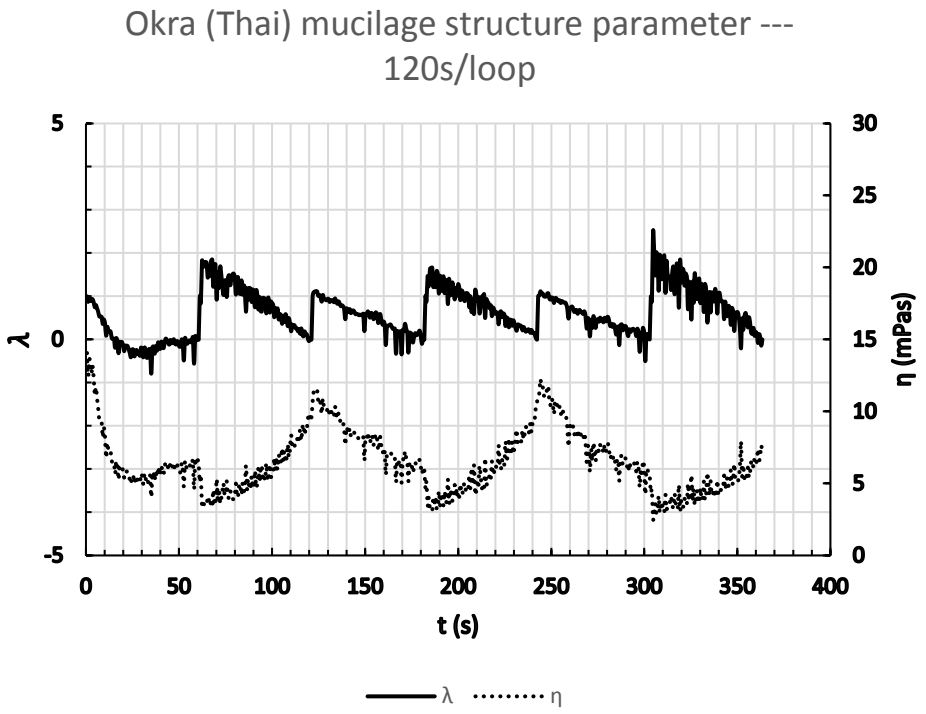

Fig. 4.23 Structure parameter of okra (Thai) mucilage (120s/loop)

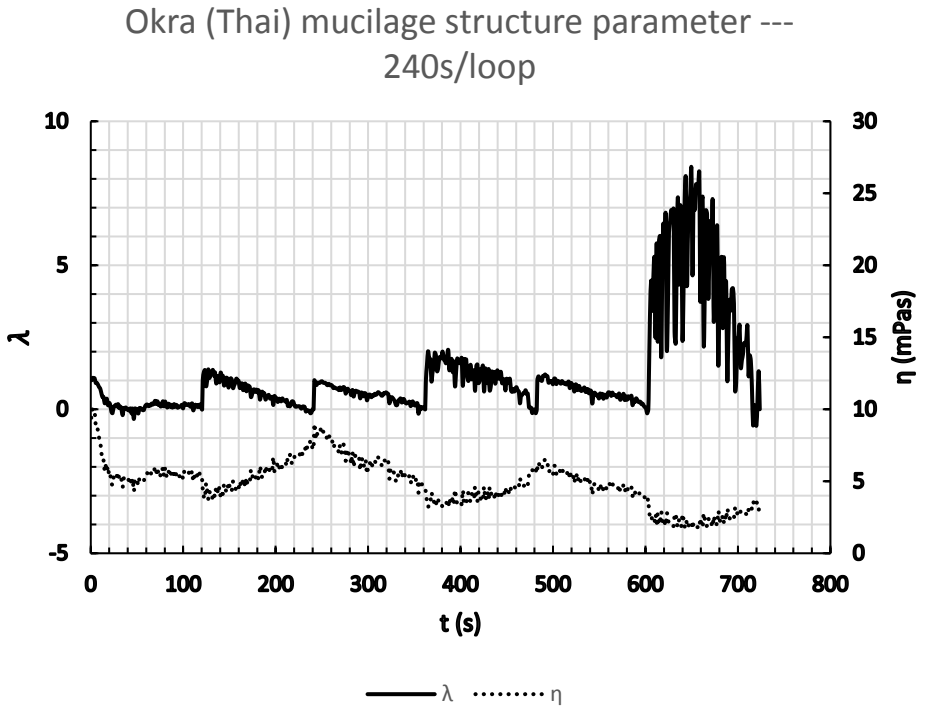

Fig. 4.24 Structure parameter of okra (Thai) mucilage (240s/loop)

From the structure parameter as a function of the developing time, we would find that to the okra mucilage's structure would break down at first (first ramping up, $d\lambda/dt<0$) and arrive at equilibrium zone around 50~60s^{-1} (first ramping up, $d\lambda/dt=0$). Then, as the fluid flows, either the ramping up or the ramping down curves showed that the structure of okra mucilage kept breaking down, except the last curve of the 240s loop.

This observation might related to the probability of inter-particle friction and collision increased with rising concentration reported by (Liu et al. 2012). And it had a close relationship with the increased viscous forces and energy consumption reported by (Wei et al. 2015). In this case, it suggested that when the shearing history was enough long, the okra biopolymers number concentration would increase. This might give okra mucilage structure much more chance to interact with each other. In another word, when the cone's rotation speed was suddenly decreased, a part of the okra mucilage structure could not follow well. This part of structures would still keep at high shear strain speed rotation. Then it might contradict to the other parts of okra mucilage structure (Fig. 4.25). So that, the accumulation of biopolymers would happen. That let the last structure parameter curve of the okra mucilage showed building up (240s loop, the beginning of 3rd ramping down, $d\lambda/dt>0$) for a short time. It hinted that when the shearing history was enough long, the mucilage structures would be turn from large groups into small crops.

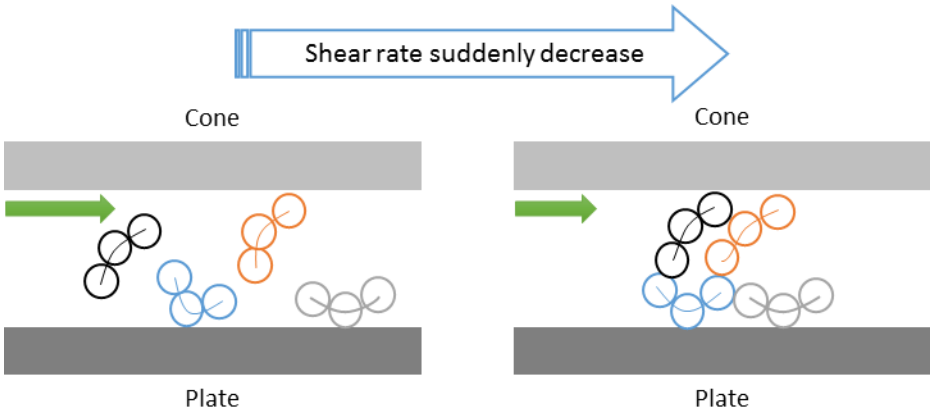

Fig. 4.25 Transitory structure building up of okra mucilage

4.6 Rotation time curve

4.6.1 Development curve at shear rate $10s^{-1}$

From the Fig. 4.27 ~ Fig. 4.31, the result of shear stress's development curve at fix shear rate $10s^{-1}$ were displayed. In those figures, the cycling structure unit were found (Fig. 4.26). To describe the cycling units, a group of parameters were introduced.

Where:

t_0 is the time that the structure of okra mucilage starts to develop (decreasing part at beginning),

n is the number of cycling units "M" during the testing time,

t_λ is the period time of a cycling unit,

f is the frequency of the cycling units,

σ_λ is the average amplitude of the cycling units.

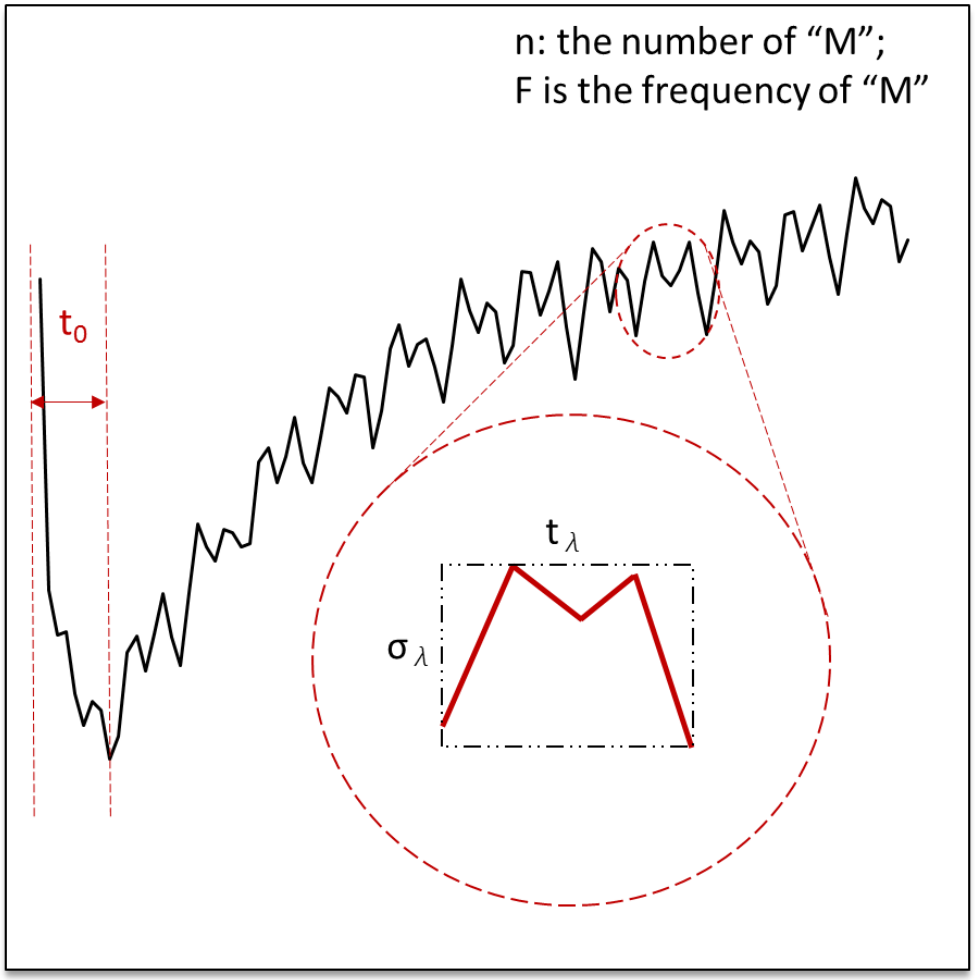

Fig. 4.26 The cycling unit of the okra mucilage rotation time curve at $10s^{-1}$

Table. 4.16 Parameters of Okra (Philippines) mucilage rotation time curves at $10s^{-1}$

Okra 4	t_0 (s)	n	t_λ (s)	f (Hz)	σ_λ (mPa)
Test 1	43	13	36.00	0.03	9
Test 2	48	13	36.00	0.03	9
Test 3	48	13	36.00	0.03	8

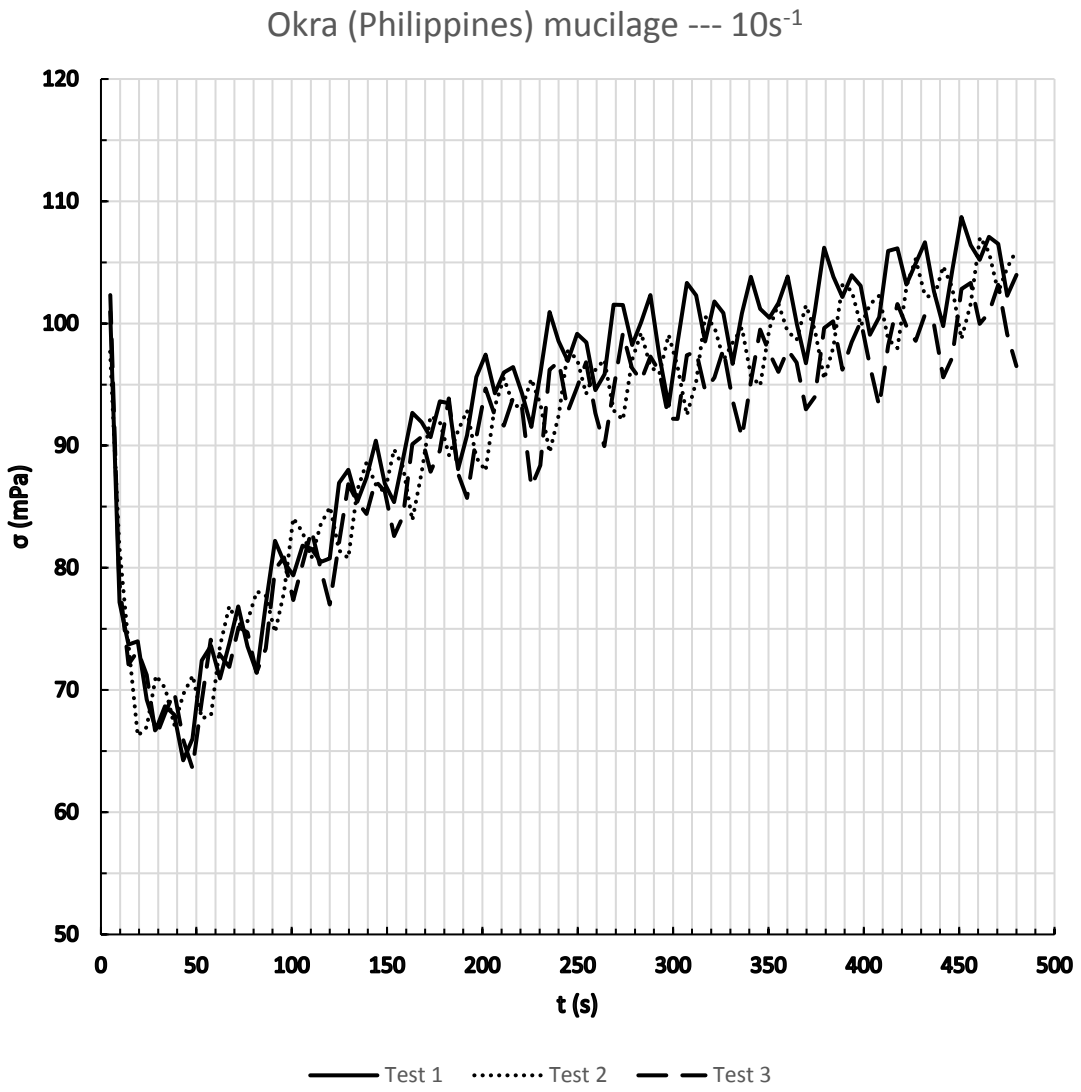

Fig. 4.27 Okra (Philippines) mucilage rotation time curves at $10s^{-1}$

Table. 4.17 Parameters of needle pre-sheared okra (Philippines) mucilage rotation time curves at $10s^{-1}$

Okra 4	t_0 (s)	n	t_λ (s)	f (Hz)	σ_λ (mPa)
Test 1	14	14	35.85	0.03	8
Test 2	14	14	35.85	0.03	8
Test 3	19	13	36.00	0.03	10

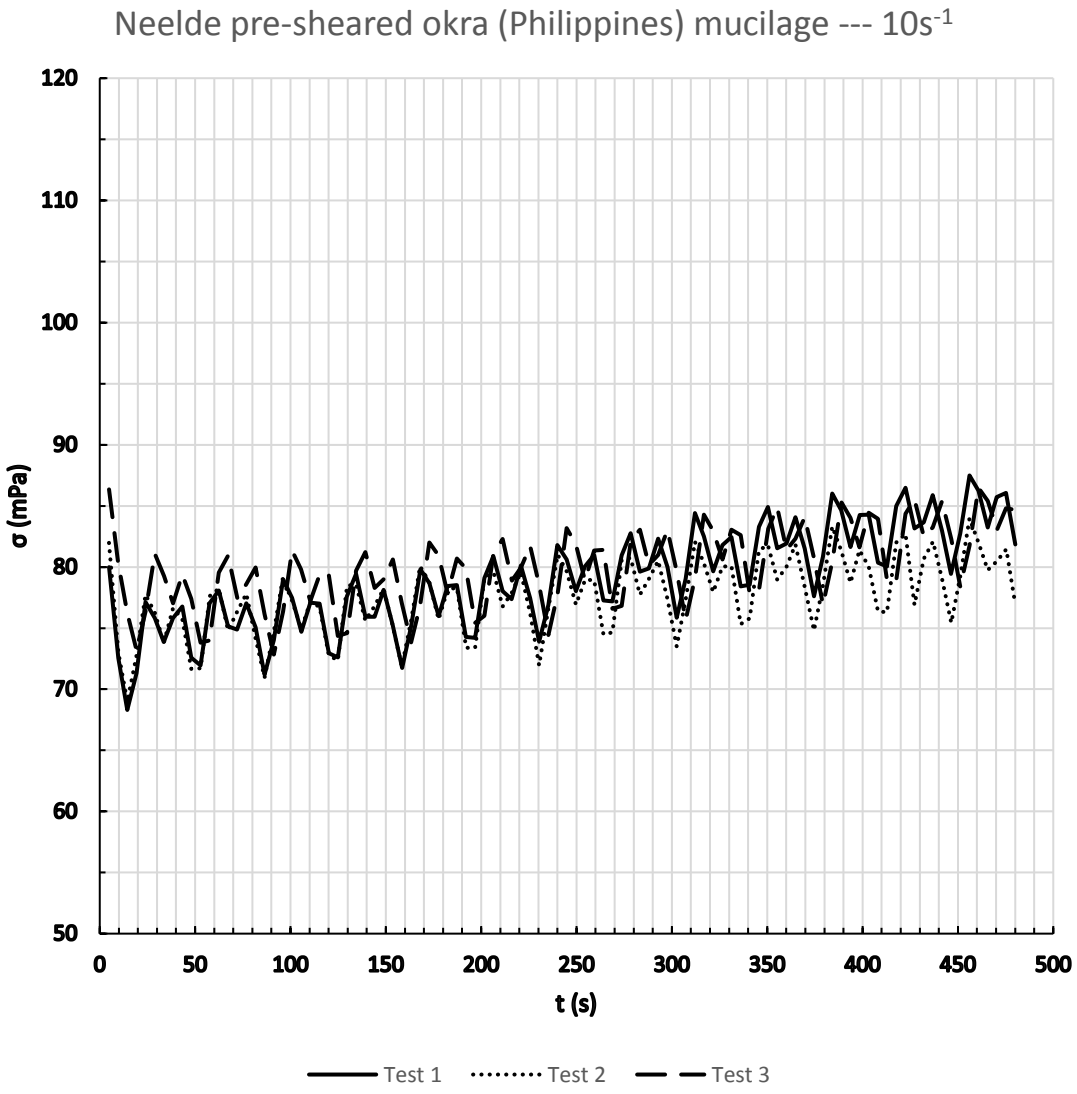

Fig. 4.28 Needle Pre-sheared okra (Philippines) mucilage rotation time curves at $10s^{-1}$

Table. 4.18 Parameters of 24h storage okra (Philippines) mucilage rotation time curves at $10s^{-1}$

Okra 4	t_0 (s)	n	t_λ (s)	f (Hz)	σ_λ (mPa)
Test 1	33	13	36.00	0.03	6
Test 2	24	13	36.00	0.03	6
Test 3	38	13	36.00	0.03	5

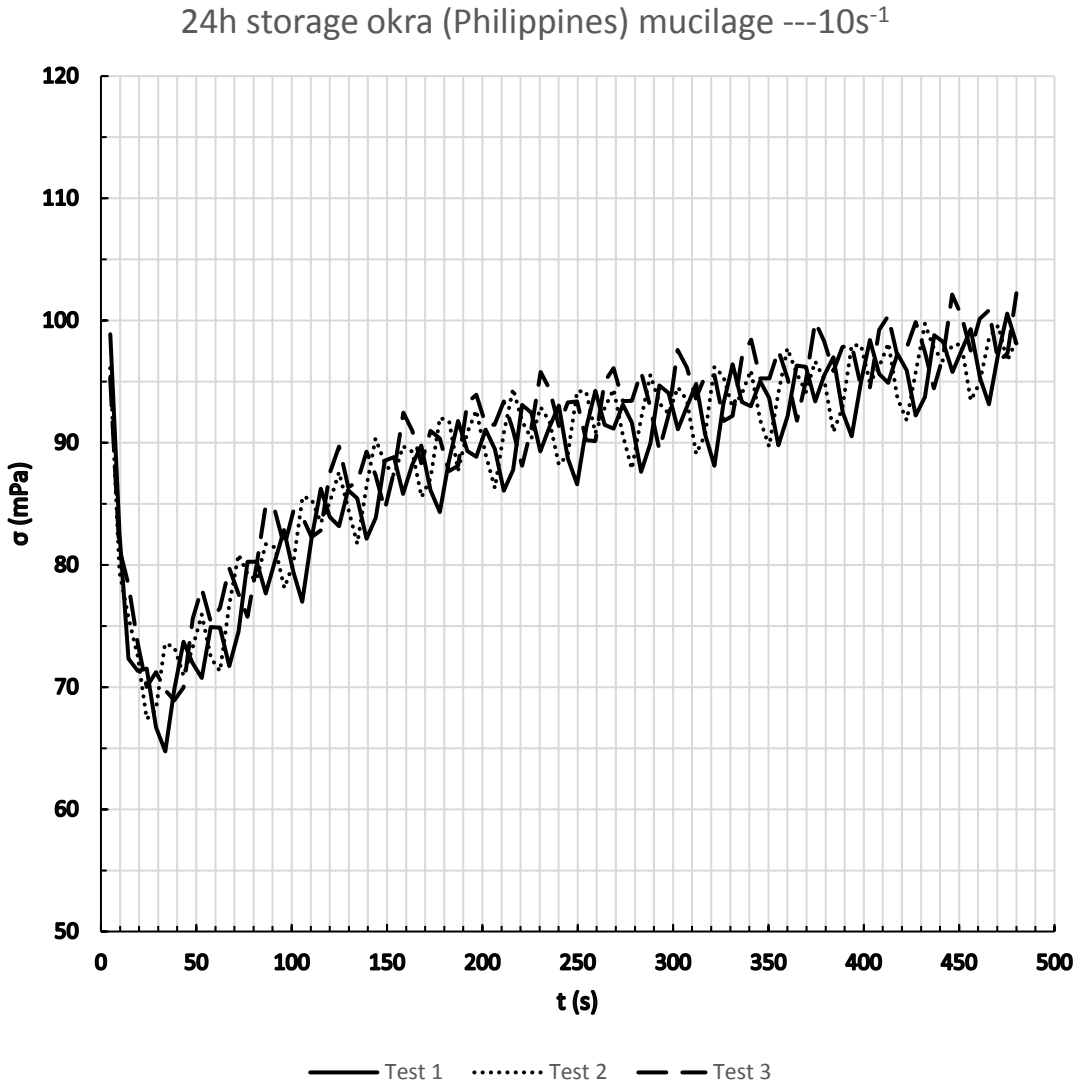

Fig. 4.29 24h storage okra (Philippines) mucilage rotation time curves at $10s^{-1}$

Table. 4.19 Parameters of 24h storage cone and plate sheared okra (Philippines) mucilage rotation time curves at $10s^{-1}$

Okra 4	t_0 (s)	n	t_λ (s)	f (Hz)	σ_λ (mPa)
Test 1	19	13	36.00	0.03	7
Test 2	19	13	36.00	0.03	6
Test 3	24	13	36.00	0.03	7

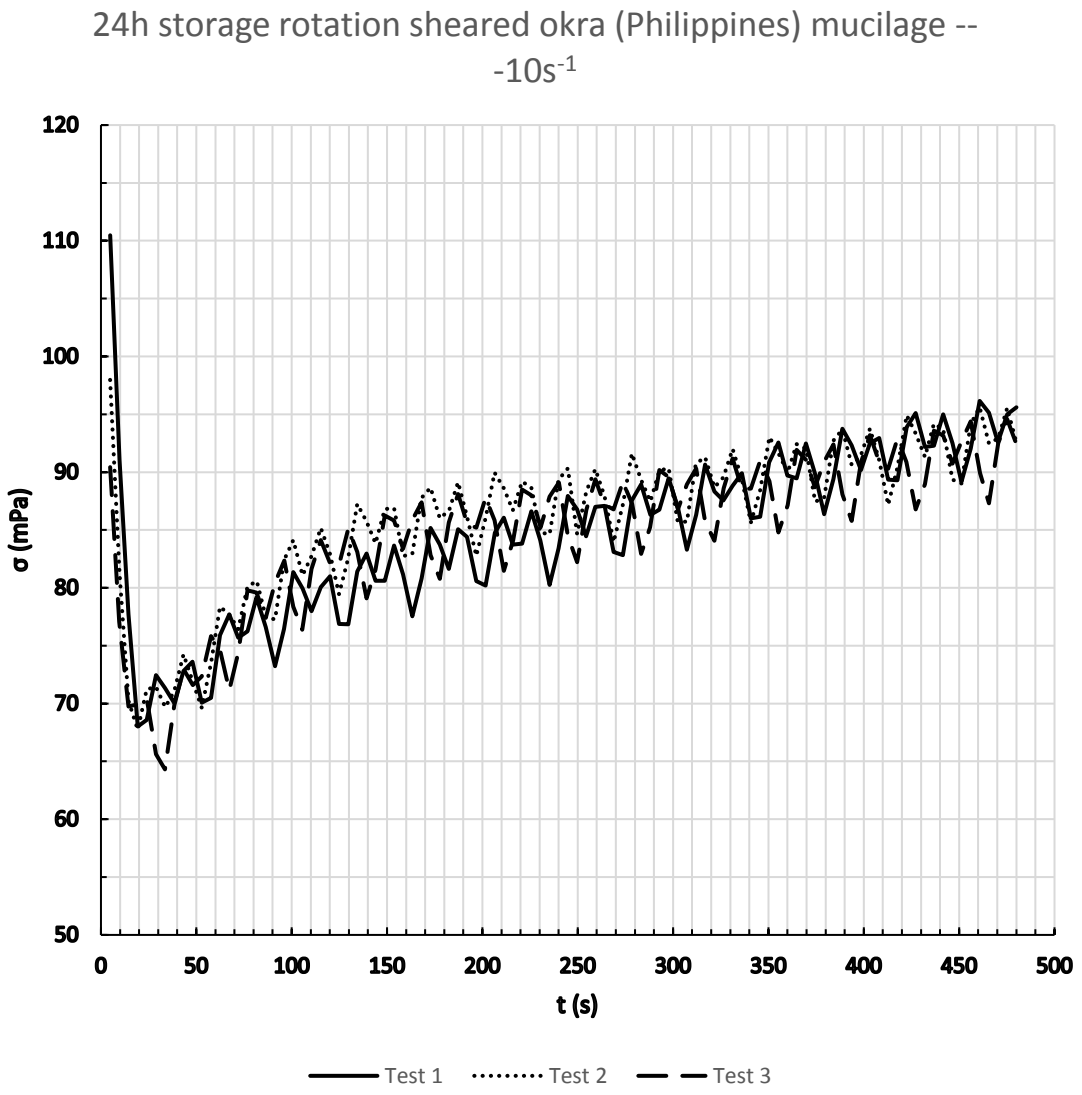

Fig. 4.30 24h storage cone and plate sheared okra (Philippines) mucilage rotation time curves at $10s^{-1}$

Table. 4.20 Parameters of 24h storage needle pre-sheared okra (Philippines) mucilage rotation time curves at $10s^{-1}$

Okra 4	t_0 (s)	n	t_λ (s)	f (Hz)	σ_λ (mPa)
Test 1	5	14	35.77	0.03	6
Test 2	9	14	34.69	0.03	6
Test 3	4	14	35.85	0.03	6

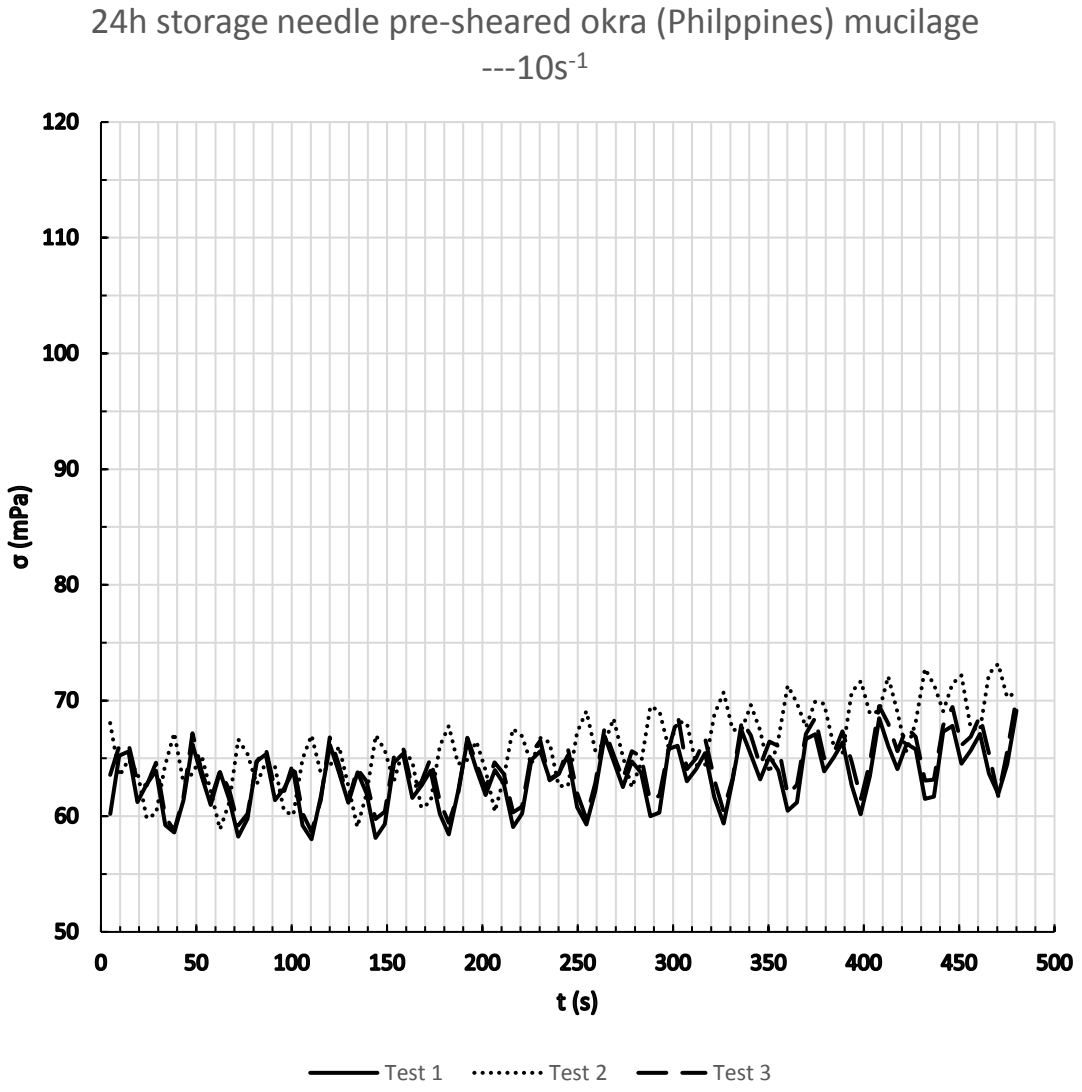

Fig. 4.31 24h storage needle pre-sheared okra (Philippines) mucilage rotation time curves at $10s^{-1}$

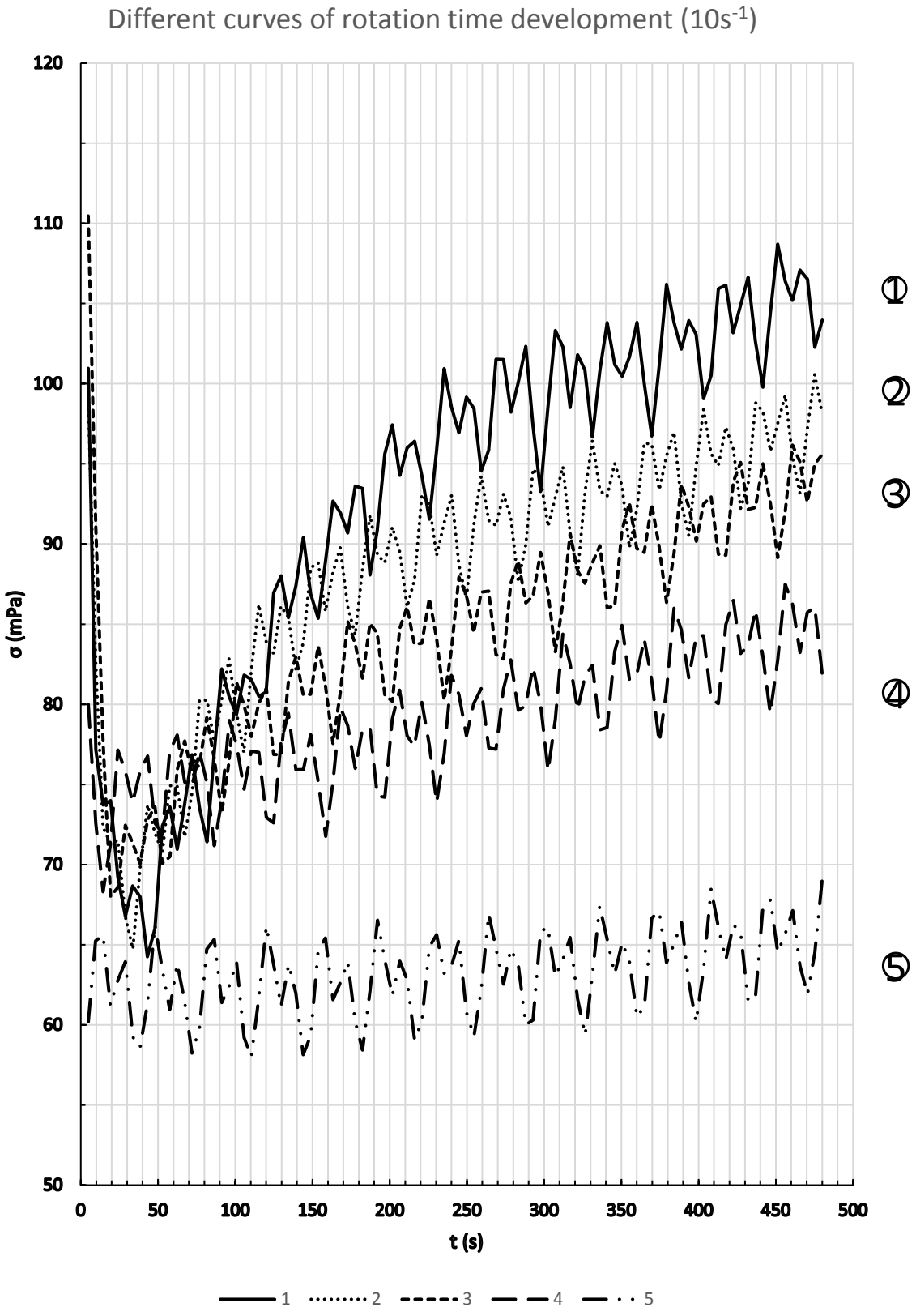

Fig. 4.32 Different curves of rotation time development ($10s^{-1}$)

To Fig. 4.27 (curve 1 shown in Fig. 4.32), given the all normal conditions to the experiment, the constant shear rate would drug the okra mucilage to flow.

When the shear rate was not high enough, the cycling units “M” shape existed. That hinted the biopolymers interacted with themselves during the mucilage’s flowing by round trip. This property was described as that the structure of the aggregates between some repeating process of destruction, reconstruction and agglomeration in report (Wang et al. 2011).

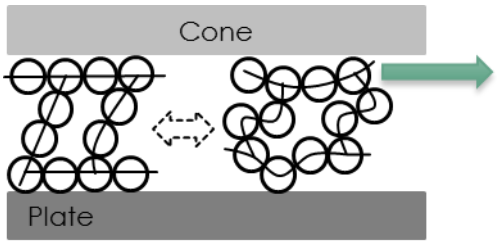

Fig. 4.33 The biopolymer under reconstruction of okra mucilage

In addition, according to the viscoelastic theory, the curve before the time t_0 kept linear declining. It was because that the okra mucilage’s elastic element part ($\sigma_{elastic} \propto \int d\dot{\gamma}/dt$) needed time to respond to the sudden deformation caused by the constant shear rate which was higher than this yield strain speed. Thus, at the beginning, the whole shear stress response shown the linear viscous ($\sigma_{viscosity} \propto d\dot{\gamma}/dt$). After that, the whole development curve showed both okra mucilage’s elastic and viscous elements was developing under the constant strain speed. Hence, the development curve as the function of time showed an exponential function trend ($\sigma(t) = \sigma_{elasticity} + \sigma_{viscosity}$; To Maxwell model: $\sigma(t) = \mu\dot{\gamma}(1 - e^{-\frac{Et}{\mu}})$).

- Okra mucilage comparing with the needle pre-sheared okra mucilage (Fig. 4.27 & Fig. 4.28; or Curve 1&4 in Fig 4.32)

It is not hard to find that the t_0 was disappearing in the development curves of needle presheared okra mucilage. It hinted that their elastic elements would be dissolved after the needle giving the structure a shear history effect. Meanwhile, the linear increasing behavior of the whole curve also proved that the elastic element was dissipating. This loose in elasticity might be due to the irreversible rearrangement of the flowing constituents of the aggregates (Jitianu et al. 2009).

However, units' repeating deforming property of the pre-sheared okra mucilage was not disappeared, because the “M” size units still existed.

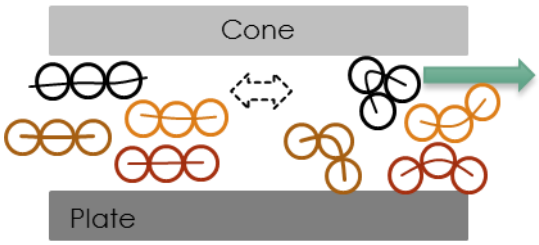

Fig. 4.34 The biopolymer under reconstruction of pre-sheared okra mucilage

On the other hand, the number of "M" shape structures had a bit higher after the shear history effect. It could be explained that the shear history effect let the biopolymers have more chances to interact. Thus, the number would be increased.

- Okra mucilage comparing with the 24h storage okra mucilage (Fig. 4.27 & Fig. 4.29; or Curve 1&2 in Fig. 4.32)

The decreased σ_λ provided the evidence that the okra mucilage had lost the activity of its biopolymers. Meanwhile, the lower shear stress curve and a little decrease in the t_0 also hinted that okra mucilage was losing its activity after one day storage. That was because the enzymatic hydrolysis process (biodegradation) would have a sensitive relationship with structure and viscoelastic energy (Tayal et al. 1999).

- 24h storage series group (Fig 4. 29, Fig 4. 30, Fig 4. 31; or Curve 2&3&5 in Fig. 4.32)

From the three different groups different from the treatments, all of them showed that the repeating reconstruction parameter $\sigma\lambda$ had a close value. This gave a view that the okra mucilage biopolymers' interaction activity would not be influenced by the small magnanimity strain speed applied, but the okra mucilage's biological activity did.

Moreover, the t_0 of the needle sheared okra mucilage was the shortest among all these three tests. The cone and plate sheared okra mucilage t_0 was a bit lower than the standard 24h storage okra mucilage t_0's value. That showed the cone and plate sheared okra mucilage's elastic element may not disappear as far as the needle sheared one, but still decreased. In addition, the whole curve's trend also showed that the cone and plate sheared okra mucilage still reserved nearly the most amount of elastic elements. This might because the rotation sheared process's shear history was $10s^{-1}$ for 8min. This intensity level was much lower than the 1min process through needle for average shear rate $13000s^{-1}$.

4.6.2 Development curve at shear rate 500s^{-1}

From the Fig. 4.36 ~ Fig. 4.40, the result of shear stress's development curve at fix shear rate 500s^{-1} were displayed.

In this section, the curves would be divided into 4 parts:

t_1 is the viscoelastic system range under the positive response to large constant shear rate. The structure would develop following the fluid current.

t_2 is the viscoelastic system range that the okra mucilage was trying to maintain the balance by its networks. In this part, the flow would arrive at a short plateau, because the fluid had reached an equilibrium structure following the shear rate. The response stress is σ_2.

t_3 is the viscoelastic system range where the shear degradation happened.

t_4 is the viscoelastic system range would arrive at a new balance plateau, where the elastic element was totally disappearing and the viscous element was the only protagonist of the system. Thus, the curve shows linear and the stable. The responed stress is σ_4.

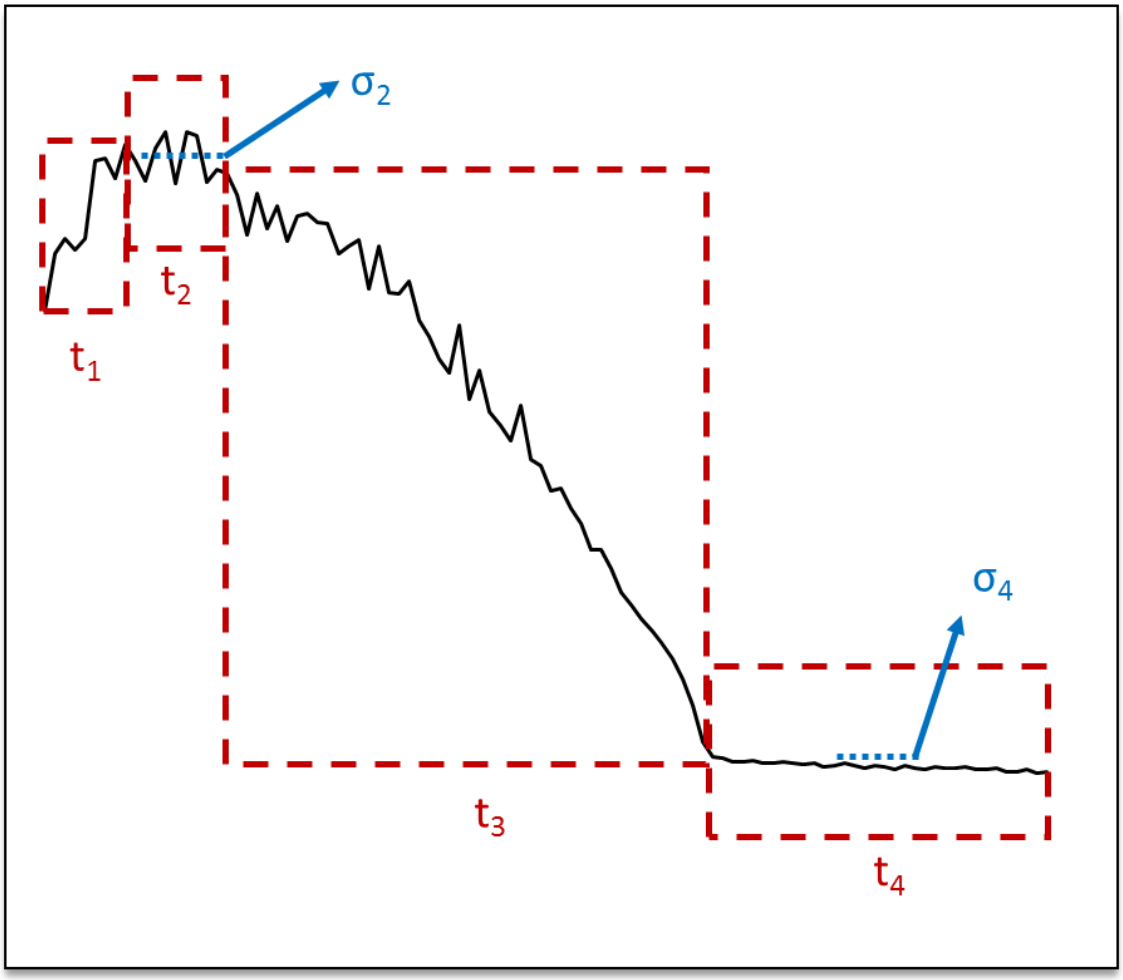

Fig. 4.35 Parameters of rotation time curve at 500s^{-1}

Table. 4.21 Parameters of okra (Philippines) mucilage rotation time curves at $500s^{-1}$

Okra 4	t_1 (s)	t_2 (s)	σ_2 (mPa)	t_3 (s)	t_4 (s)	σ_4 (mPa)
Test 1	33	48	3080	240	159	1070
Test 2	24	67	3100	230	159	1090
Test 3	28	77	3150	216	159	1050

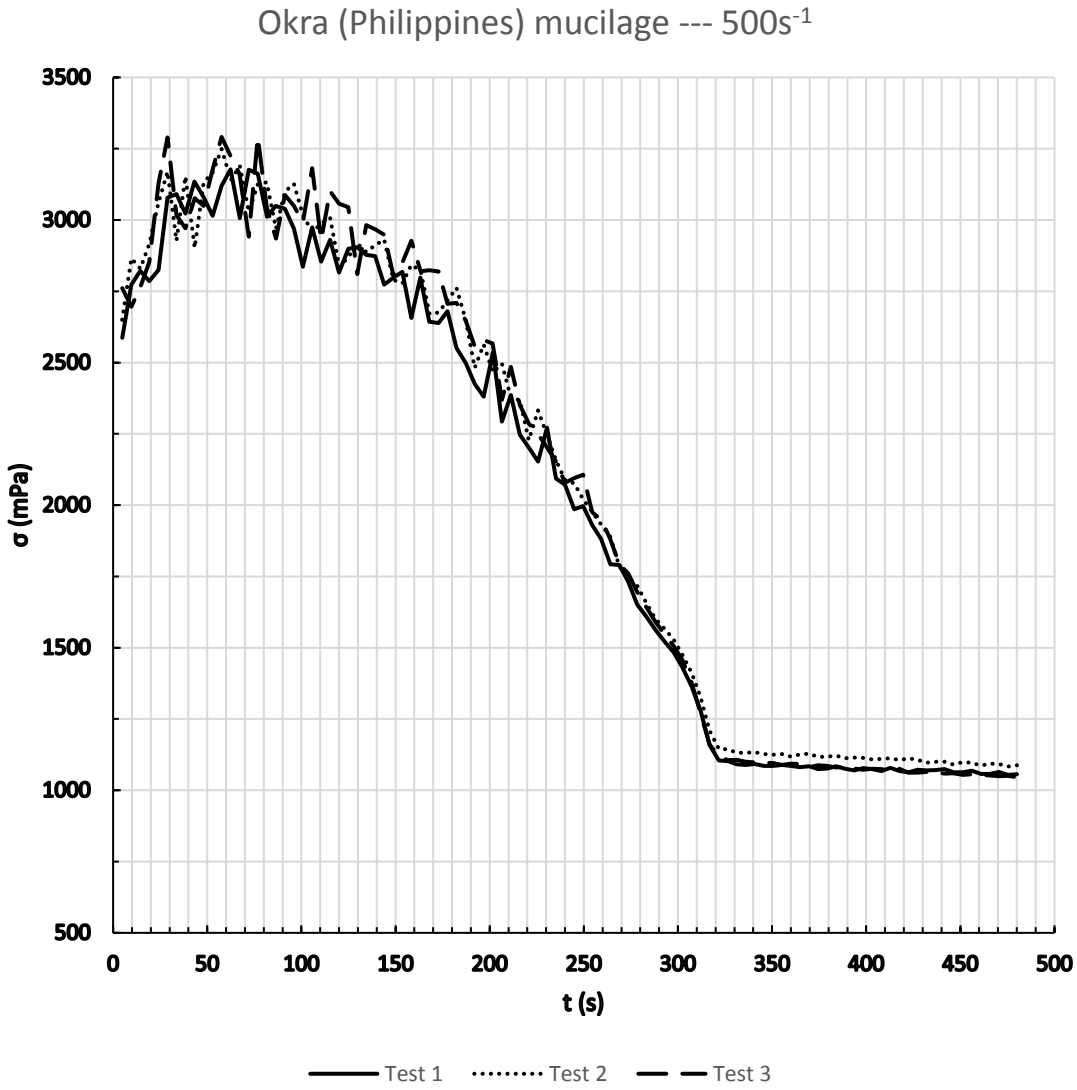

Fig. 4.36 Okra (Philippines) mucilage rotation time curves at $500s^{-1}$

Table. 4.22 Parameters of needle pre-sheared okra (Philippines) mucilage rotation time curves at $500s^{-1}$

Okra 4	t_1 (s)	t_2 (s)	σ_2 (mPa)	t_3 (s)	t_4 (s)	σ_4 (mPa)
Test 1	52	0	1980	116	312	1500
Test 2	52	0	1940	106	322	1550
Test 3	38	29	1880	87	317	1500

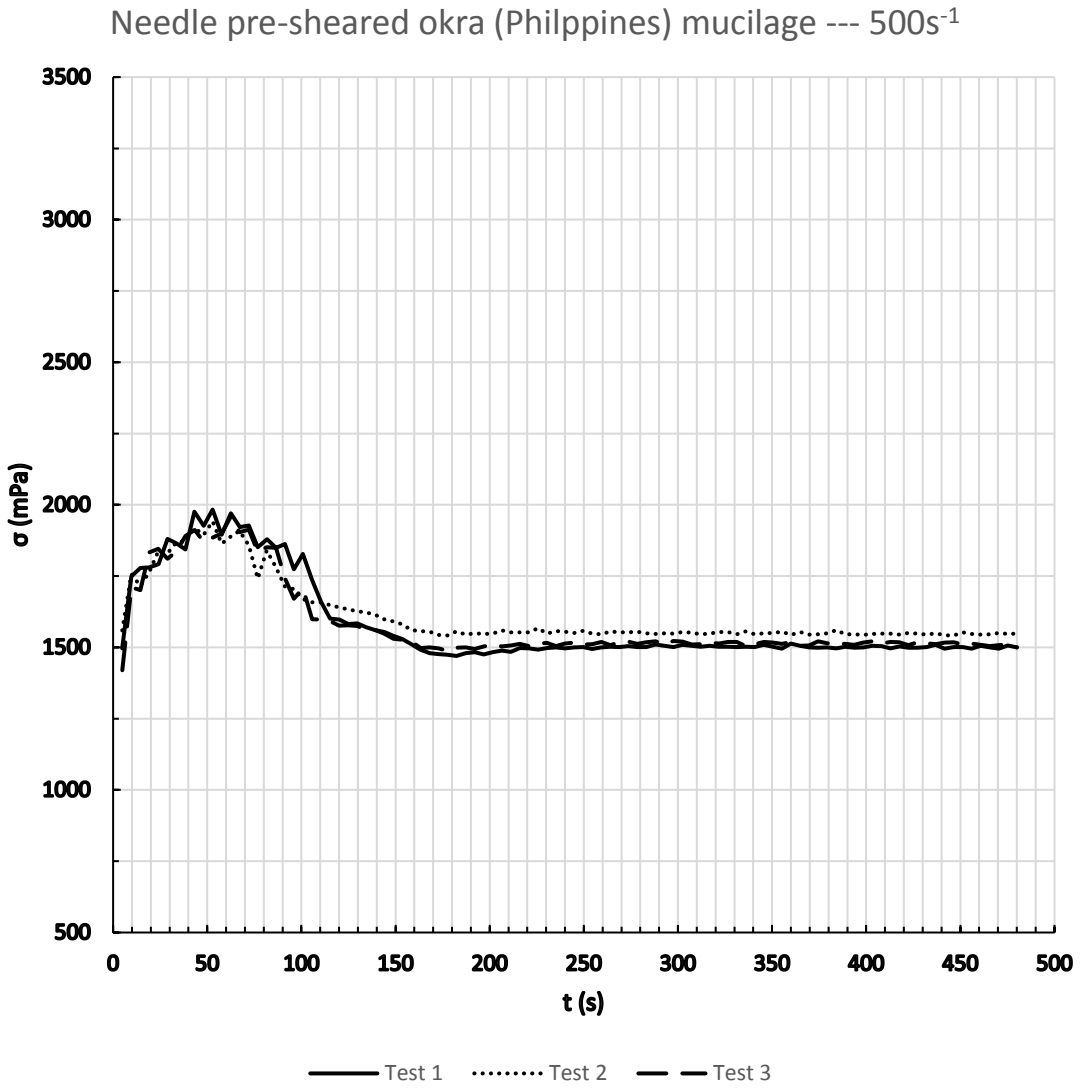

Fig. 4.37 Needle pre-sheared okra (Philippines) mucilage rotation time curves at $500s^{-1}$

Table. 4.23 Parameters of 24h storage okra (Philippines) mucilage rotation time curves at $500s^{-1}$

Okra 4	t_1 (s)	t_2 (s)	σ_2 (mPa)	t_3 (s)	t_4 (s)	σ_4 (mPa)
Test 1	48	76	2670	192	164	980
Test 2	48	72	2680	192	168	1000
Test 3	33	96	2700	187	164	980

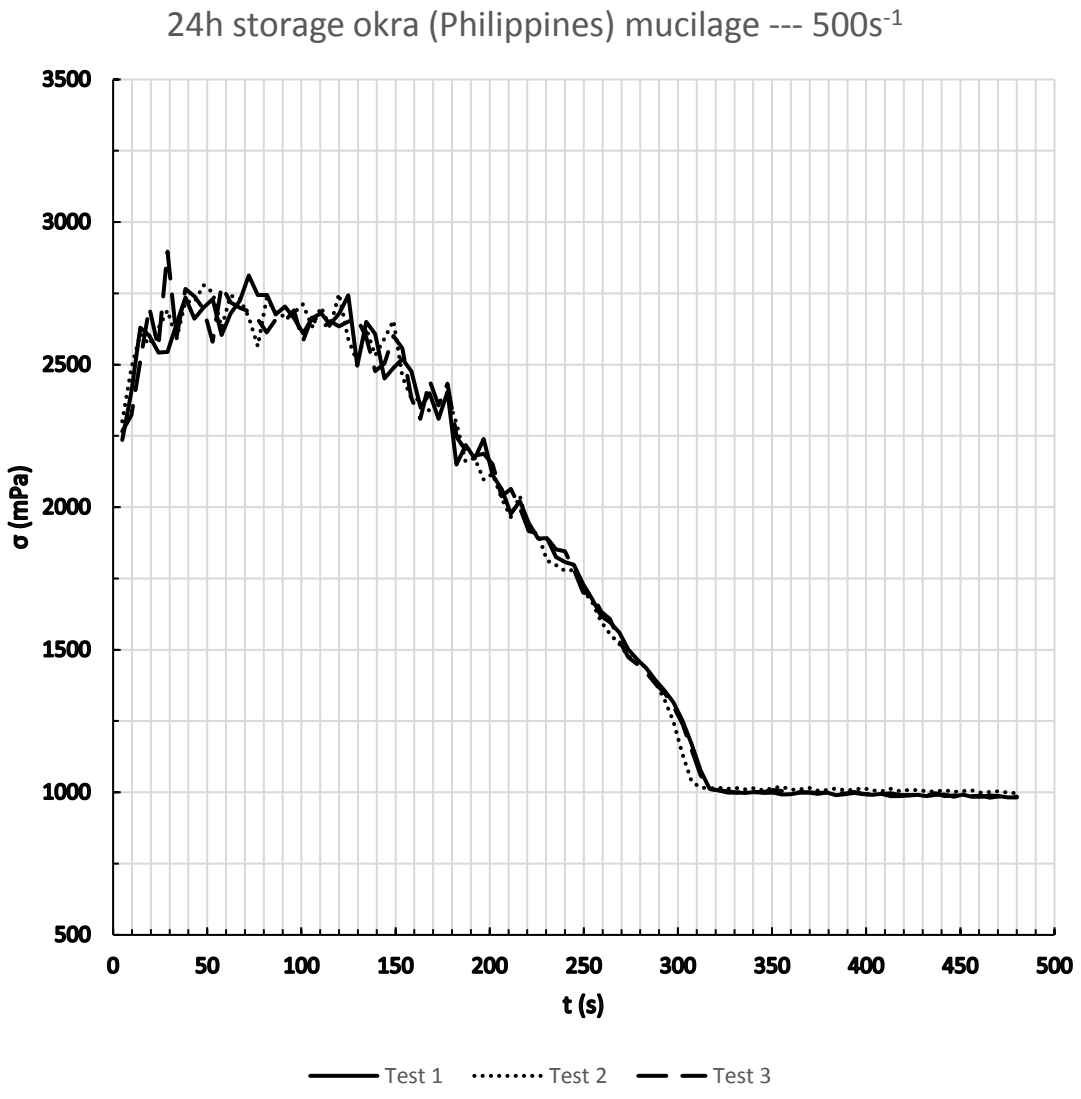

Fig. 4.38 24h storage okra (Philippines) mucilage rotation time curves at $500s^{-1}$

Table. 4.24 Parameters of 24h storage cone and plate sheared okra (Philippines) mucilage rotation time curves at $500s^{-1}$

Okra 4	t_1 (s)	t_2 (s)	σ_2 (mPa)	t_3 (s)	t_4 (s)	σ_4 (mPa)
Test 1	57	10	2290	197	216	1200
Test 2	57	29	2240	168	226	1200
Test 3	24	52	2250	188	216	1190

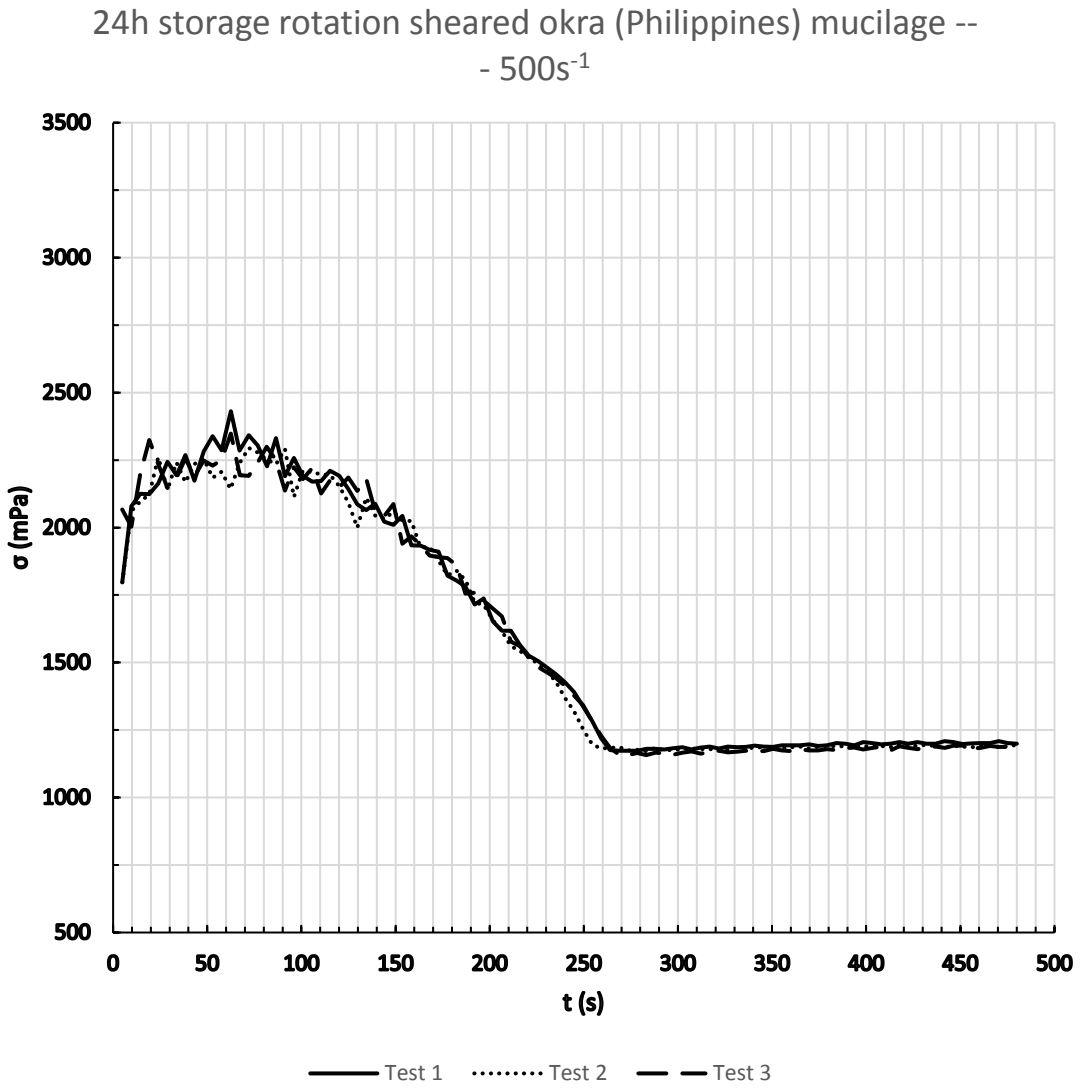

Fig. 4.39 24h storage cone and plate sheared okra (Philippines) mucilage rotation time curves at $500s^{-1}$

Table. 4.25 Parameters of 24h storage needle pre-sheared okra (Philippines) mucilage rotation time curves at $500s^{-1}$

Okra 4	t_1 (s)	t_2 (s)	σ_2 (mPa)	t_3 (s)	t_4 (s)	σ_4 (mPa)
Test 1	9	34	1400	19	418	1450
Test 2	14	38	1440	10	418	1450
Test 3	14	24	1420	19	423	1450

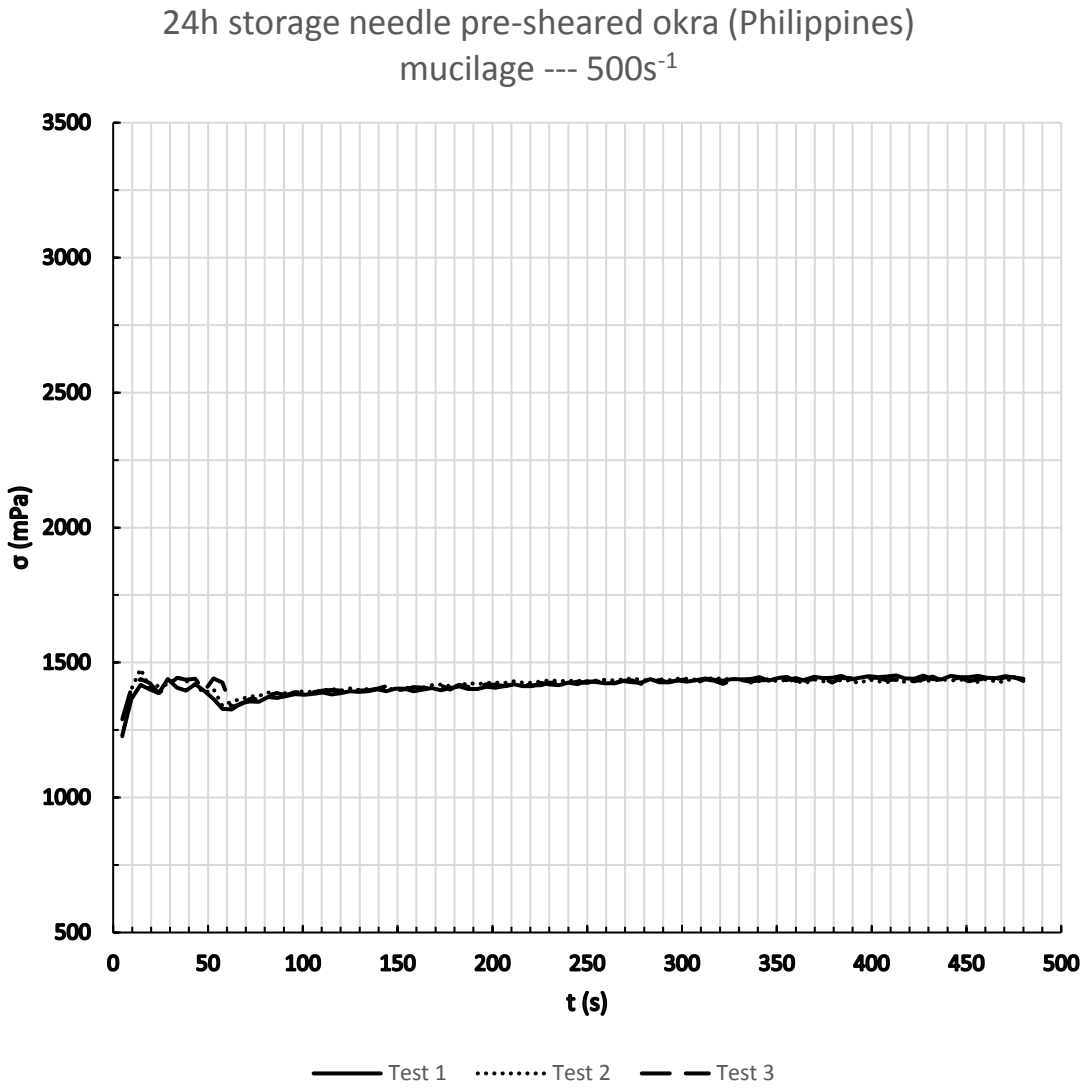

Fig. 4.40 24h storage needle pre-sheared okra (Philippines) mucilage rotation time curves at $500s^{-1}$

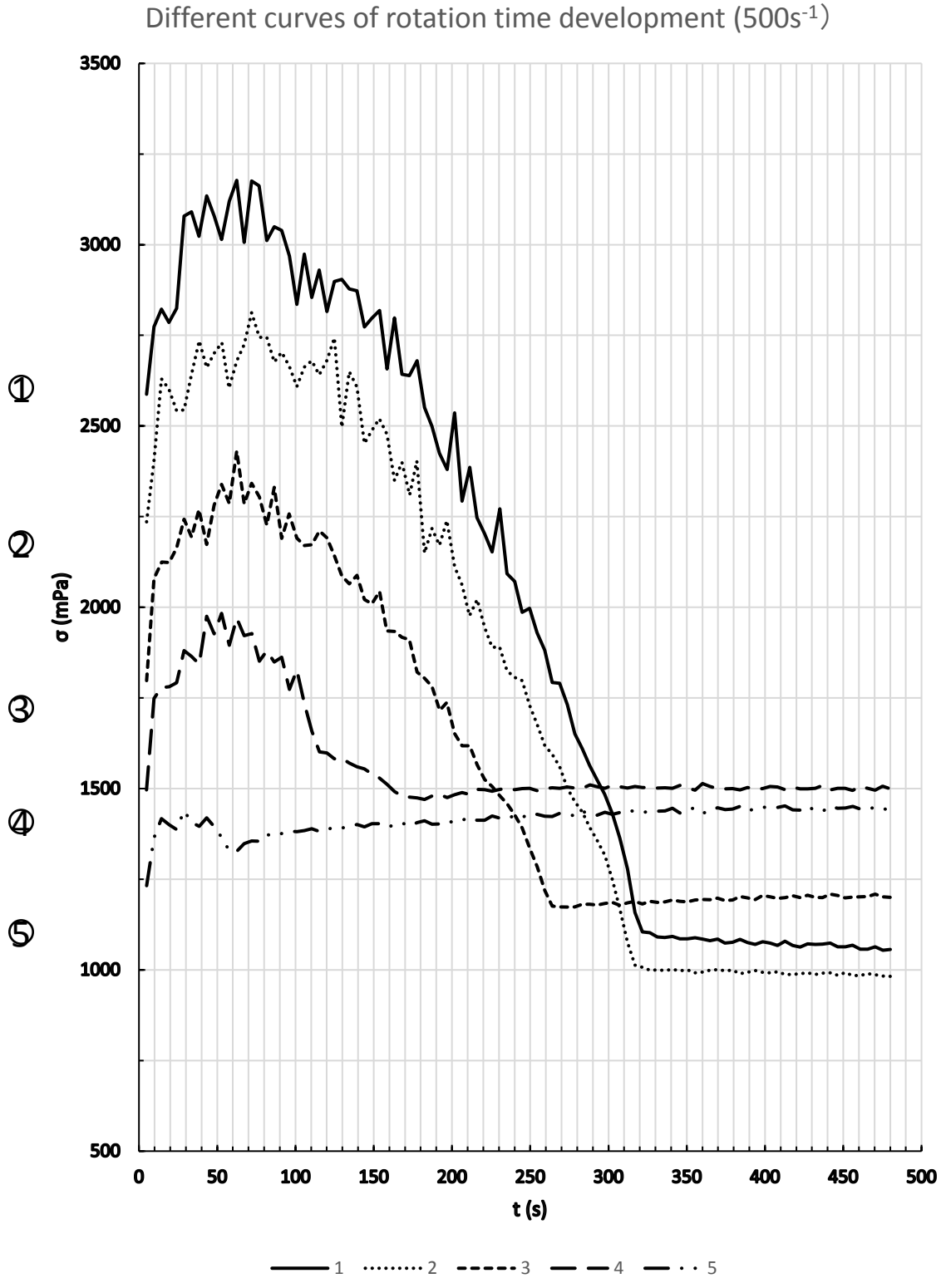

Fig. 4.41 Different curves of rotation time development (500s^{-1})

To Fig. 4.36 (curve 1 shown in Fig. 4.41), given the all normal conditions to the experiment, the constant shear rate would drug the okra mucilage to flow.

The initial increase in stress represents the elastic response of the material, while a decrease of the stress value indicates the gradual structure breakdown (Tárrega et al., 2006). This transition from viscoelastic to viscous flow is manifested as a peak in shear stress response which corresponds to the yield stress value (Sad 2008). In a series of experiments, at low shear rate 10s-1, the material is slow to respond and the stress increases to a relatively constant value. This would like a shear rate style "creep" experiment to complex. While using the higher shear rates (over than the transition point), the peak in the stress occurred like the yield stress. After that the stress response would decay and decrease to a constant value.

- Okra mucilage comparing with the needle presheared okra mucilage (Fig. 4.36, Fig. 4.37; or Curve 1&4 in Fig. 4.41)

It is not hard to find that the total time of t_1, t_2 and t_3 of the needle pre-sheared okra mucilage system was much less than the normal one. It hinted that the needle pre-sheared okra mucilage would arrive at the final viscous balance in a shorter time. That might because the needle shear history effect had already weakened the system's elastic element strength. In the end, the phenomenon that the σ_4 of the needle presheared was higher than the normal one was found. That was because needle shear stress let the large okra structure groups into small crops, which would increase the number concentration. Thus, the viscous forces and energy consumption were increased.

- Okra mucilage comparing with the 24h storage okra mucilage (Fig. 4.36, Fig. 4.38; or Curve 1&2 in Fig. 4.41)

Comparing with the fresh okra mucilage development curve, the longer t_4 showed that the 24h storage okra mucilage would reach the final balance in shorter time. Meanwhile, both the σ_2 and σ_4 were lower than the fresh one. These all hint that the lower biopolymers' activity that the 24h prevented okra mucilage contained. The particles in 24h storage okra mucilage could not assemble and pack effectively.

- 24h series group (Fig. 4.38, Fig. 4.39&Fig. 4.40; or Curve 2, 3&5 in Fig. 4.41)

The higher σ_4 and the lager t_4 time of the needle pre-seared okra mucilage, comparing with the rotation sheared okra mucilage, showed that the needle pre-sheared process would bring a more distinct effect over than the cone and plate sheared one, due to their different intensity as mentioned before.

4.7 Observation

4.7.1 Okra protein observation

The Tyndall effect of the okra mucilage was shown in Fig. 4.42 and Fig. 4.43 compared with water, which was on the left hand side. The okra mucilage's component showed much more heterogeneous and larger than the pre-sheared okra mucilage.

Fig. 4.42 Okra mucilage under the green leaser

Fig. 4.43 Pre-sheared okra mucilage under the green leaser

4.7.2 Fluorescent microspheres-added mucilage state's observation

After well shaking of the fluid which had already added the fluorescent microspheres, the microspheres' state was observed in Fig. 4.44. Comparing with the other two solute's state, the pre-sheared okra mucilage could be a nice solvent to let the microspheres evenly distributed in.

On the other hand, after 5 hours, the silk-shape of the microspheres in the okra mucilage were thicken and the upper layer of the pre-sheared okra mucilage became clear. It hinted that the mucilage was losing active energy to lock the microspheres' Brownian motion.

[1] (t=0min) [2] (t=5min)

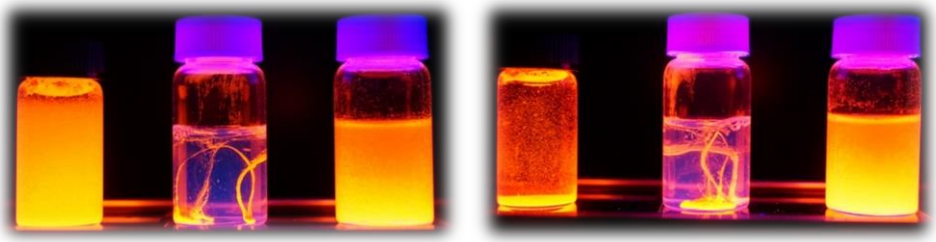

(A) **(B)** **(C)** **(A)** **(B)** **(C)**

[3] (t=15min) [4] (t=300min)

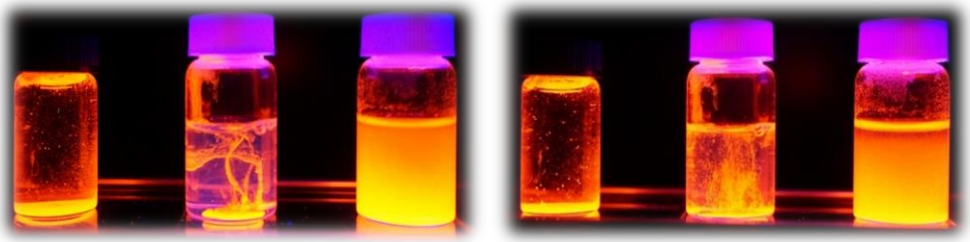

(A) **(B)** **(C)** **(A)** **(B)** **(C)**

Fig. 4.44 Fluorescent microspheres-added mixture;

Water **(A)**/Okra mucilage **(B)**/Pre-sheared mucilage **(C)**

4.7.3 Dry result observation

The crystals of okra mucilage were observed in Fig. 4.45 and Fig. 4.46. The crystal result of the pre-sheared okra mucilage had the rough structures comparing with the non-sheared one. That might because the okra mucilage without the shear history had a more comparative dense structure.

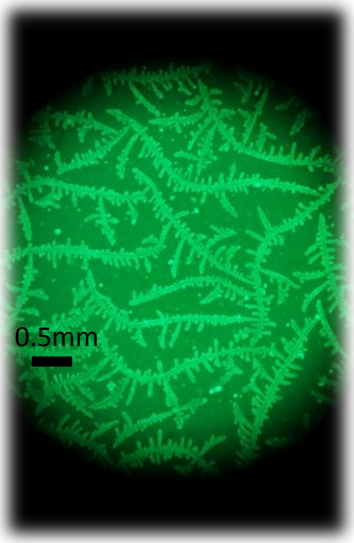

Fig. 4.45 Dry result of okra mucilage

Fig. 4.46 Dry result of pre-sheared okra mucilage

VI. Conclusion

5. Conclusion

Okra mucilage is a very interesting complex fluid.

- A shear history effect would cause okra mucilage's viscosity much smaller at high shear rate range (from $100s^{-1}$ ~$1000s^{-1}$) as a common result. At low shear rate (0.1s-1~10s-1), this phenomenon was not prominent probably because the time scale caused by the shear rate was lower than the relaxation time. That would not let the structure be easily disrupted, stretch out and entanglement.
- A shear history effect would let the elastic element part of okra mucilage decrease. On the opposite, the viscous element part would increase. That might because the shear history effect break the large biopolymer groups into small crops. In another word, the mid of large biopolymer's bunch were disintegrated (no longer networks), and it would do effect to the viscous energy consumption by accumulation.
- Due to the shear effect, the pre-sheared okra mucilage could be a nice solvent to let the substance evenly distributed in.

This effect is beneficial for some aspects, but unfriendly at another application. For example, for the structural stability of ice cream which was mentioned in food processing in background part of this paper, a stable grid structure is trying to be required. Therefore, when preparing okra polysaccharide process, adding shear force should be avoided as much as possible for the interior elastic energy consumption of okra. Because the energy consumption will lead a coarseness of crystallization and poor mesh. This will has a negative impact on the ice cream stability system. On the other hand, for example, in the future, I will try to pump the okra mucus into the liver to achieve some pathological adjustment. If the okra mucus still has the high viscosity, large macromolecular group and network, this is obviously not so beneficial. Because, the high viscosity will cause an excessive resistance in the capillaries. It is possible to deepen the damage to the soft tissue and cells. Moreover, the existence of large grids and macromolecular groups may prevent the exchange of oxygen or some other nutrition molecules for cell and soft tissues.

Overall, the rheological properties and the shear history effect on okra mucilage have been discovered and explored in this paper. This will give a more detailed information of for okra mucilage's flow characteristic. Thus, a much better fitted simulation of okra mucilage can be set up in the future.

VII. Reference

6. Reference

Agarwal M, Srinivasan R, Mishra A. 2001. Study on flocculation efficiency of okra gum in sewage waste water. *Macromol. Mater. Eng.* 286(9):560–63

Akram S, Bashir S, Noreen S, Muqeet A, Riffat S, Abbas M. 2018. International Journal of Biological Macromolecules Polymeric microspheres of okra mucilage and alginate for the controlled release of oxcarbazepine : In vitro & in vivo evaluation. *Int. J. Biol. Macromol.* 111:1156–65

Alamri MS. 2014. Okra-gum fortified bread : formulation and quality. . 51(October):2370–81

Alamri MS, Mohamed AA, Hussain S. 2012. Effect of okra gum on the pasting, thermal, and viscous properties of rice and sorghum starches. *Carbohydr. Polym.* 89(1):199–207

Alamri MS, Mohamed AA, Hussain S. 2013. Effects of alkaline-soluble okra gum on rheological and thermal properties of systems with wheat or corn starch. *Food Hydrocoll.* 30(2):541–51

Alba K, Ritzoulis C, Georgiadis N, Kontogiorgos V. 2013. Okra extracts as emulsi fi ers for acidic emulsions. . 54:1730–37

Alqasoumi SI. 2012. "Okra" Hibiscus esculentus L.: A study of its hepatoprotective activity. *Saudi Pharm. J.* 20(2):135–41

Anastasakis K, Kalderis D, Diamadopoulos E. 2009. Flocculation behavior of mallow and okra mucilage in treating wastewater. *Desalination*. 249(2):786–91

Archana G, Sabina K, Babuskin S, Radhakrishnan K, Fayidh MA, et al. 2013. Preparation and characterization of mucilage polysaccharide for biomedical applications. *Carbohydr. Polym.* 98(1):89–94

Armstrong MJ, Beris AN, Wagner NJ. Dynamic Shear Rheology of Thixotropic Suspensions: Comparison of Structure-Based Models with Large Amplitude Oscillatory Shear Experiments Matthew J. Armstrong, Antony N. Beris, Norman J. Wagner. . (2009):1–32

Björn A, Segura De P, Monja L, Karlsson A, Ejlertsson J, Svensson BH. 2012. Rheological Characterization. *Biogas*. 408

Chen J, Chen W, Duan F, Tang Q, Li X, et al. 2019. Food Hydrocolloids The synergistic gelation of okra polysaccharides with kappa-carrageenan and its influence on gel rheology , texture behaviour and microstructures. *Food Hydrocoll.* 87(July 2018):425–35

Chen Y, Zhang J, Sun H, Wei Z. 2014. International Journal of Biological Macromolecules Pectin from Abelmoschus esculentus : Optimization of extraction and rheological properties. *Int. J. Biol. Macromol.* 70:498–505

Coelho EC, Barbosa KCO, Soares EJ, Siqueira RN, Freitas JCC. 2016. Okra as a drag reducer for high Reynolds numbers water flows. *Rheol. Acta*. 55(11–12):983–91

Cui S, Wang Q. 2005. *Understanding the Physical Properties of Food Polysaccharides*

Freitas TKFS, Oliveira VM, Souza MTF De, Geraldino HCL, Almeida VC, et al. 2015. Optimization of coagulation-flocculation process for treatment of industrial textile wastewater using okra (A . esculentus) mucilage as natural coagulant. *Ind. Crop. Prod.* 76:538–44

Gemede HF, Haki GD, Beyene F, Woldegiorgis AZ, Rakshit SK. 2016a. Proximate, mineral, and antinutrient compositions of indigenous Okra (Abelmoschus esculentus) pod accessions: implications for mineral bioavailability. *Food Sci. Nutr.* 4(2):223–33

Gemede HF, Ratta N, Haki GD, Woldegiorgis AZ, Beyene F. 2016b. Nutritional Quality and Health Benefits of Okra (Abelmoschus Esculentus) : A Review NutritionalQualityandHealthBenefitsofOkraAbelmoschusEsculentusAReview. . (June 2014):

Georgiadis N, Ritzoulis C, Sioura G, Kornezou P, Vasiliadou C, Tsioptsias C. 2011. Contribution of okra extracts to the stability and rheology of oil-in-water emulsions. *Food Hydrocoll.* 25(5):991–99

Ghica MV, Hîrjău M, Lupuleasa D, Dinu-Pîrvu CE. 2016. Flow and Thixotropic Parameters for Rheological Characterization of Hydrogels. *Molecules*. 21(6):

Ghori MU, Alba K, Smith AM, Conway BR, Kontogiorgos V. 2014. Food Hydrocolloids Okra extracts in pharmaceutical and food applications. *Food Hydrocoll.* 42:342–47

H. W, G. C, D. R, S.-T. Y. 2014. Hypolipidemic activity of okra is mediated through inhibition of lipogenesis and upregulation of cholesterol degradation. *Phyther. Res.* 28(2):268–73

Huang C, Wang C, Lin C, Lin H, Peng C. 2017. The nutraceutical benefits of subfractions of Abelmoschus esculentus in treating type 2 diabetes mellitus. . 2–13

Jenkins DJA, Kendall CWC, Marchie A, Faulkner DA, Wong JMW, et al. 2005. Direct comparison of a dietary portfolio of cholesterol-lowering foods with a statin in hypercholesterolemic participants. *Am. J. Clin. Nutr.* 81(2):380–87

Karim MR, Islam MS, Sarkar SM, Murugan AC, Makky EA, et al. 2014. Anti-amylolytic activity of fresh and cooked okra (Hibiscus esculentus L.) pod extract. *Biocatal. Agric. Biotechnol.* 3(4):373–77

Kaur G, Singh D, Brar V. 2014. Bioadhesive okra polymer based buccal patches as platform for controlled drug delivery. *Int. J. Biol. Macromol.* 70:408–19

Kontogiorgos V, Margelou I, Georgiadis N, Ritzoulis C. 2012. Rheological characterization of okra pectins. *Food Hydrocoll.* 29(2):356–62

Kpodo FM, Agbenorhevi JK, Alba K, Bingham RJ, Oduro IN, et al. 2017. Food Hydrocolloids Pectin isolation and characterization from six okra genotypes. *Food Hydrocoll.* 72:323–30

Li Y-X, Yang Z-H, Lin Y, Han W, Jia S-S, Yuan K. 2016. Antifatigue effects of ethanol extracts and polysaccharides isolated from Abelmoschus esculentus. *Pharmacogn. Mag.* 12(47):219

Ling FWM, Abdulbari HA. 2017. Drag reduction by natural polymeric additives in PMDS microchannel: Effect of types of additives. *MATEC Web Conf.* 111:1001

Liu J, Zhao Y, Wu Q, John A, Jiang Y, et al. 2018. Structure characterisation of polysaccharides in vegetable “okra” and evaluation of hypoglycemic activity. *Food Chem.* 242(July 2017):211–16

Liu J zhong, Wang R kun, Gao F yan, Zhou J hu, Cen K fa. 2012. Rheology and thixotropic properties of slurry fuel prepared using municipal wastewater sludge and coal. *Chem. Eng. Sci.* 76:1–8

Lousinian S, Dimopoulou M, Panayiotou C, Ritzoulis C. 2017. Self-assembly of a food hydrocolloid: The case of okra mucilage. *Food Hydrocoll.* 66:190–98

Majd NE, Ph D, Tabandeh MR, Ph D, Shahriari A, et al. 2018. Okra (Abelmoscus esculentus) Improved Islets Structure , and Down-Regulated PPARs Gene Expression in Pancreas of High-Fat Diet and Streptozotocin-Induced Diabetic Rats. . 20(1):31–40

Meister JJ, Anderle K, Merriman G. 1983. Rheology of Aqueous Solutions of Okra Mucilage F. *J. Rheol. (N. Y. N. Y).* 27(1):37–46

Messing J, Thöle C, Niehues M, Shevtsova A, Glocker E, et al. 2014. Antiadhesive properties of Abelmoschus esculentus (okra) immature fruit extract against Helicobacter pylori adhesion. *PLoS One*. 9(1):

Mishra A, Clark JH, Pal S. 2008. Modification of Okra mucilage with acrylamide: Synthesis, characterization and swelling behavior. *Carbohydr. Polym.* 72(4):608–15

Mishra N, Kumar D, Rizvi SI. 2016. Protective Effect of Abelmoschus esculentus Against Alloxan-induced Diabetes in Wistar Strain Rats. . 13(6):634–46

Ndjouenkeu R, Goycoolea FM, Morris ER, Akingbala JO. 1996. Rheology of okra (Hibiscus esculentus L.) and dika nut (Irvingia gabonensis) polysaccharides. *Carbohydr. Polym.* 29(3):263–69

Ohtani K, Okai K, Yamashita U, Yuasa I, Misaki A. 1995. Characterization of an acidic polysaccharide isolated from the leaves of corchorus olitorius (moroheiya). *Biosci. Biotechnol. Biochem.* 59(3):378–81

Panneerselvam K, Ramachandran S, Sabitha V, Naveen K. 2011. Antidiabetic and antihyperlipidemic potential of Abelmoschus esculentus (L.) Moench. in streptozotocin-induced diabetic rats. *J. Pharm. Bioallied Sci.* 3(3):397

PFITZNER J. 1976. Poiseuille and his law. *Anaesthesia*. 31(2):273–75

Principles THE, Of A, Rule THEC. Thermal Analysis & Rheology THE PRINCIPLES AND APPLICATIONS OF THE COX-MERZ RULE

Qasem AAA, Alamri MS, Mohamed AA, Hussain S, Mahmood K, Ibraheem MA. 2017. Effect of okra gum on pasting and rheological properties of cake-batter. *J. Food Meas. Charact.* 11(2):827–34

Rheology EF, Derived M, Foods N. 2017. Shear and Extensional Flow Rheology of Mucilages Derived from Natural Foods. . 45(2):91–99

Ritzoulis C. 2017. Mucilage formation in food: a review on the example of okra. *Int. J. Food Sci. Technol.* 52(1):59–67

Roy A, Shrivastava SL, Mandal SM. 2014. Functional properties of Okra Abelmoschus esculentus L. (Moench): traditional claims and scientific evidences. *Plant Sci. Today*. 1(3):121–30

Sad N. 2008. Determining the Yield - Importance and Shortcomings. *Food Process.* 35:143–49

Saravanan S, Pandikumar P, Pazhanivel N, Paulraj MG, Ignacimuthu S. 2013. Hepatoprotective role of Abelmoschus esculentus (Linn.) Moench., on carbon tetrachloride-induced liver injury. *Toxicol. Mech. Methods*. 23(7):528–36

Schets FM, De Man H. 2017. Risico-inventarisatie waterspeelplaats Zuiderpret, Den Haag

Sengkhamparn N, Bakx EJ, Verhoef R, Schols HA, Sajjaanantakul T, Voragen AGJ. 2009. Okra pectin contains an unusual substitution of its rhamnosyl residues with acetyl and alpha-linked galactosyl groups. *Carbohydr. Res.* 344(14):1842–51

Sengkhamparn N, Sagis LMC, Vries R De, Schols HA, Sajjaanantakul T, Voragen AGJ. 2010. Food Hydrocolloids Physicochemical properties of pectins from okra (Abelmoschus esculentus (L .) Moench). *Food Hydrocoll.* 24(1):35–41

Sheu SC, Lai MH. 2012. Composition analysis and immuno-modulatory effect of okra (Abelmoschus esculentus L.) extract. *Food Chem.* 134(4):1906–11

Siah C, Fong M, Robinson J, Binner E. 2015. Optimisation of extraction and sludge dewatering ef fi ciencies of bio- fl occulants extracted from Abelmoschus esculentus (okra). *J. Environ. Manage.* 157:320–25

Sun A, Gunasekaran S. 2009. *Yield Stress in Foods: Measurements and Applications*, Vol. 12

Systems F. M o m e n t u m a n a ly s i s o f flow systems. *Most*. 559–604

Tayal A, Pai VB, Khan SA. 1999. Rheology and microstructural changes during enzymatic degradation of a guar-borax hydrogel. *Macromolecules*. 32(17):5567–74

Wang Y, Wu X, Yang W, Zhai Y, Xie B, Yang M. 2011. Aggregate of nanoparticles : rheological and mechanical properties. . 3–8

Wee MSM, Matia-Merino L, Goh KKT. 2015. Time- and shear history-dependence of the rheological properties of a water-soluble extract from the fronds of the black tree fern, *Cyathea medullaris*. *J. Rheol. (N. Y. N. Y).* 59(2):365–76

Wei Y, Lin Y, Xie R, Xu Y, Yao J, Zhang J. 2015. The flow behavior , thixotropy and dynamical viscoelasticity of fenugreek gum. *J. Food Eng.* 166:21–28

Woolfe ML, Chaplin MF, Otchere G. 1977. Studies on the mucilages extracted from okra fruits (Hibiscus esculentus L.) and baobab leaves (Adansonia digitata L.). *J. Sci. Food Agric.* 28(6):519–29

Xia F, Zhong Y, Li M, Chang Q, Liao Y, et al. 2015. Antioxidant and anti-fatigue constituents of Okra. *Nutrients*. 7(10):8846–58

Xie J, Jin YC. 2016. Parameter determination for the cross rheology equation and its application to modeling non-Newtonian flows using the WC-MPS method. *Eng. Appl. Comput. Fluid Mech.* 10(1):111–29

Xu K, Guo M, Du J. 2017. Molecular characteristics and rheological properties of water-extractable polysaccharides derived from okra (Abelmoschus esculentus L .). *Int. J. Food Prop.* 20(1):899–909

Yuan B, Ritzoulis C, Chen J. 2018a. Extensional and shear rheology of a food hydrocolloid. *Food Hydrocoll.* 74:296–306

Yuan B, Ritzoulis C, Chen J. 2018b. Extensional and shear rheology of okra hydrocolloid–saliva mixtures. *Food Res. Int.* 106(July 2017):204–12

Yuennan P, Sajjaanantakul T, Goff HD. 2014. Effect of okra cell wall and polysaccharide on physical properties and stability of ice cream. *J. Food Sci.* 79(8):

Zafer O, Ortac D, Cemek M, Karaca T. 2018. In vivo anti-ulcerogenic effect of okra (Abelmoschus esculentus) on ethanol-induced acute gastric mucosal lesions. . 56(1):165–75

Zaharuddin ND, Noordin MI, Kadivar A. 2014. The use of hibiscus esculentus (Okra) gum in sustaining the release of propranolol hydrochloride in a solid oral dosage form. *Biomed Res. Int.* 2014(August):

Zhang T, Xiang J, Zheng G, Yan R, Min X. 2018. Preliminary characterization and anti-hyperglycemic activity of a pectic polysaccharide from okra (Abelmoschus esculentus (L .) Moench). *J. Funct. Foods*. 41(November 2017):19–24

Zheng W, Zhao T, Feng W, Wang W, Zou Y, et al. 2014. Purification , characterization and immunomodulating activity of a polysaccharide from flowers of Abelmoschus esculentus. *Carbohydr. Polym.* 106:335–42